ABSTRACT

Title of dissertation: HADRONIC INTERACTIONS IN LARGE N_c QCD: STUDIES OF EXCITED BARYON DECAYS AND SCATTERING RELATIONS

Daniel C. Dakin, Doctor of Philosophy, 2005

Dissertation directed by: Professor Thomas D. Cohen
Department of Physics

Decays and scattering events are two of the principal ways to learn about particle physics. Decays, in which a particle spontaneously disintegrates and we examine the debris, are quantified by a decay width. The decay of a resonance state provides information about the structure of the state and the interaction between its components. In particular, we can learn about the dynamics of quarks and gluons by studying the decay of hadrons. Scattering, in which particles are directed towards each other and interact, are quantified by partial-wave amplitudes. These amplitudes give us information about the interaction between the scattered particles.

In principle, all of hadronic physics follows from quantum chromodynamics (QCD), which describes the interactions of quarks and gluons. However, the techniques of perturbation theory are not applicable to QCD at low energy because the strong coupling constant (the natural choice for the expansion parameter) is large at the energy scale of hadronic physics. A powerful model-independent method is the $1/N_c$ expansion in which the number of quark color degrees of freedom (N_c)

is treated as a large number. This thesis presents the application of the $1/N_c$ expansion to the calculation of physical observables for excited baryons, pion-nucleon scattering, and pion photoproduction.

The framework of the contracted SU(4) group that emerges in large N_c QCD is applied to the study of excited baryon decays. The N_c power scaling of the excited baryon's decay width depends on the symmetry of its spin-flavor wavefunction. The scaling with N_c for different symmetries is discussed in the context of a quark-shell model that permits mixing of different symmetry types. The subtle issues concerning the legitimacy of applying the contracted SU(4) group theory to excited baryons are discussed.

The contracted SU(4) spin-flavor symmetry severely restricts the angular momentum and isospin dependence of partial-wave amplitudes. The consequences of this restriction on pion-nucleon scattering and pion photoproduction are discussed. In particular, model-independent linear relations among different hadronic scattering amplitudes holding to leading order in $1/N_c$ are obtained and compared with experimental data. The group-theoretic structure of large N_c QCD allows for a systematic expansion of scattering amplitudes in powers of $1/N_c$ which leads to model-independent relations holding to next-to-leading order in $1/N_c$. These relations are derived and shown to compare more favorably with experiments to the extent expected for the $1/N_c$ expansion.

HADRONIC INTERACTIONS IN LARGE N_c QCD: STUDIES OF EXCITED BARYON DECAYS AND SCATTERING RELATIONS

by

Daniel C. Dakin

Dissertation submitted to the Faculty of the Graduate School of the
University of Maryland, College Park in partial fulfillment
of the requirements for the degree of
Doctor of Philosophy
2005

Advisory Committee:

Professor Thomas D. Cohen, Chair/Advisor
Professor Elizabeth Beise
Professor Xiangdong Ji
Professor Alice C. Mignerey
Professor Stephen J. Wallace

This thesis is dedicated to my best friend, b and the Quantum Mechanics Pirates.

ACKNOWLEDGMENTS

It's pronounced nuclear. Nu-cu-ler. – Homer Simpson

I would like to begin by thanking my advisor, Professor Tom Cohen, for all his help over the years. His combination of guidance, patience, and a wealth of knowledge made my research fruitful and fun. I believe that the course set by Tom and Boris Gelman over my first summer will take me to many exciting areas of physics.

My collaborators, Abhi Nellore of the University of Maryland and Rich Lebed and Dan Martin of Arizona State University have taught me lot and I am glad that I had the chance to work with them.

Academic research would be impossible without the help of the physics department staff. Loretta Robinette deserves many thanks for all the time and effort she devoted to me. Also, Dottie Brosious provided the template for this thesis.

My family, especially Mom & Dad & Tom, has been very supportive while I avoided the "real world" for four more years. I enjoyed studying and working at my grandparents' places on Long Island and in Ocean City, Maryland.

Graduate school would be unbearable torture without the friendship of the Quantum Mechanics Pirates, the honorary members, and the TQHN group. I had a great time working on the homework sets and going to lunch. 12:30, lobby.

The best thing about Maryland is my bestfriend, fiance, and future wife, Beth

Rogers. We make a great team and I am so happy that we shared graduate school together. I look forward to sharing the rest of our lives, too.

TABLE OF CONTENTS

LIST OF TABLES

LIST OF FIGURES

Chapter 1

Introduction: Methods of Quantum Chromodynamics

1.1 QCD and Hadronic Physics

The strong interaction sector of the Standard Model includes the basic ingredients of matter, protons and neutrons, which are found in the atomic nucleus and provide fusion fuel for stars. This sector is described by the theory of quantum chromodynamics (QCD) where the fundamental degrees of freedom of the QCD Lagrangian [1] are spin-1/2 quarks and spin-1 gluons. Each quark takes on one of the three values of a label called *color* [2] that plays a role similar to that of electric charge in quantum electrodynamics (QED). The interaction between the quarks and the gluons is then determined by gauging the local SU(3)-color symmetry.

Quantum chromodynamics exhibits a phenomena called *color confinement*, which states that the asymptotic states of QCD are colorless. While color confinement is currently not totally understood within the theory of QCD, it is firmly based on the empirical fact that quarks or gluons have not been observed in nature. The observed particles of QCD are colorless bound states of quarks and gluons, called hadrons which fall into two classes: mesons and baryons. Mesons are spin-0 or -1 hadrons with the quantum numbers of a quark–anti-quark pair. Baryons are spin-$\frac{1}{2}$ or -$\frac{3}{2}$ hadrons with the quantum numbers of a three-quark composite.

One goal of hadronic physics is to understand the properties and interactions

of mesons and baryons using QCD. However, the dimensionless QCD coupling g is of order unity at the low energies (on the order of the QCD scale parameter, $\Lambda_{\rm QCD} \approx 200$ MeV) and large distances (on the order of the proton radius ~ 1 fm) relevant to hadronic physics. This means that the powerful techniques of perturbation theory using the coupling as an expansion parameter developed for QED ($g_{\rm QED} \sim 1/137$) are inapplicable. The large value of the coupling at small energies is due to the phenomenon of asymptotic freedom [3] exhibited by non-Abelian gauge groups like SU(3)-color. Asymptotic freedom also hints at a partial explanation for color confinement: low-energy colored quarks and gluons interact strongly with each other and condense into colorless states (hadrons). According to asymptotic freedom, the QCD coupling is small at high energies (and short distances) and thus is a suitable perturbation parameter in this regime. Research using perturbative QCD at high energies has enjoyed a lot of success. For example, Bjorken scaling and deviations from scaling in the context of deep inelastic lepton-hadron scattering are well understood [4, 5].

In the hadronic physics energy regime, progress is made by constructing models that encode varying levels of QCD features. Among the popular and successful models are the quark model [6], the MIT bag model [7], the vector dominance model [8], and the Skyrme model [9, 10]. We briefly describe these below.

The quark model of Gell-Mann and Ne'eman [6] provided the genesis for quantum chromodynamics. In this model, the known hadrons are imagined to be composed of point-like entities called *constituent* quarks with electric charges in multiples of $\frac{1}{3}$ and a color label. The quarks are spin-$\frac{1}{2}$ and come in six flavors with increasing

mass, {up, down, strange, charm, top, bottom}. Although they share the same name, the quarks of the QCD Lagrangian and the quark model have no obvious connection. A constituent quark is an object made up of quarks and gluons that has the quantum numbers (spin, color, baryon number, etc.) of a single quark. The interaction between constituent quarks in the quark model is not based directly on QCD, but on phenomenological parameters chosen so that the predicted hadronic masses fit the observed spectrum. Despite its shortcomings, this model has been very helpful for understanding hadronic properties.

The original quark model only considered the three lightest flavors, $q = (u, d, s)$ and assumes that their masses are small compared to $\Lambda_{\rm QCD}$. This hypothesis explains the observation that hadrons with masses below ~ 1700 MeV can be grouped into SU(3)-flavor multiplets if mesons are taken as $q\bar{q}$ pairs and baryons as qqq composites. Isospin is a sub-group of this approximate SU(3)-flavor symmetry. An SU(2) isospin quantum number is assigned to particles that can be grouped together by mass and other properties (strangeness, etc.). For example, the proton and neutron form an isospin-$\frac{1}{2}$ doublet with mass ≈ 939 MeV, called a nucleon. Other multiplets that will be important in this thesis are the pions (π^+, π^0, π^-) with isospin 1 and mass ≈ 138 MeV, and the deltas (Δ^{++}, Δ^+, Δ^0, Δ^-) with isospin $\frac{3}{2}$ and mass ≈ 1232 MeV. Since QCD respects the isospin symmetry, the total isospin of a hadronic system is conserved in strong interaction processes.

In the MIT bag model, a hadron is modeled as a spherical ("bag-like") cavity in the QCD vacuum that contains free quarks. The QCD vacuum provides the external pressure needed to stabilize the hadron and color confinement is explic-

itly incorporated by choosing appropriate color values for the quarks. Calculations within this model of the hyperfine mass splittings in the hadronic spectrum match a lot of experimental data nicely [7].

Even before the quark model or QCD, J.J. Sakurai [8] attempted to model the strong interaction as a gauge theory where the vector mesons $\rho(770)$, $\omega(782)$, and $\phi(1020)$ play the role of the gauge bosons. The so called vector dominance model has successfully explained many phenomenological aspects of hadronic physics such as form factors, absorption cross sections, and πN and NN scattering.

An effective theory of pions with a close connection to the vector dominance model is due to T.H. Skyrme [9, 10]. It is an extension of the non-linear sigma model, which is based on chiral symmetry. This symmetry follows from the fact that the up and down quark masses are very close to zero and the QCD Lagrangian restricted to these flavors is invariant under $\mathrm{SU}_L(2)\times\mathrm{SU}_R(2)$ transformations. The Skyrme Lagrangian is given by

$$\mathcal{L} = \frac{1}{4} f_\pi^2 \,\mathrm{Tr}(\partial_\mu U \partial^\mu U^\dagger) + \frac{1}{32e^2}\mathrm{Tr}\left[(\partial_\mu U)U^\dagger, (\partial_\nu U)U^\dagger\right]^2, \tag{1.1}$$

where $U = \exp(i\vec{\tau}\cdot\vec{\pi}/f_\pi) \in \mathrm{SU}(2)$, $\vec{\pi}$ represents the pion fields, and $\vec{\tau}$ is the set of Pauli matrices acting in isospin space. The pion decay constant, $f_\pi \approx 93$ MeV, is a fundamental parameter that governs low-energy hadronic physics. Skyrme noted that the equations of motion derived from Eq. (1.1) include static classical solutions of finite size and energy (called *solitons*), with a conserved topological quantum number (charge), b. Skyrme suggested that the number b can be identified with the baryon number and furthermore that the $b = 1$ solitons are nucleons. That a meson

(boson) theory can describe baryons (fermions) is not obvious *a priori* [11], but the hypothesis has provided many good predictions (within 30% accuracy) for baryonic properties like magnetic moments, couplings, and charge radii [12].

Chiral symmetry is spontaneously broken by the QCD vacuum. According to Goldstone's theorem, a continuous symmetry that is spontaneously broken is accompanied by a zero-mass boson field. The anomalously low mass of the pions compared to other hadronic masses makes them a good candidate for the Goldstone bosons. The non-zero mass of the pions is explained by the fact that chiral symmetry is broken by the non-zero masses of the up and down quarks. Given the low mass of the pions compared to the nucleon mass, it is possible to implement an expansion for observables in the perturbation parameter $m_\pi/m_N \approx 0.15$. Chiral perturbation theory has yielded many useful results for scattering lengths and cross sections [13, 14].

One of the few non-perturbative and model-independent approaches to understanding hadronic physics is lattice QCD [15]. This method is implemented by discretizing the space-time continuum into a 3+1 dimensional lattice and formulating QCD in path integral language at each point. The integrals involved can then be computed on large computers to calculate observables, like the hadronic mass spectrum. A serious drawback to this approach is the difficultly encountered when one attempts to compute time-dependent quantities like those relevant to decay and scattering processes.

Although the above techniques have sustained hadronic physics for decades, we continue to search for a model-independent approach that reflects all the features

of QCD. In the following section, we introduce one such approach that has had some success: The $1/N_c$ expansion of QCD, where the number of quark colors, N_c is treated as a large number [16]. It is an empirical fact that $N_c = 3$ in our universe. Historically, the three colors were introduced to explain the symmetry of baryon wavefunctions in the quark model in light of the Pauli exclusion principle [2]. The three colors also explain the measured decay rate for $\pi^0 \to \gamma\gamma$ and the ratio, $R \equiv \sigma(e^+e^- \to \text{hadrons})/\sigma(e^+e^- \to \mu^+\mu^-)$ for energies away from thresholds for new quark flavor production. Despite its fixed value in nature, treating N_c as an arbitrarily large number yields a predictive field theory of hadrons.

1.2 Large N_c QCD and All That

As mentioned above, the QCD coupling constant g becomes large at low energies through the workings of asymptotic freedom. We therefore cannot perform a perturbative expansion in powers of g as done in QED and are thus deprived of the physical insights usually gained from perturbation theory. Given the absence of any other useful expansion parameter, 't Hooft [16] suggested generalizing the number of QCD quark colors to N_c and assuming it to be a large number. That is, rather than study the SU(3)-color gauge group, we should focus on SU(N_c)-color and calculate observables with an expansion in powers of $1/N_c$. This is done with the hope that the two worlds described by the $N_c \to 3$ and $N_c \to \infty$ limits have similar properties.

To implement this idea, 't Hooft re-scaled the coupling constant, $g \mapsto g/\sqrt{N_c}$ while keeping Λ_{QCD} fixed. This serves to produce a nontrivial and predictive theory

of strong interactions at all energy scales. It also gives the one-loop gluon polarization and other diagrams a smooth limit (*i.e.*, approaches a finite value) as $N_c \to \infty$ with $g^2 N_c$ fixed. The main advantage of a large number of colors is the simplification of QCD that occurs when summing over the color indices in Feynman diagrams containing quarks and gluons. This follows from the fact that there are $N_c^2 - 1$ gluon fields (represented by trace-less $N_c \times N_c$ matrices) and N_c quark states. The color sum contributes a unique N_c-dependent combinatorial factor to each diagram that becomes either large or small as $N_c \to \infty$. The immediate consequence of this scaling and the combinatorics of the SU(N_c)-color group is that only diagrams that lie in a plane (called planar diagrams) contribute to matrix elements as $N_c \to \infty$. All other diagrams–those that contain quark loops or for which one cannot draw all the particle lines in a plane without crossing them (non-planar)–are suppressed by a factor of $1/N_c$ or higher. Therefore, large N_c QCD provides an *organization* of Feynman diagrams into a hierarchy of classes according to their N_c scaling.

In large N_c QCD, color confinement is assumed to occur for N_c greater than three. If color confinement did not persist as $N_c \to \infty$, the theory would have little phenomenological value since colored QCD states have not been observed. By applying the $1/N_c$ expansion to the theory of mesons, one can show that there are an infinite number of pure $q\bar{q}$ states with masses independent of N_c [*i.e.*, mass $\sim O(N_c^0)$], decay amplitudes of order $O(N_c^{-1/2})$, and meson-meson elastic scattering amplitudes of order $O(N_c^{-1})$. Therefore, the large N_c limit of QCD becomes a theory of stable and non-interacting mesons. Also, the matrix element for a current to create a meson is $O(N_c^{1/2})$ and each additional meson at a vertex contributes another suppression

factor of $N_c^{-1/2}$. Thus the pion decay constant, which governs most of low-energy hadronic physics scales as $f_\pi \sim O(N_c^{1/2})$.

Incorporating baryons into the framework of the $1/N_c$ expansion was pioneered by Witten [17]. In order to form a color singlet as required by color confinement, baryons become a bound state of N_c quarks. At this point, we insist that N_c be an odd number to form a fermionic bound state. The N_c quarks are described by a Hartree mean field approximation in which each quark moves in an $O(N_c^0)$ potential created by the other $N_c - 1$ quarks. Witten's N_c power counting rules follow from this formalism and predict that the baryon has a mass of order $O(N_c^1)$, with a size and shape independent of N_c [*i.e.*, $O(N_c^0)$].

1.3 Applications of N_c Power Counting Rules

It is possible to use the N_c power counting rules to investigate several hadronic processes. For example, baryon-baryon scattering cross sections are shown to have a smooth large N_c limit if the baryon momentum is of order $O(N_c^1)$. Momenta of order $O(N_c^0)$ are encountered in an analysis of the nucleon-nucleon potential [18, 19, 20], while the $p \sim O(N_c^{1/2})$ regime in nucleon-nucleon scattering was explored in Refs. [21, 22]. In the latter regime, it was shown that predictions for nucleon-nucleon scattering observables derived from time-dependent mean-field theory are still valid, thus relaxing Witten's above restriction that the baryon momentum must be of order $O(N_c^1)$. Despite the validity of the predictions, empirical evidence did not support the claims of Ref. [21] for a subtle reason. As shown in Ref. [22], the

expansion is effectively in the parameter $(\beta N_c)^{-1/2}$, where β is the ratio of m_π to typical hadronic energy scales. Given the approximate chiral symmetry of QCD discussed in Sec. 1.1, β is a small number and thus the expansion converges slowly and prevents us from making precise numerical predictions.

Meson-baryon scattering has a smooth and non-trivial large N_c limit when meson energies are of order $O(N_c^0)$. This result of Witten's counting rules will be crucial for describing the spin-flavor properties of baryons, as noted below. The counting rules also show that scattering with an excited baryon does not have a smooth limit. In fact, the amplitude for meson + baryon $\rightarrow$ meson + excited baryon is of order $O(N_c^{-1/2})$ [23]. This scaling will be important in our discussion of excited baryon decays in Chapter 2. The cross sections for the production or annihilation of a baryon–anti-baryon pair in mesonic reactions vanish exponentially for large N_c [*i.e.*, e^{-N_c}]. This follows from the difficulty in creating or destroying a large number (N_c) of quark pairs.

Witten elegantly summarized the above results for large N_c baryons [17] by proposing that they are solitons of a weakly-interacting meson theory. As noted above, the mesons of large N_c QCD have an effective coupling of order $O(N_c^{-1})$. Baryon properties like mass [$m \sim O(N_c^1)$] and size [$\langle r^2 \rangle \sim O(N_c^0)$] scale with this effective coupling constant like those of a soliton.

A popular way to realize this idea is the Skyrme model introduced in Sec. 1.1. In the Skyrme model, baryons are solitons with a conserved topological number interpreted as the baryon number. However, the solitons do not have the proper (fixed) spin and isospin quantum numbers to describe a baryon, so the correct

quantum numbers are generated by rotating (or quantizing) the soliton in spin-isospin space. The quantized baryon states have equal isospin and spin ($I = J$); this describes the nucleons ($I = J = \frac{1}{2}$) and deltas ($I = J = \frac{3}{2}$). The rotational energy contributes to the baryon mass as $m_J = m + \frac{1}{2\lambda}J(J+1)$, where $m \sim O(N_c^1)$ is the soliton mass and $\lambda \sim m\langle r^2 \rangle \sim O(N_c^1)$ is its moment of inertia. This yields an important relation [12] between the mass of the deltas and nucleons: $m_\Delta - m_N \sim O(N_c^{-1})$.

Using large N_c QCD as a guide, one can formulate pion-baryon scattering and pion photoproduction in the Skyrme model with considerable success [25, 24, 26, 27]. Several relations among static and dynamic observables from the Skyrme model are found to be independent of the model parameters such as f_π and indeed hold true for any chiral soliton model [28]. For example, the Skyrme model predicts that $g_{\pi N\Delta}/g_{\pi NN} = \frac{3}{2}$ for pion couplings. This is experimentally confirmed within one percent, whereas typical Skyrme model predictions are within 30% [12]. This strongly suggests that these model-independent predictions are more general results that follow directly from pure large N_c QCD arguments. In the following section, we present an approach to large N_c QCD that is independent of any models.

1.4 Large N_c Consistency Conditions

A completely model-independent approach to large N_c QCD follows from consistent N_c power counting in low-energy pion-baryon scattering. This approach begins by considering the scattering of pions off of baryons [$m \sim O(N_c^1)$] with energies

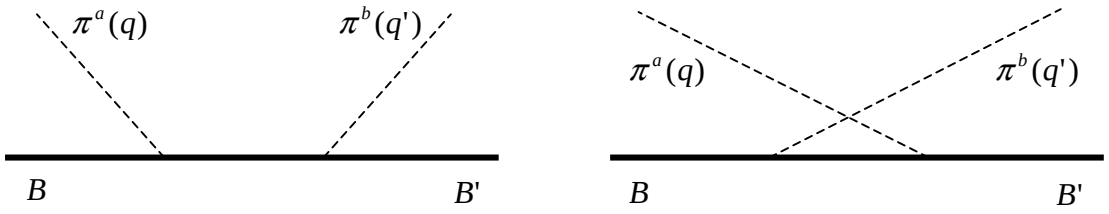

Figure 1.1: Tree-level diagrams that contribute to leading order in $1/N_c$ for pion-baryon scattering.

of order $O(N_c^0)$. To calculate the amplitude for pion-baryon scattering, we must evaluate the two tree-level Feynman diagrams shown in Fig. 1.1. The evaluation requires a knowledge of the pion-nucleon vertex factor and baryon propagator. The vertex factor follows after recalling that pions are pseudo-Goldstone bosons of the broken chiral symmetry and thus are derivatively coupled to the axial vector baryon current with the form:

$$g_A \left\langle B' \left| \bar{q}\gamma^i\gamma_5\tau^a q \right| B \right\rangle \partial_i\pi^a/f_\pi, \tag{1.2}$$

where the axial coupling $g_A \sim O(N_c^1)$ and pion decay constant $f_\pi \sim O(N_c^{1/2})$. The matrix element of the axial current is parameterized in terms of an order $O(N_c^0)$ spin-flavor operator by $\langle B'|\bar{q}\gamma^i\gamma_5\tau^a q|B\rangle = X^{ia}$. Using the heavy baryon propagator $[i/p\cdot v]$ for a baryon at rest $[\,v=(1,0,0,0)\,]$, which is appropriate since $m \sim O(N_c^1)$, the amplitude is

$$\mathcal{A} = -i\left(\frac{g_A}{f_\pi}\right)^2 \frac{q^i q'^j}{q^0}\left[X^{ia}, X^{jb}\right], \tag{1.3}$$

where we sum over all possible baryon intermediate spin and isospin states. Naive power counting based on the appearance of $(g_A/f_\pi)^2 \sim O(N_c^1)$ implies the amplitude is also of order $O(N_c^1)$, which violates unitarity and is inconsistent with Witten's

argument that the scattering cross section has a smooth large N_c limit. It is possible to control this divergence if a set of intermediate baryons, degenerate to leading order in $1/N_c$, contributes to the sum and cancels a factor of N_c. The spin-flavor operator X^{ia} for these baryons must satisfy the following (minimal) condition on their commutator [29, 30]:

$$\left[X^{ia}, X^{jb}\right] \sim O(N_c^{-1}). \tag{1.4}$$

Therefore the commutator vanishes in the large N_c limit and forms part of the Lie algebra for a contracted SU(4) spin-flavor symmetry:

$$\begin{aligned}
\left[J^i, X^{jb}\right] &= i\epsilon_{ijk} X^{kb}, \\
\left[I^a, X^{jb}\right] &= i\epsilon_{abc} X^{jc}, \\
\left[J^i, J^j\right] &= i\epsilon_{ijk} J^k, \\
\left[I^a, I^b\right] &= i\epsilon_{abc} I^c, \\
\left[I^a, J^i\right] &= 0\,,
\end{aligned} \tag{1.5}$$

where J^i and I^a are the generators of spin and isospin transformations, respectively.

The simplest irreducible representation [29] of the contracted SU(4) group is an infinite tower of degenerate baryons with $I = J = \frac{1}{2}, \frac{3}{2}, \frac{5}{2}, \cdots, \frac{N_c}{2}$. The states with $I = J = \frac{1}{2}$ and $I = J = \frac{3}{2}$ are identified with the observed nucleons and deltas, respectively. The others are merely large N_c QCD artifacts. We note that these are the same states found in the Skyrme model and the large N_c non-relativistic quark model. We also find that the states are degenerate with a spin-dependent mass splitting of order $O(N_c^{-1})$, confirming the previous Skyrme-model result that

$m_\Delta - m_N \sim O(N_c^{-1})$.

The contracted SU(4) symmetry allows us to make model-independent predictions based only on group theory methods. The Skyrme model also contains this symmetry [29], providing evidence for our suggestion that those predictions that are independent of any model parameters are truly (model-independent) results of large N_c QCD.

The contracted SU(4) symmetry also provides us with a systematic method for including $1/N_c$ corrections to predictions. For example, it is shown that the next-to-leading order correction to the $g_{\pi N\Delta}/g_{\pi NN}$ ratio vanishes, implying that $g_{\pi N\Delta}/g_{\pi NN} = \frac{3}{2}[1 + O(N_c^{-2})]$ [29] and explaining why the Skyrme model prediction is so empirically accurate.

Another important result that follows from the contracted SU(4) spin-flavor symmetry is the N_c scaling of matrix elements of a general n-quark operator $\hat{O}^{(n)}_{I_0,J_0}$ with baryon number equal to zero, isospin I_0, and spin J_0. The matrix element between two baryon states scales as [32]

$$\langle B'|\hat{O}^{(n)}_{I_0,J_0}/N_c^n|B\rangle \sim 1/N_c^{|I_0-J_0|}. \tag{1.6}$$

Note that operators whose spin equals isospin have the largest matrix elements and contribute to leading order in the $1/N_c$ expansion. The results of Chapters 3 and 4 will follow directly from this relation.

Large N_c QCD has become a powerful tool for studying many aspects of hadronic and nuclear physics. It has developed over many years with a rich history of success. While its quantitative predictions are often rough, large N_c QCD

provides a framework for organizing operators and Feynman diagrams according to powers of N_c and serves as a trusty guide to QCD calculations.

1.5 Thesis Outline

This thesis presents two distinct applications of the large N_c limit to hadronic physics. In Chapter 2, we discuss the decay widths of excited baryons. It was suggested previously [33] that some spin-flavor mixed-symmetric baryon states have strong couplings of order $O(N_c^{-1/2})$ to nucleons [implying narrow widths of order $O(1/N_c)$], as opposed to the generic expectation based on Witten's counting rules of an order $O(N_c^0)$ coupling. The calculation obtaining these narrow widths was performed in the context of a simple quark-shell model. We address the question of whether the existence of such narrow states is a general property of large N_c QCD. We show that a general large N_c QCD analysis does not predict such narrow states; rather they are a consequence of the extreme simplicity of the quark model.

In Chapters 3 and 4, we show that the spin-flavor symmetry discussed in Sec. 1.4 relates partial-wave amplitudes for different hadronic scattering channels. In particular, we produce linear relations for pion-nucleon scattering (Chap. 3) and pion photoproduction (Chap. 4) that hold to leading order or next-to-leading order in the $1/N_c$ expansion. These results follow from Eq. (1.6) of Sec. 1.4. All of our predictions are tested using available data with satisfying agreement.

Throughout this thesis, we consider only two light quark flavors, the up and down quark, though our results can be generalized to include a third light flavor,

the strange quark [34].

This thesis is based on the original work of Cohen, Dakin, Lebed, Martin, and Nellore [36, 35, 37].

-.-

Chapter 2

Excited Baryon Decay Widths

2.1 Describing Excited Baryons

Distinct excited baryon states are abundant in the hadronic spectrum, with masses ranging from 1440 to 1990 MeV [38]. These states appear as bumps in a partial-wave analysis of hadronic scattering experiments. In a typical situation, a ground-state baryon target couples to an incoming meson, creating a short-lived intermediate state, which then decays into a meson and baryon. Quantum chromodynamics provides no simple method for understanding these *resonances* or their properties, such as their mass and decay width. We usually resort to models, the standard of which is the constituent quark model of Chapter 1. However, despite its phenomenological successes, the simplest version of the quark model has a major conceptual problem: The predicted excited states are stable, implying vanishing decay widths, which is inconsistent with observations. While the excited baryons are resolvable in the spectrum, they decay rapidly and their widths are not small, but typically on the order of 200 MeV. In order to describe decays in the quark model, *ad hoc* dynamics must be introduced to account for couplings to decay channels. A more overarching problem with the quark model is that it has no direct connection with QCD as discussed in Chapter 1. Given these problems, we seek a model-independent approach to understanding excited baryons and turn to large N_c QCD.

In Chapter 1, we developed Witten's N_c power counting rules, originally without regard to hadron spin and flavor quantum numbers, and applied them to mesons and baryons. We found that the decay widths of mesons are of order $O(N_c^{-1})$, while the widths of excited baryons are of order $O(N_c^0)$. In the large N_c limit, the meson widths are vanishingly narrow; this helps explain why they are visible in the hadron spectrum. However, generic excited baryons do not have narrow widths in the large N_c limit [the size is of order $O(N_c^0)$], yet we still see them clearly in the spectrum. It is conceivable that the observed states are exceptional in that their widths do vanish as $N_c \to \infty$. One might imagine that states of this kind may appear once we account for the spin and flavor quantum numbers of the baryons, as done in the consistency condition approach to large N_c QCD. As discussed in the next section, Pirjol and Yan [33] suggested that an approach of this type yields a certain class of excited baryons with narrow widths. This class includes baryons transforming under the mixed-symmetric representation of the spin-flavor group SU(4). (This terminology will be explained in the following section; for now, accept "mixed-symmetric" as an identifying adjective.) This could be an exciting result since the observed narrow baryons are usually assigned to such a representation in simple quark models. This chapter focuses on the question of whether the narrowness of this class of states is, in fact, a model-independent consequence of large N_c QCD.

As shown in Chapter 1, the ground-state baryons of large N_c QCD form multiplets of a completely symmetric representation of a contracted SU(4) spin-flavor symmetry [30, 29]. The symmetry arises when we enforce consistent N_c power counting rules for the scattering of mesons off of ground-state baryons. Methods based

on the group theory of this symmetry provide model-independent predictions for hadronic observables and have been fruitful in describing hadronic physics. The success of the consistency condition method for describing ground-state baryons led to the question of whether the study of excited baryons could profit in a similar manner. Pirjol and Yan [33] developed such an approach in a fashion analogous to the original one of Gervias and Sakita [30] and Dashen, Jenkins, and Manohar [29]. That is, they considered pions scattering off of excited baryons and insisted that the scattering amplitudes obey unitarity and Witten's generic N_c power counting rules [17, 23]. However, it is not obvious how to formulate a *physical* scattering process with asymptotic excited baryon states. Excited baryons are resonances and decay rapidly; they cannot be used as targets in scattering experiments. Thus, the consistency condition approach is only applicable if there exist excited baryons in the large N_c world with widths that are indeed narrow. Pirjol and Yan assumed such states exist and it is not clear if their general mode-independent predictions are valid. However, if a class of narrow excited baryons exists, then the model-independent arguments can be applied to these in a legitimate way. Therefore, the existence of a class of narrow baryon states in large N_c QCD is also important for providing a theoretical justification for the elegant model-independent analysis of Ref. [33], as applied to at least this class of states.

Interestingly, Ref. [33] itself offered an argument that there exists a class of narrow excited baryons in the large N_c limit. It finds that the baryons in the mixed-symmetric representation of the spin-flavor group have widths of order $O(N_c^{-1})$, which thus vanish in the large N_c limit. This is in contrast to the generic N_c power

counting rule prediction, in which the widths are of order $O(N_c^0)$ [39]. Unfortunately, the prediction of narrow decay widths for the mixed-symmetric states in Ref. [33] was *not* based directly on the large N_c QCD consistency conditions. Rather, it arose from calculations done in the context of a simple, nonrelativistic quark model. The particular model employed was the quark-shell model to be described in Section 2.2.2. At this point, there is no cause for alarm since quark models have a long and distinguished history of successful phenomenological descriptions. In the large N_c QCD context, quark models have been used to describe the lowest-lying excited baryon states [40, 41, 42, 43, 44, 45, 46], and have revealed interesting mass degeneracy patterns [33, 39, 57]. Recently, it was shown that the quark-shell model is compatible with the more realistic picture of excited baryons as resonances in meson-baryon scattering, in the sense that both describe the same mass and width degeneracy patterns [39]. How this pattern arises in the resonance picture will be described in Sec. 3.2.

Although the quark model is useful in hadronic physics, the question of interest in this chapter is whether the prediction of narrow excited baryon states presented in Ref. [33] is a direct consequence of large N_c QCD. It is useful to note that a large number of the model-independent relations found with the consistency condition method [29, 30, 31, 47, 48, 49, 50, 51] were originally seen in the context of soliton models [28], and indeed *all* of these hold for quark models. Thus, the issue is whether the existence of narrow excited baryon states found in the quark-shell model of Ref. [33] similarly indicates a general large N_c QCD result. If so, this is an important general result in understanding excited baryons. In contrast, if the prediction is

merely an artifact of the particular choice of model, then it is far less important. In light of this, it is important to note that the model used in Ref. [33] is not completely general, as will be described in Sec. 2.2.2. It is limited in so far as it does not include admixtures of different single-particle descriptions (*i.e.*, it neglects configuration mixing).

The issue of whether the mixed-symmetric excited baryons described in the simple quark-shell model correspond to physical states in large N_c QCD is not addressed in Ref. [33]. If the states are physical, then a previously unrecognized symmetry in large N_c QCD is manifesting itself and prevents the states from decaying rapidly. In particular, the narrowness depends upon a symmetry beyond the contracted SU(4) spin-flavor symmetry deduced in Chapter 1 and Refs. [29, 30, 31, 47, 48, 49, 50, 51]. In those works the "spin" in "spin-flavor" corresponds to the total angular momentum of the baryon state in its rest frame. As shown below, the narrow states predicted in Ref. [33] depend on *two* distinct spin-flavor symmetries: one as before, in which the spin corresponds to the total angular momentum of the baryon state in its rest frame, and a second one in which the spin is purely associated with the spin of the quarks. While these two symmetries are identical for a quark-shell model with all of the quarks in the orbital ground level (s wave), they differ for more general models. The prediction of a new symmetry emerging in the large N_c limit for excited states is certainly exciting; the issue, however, is whether it is physical.

In this chapter, we show that the seemingly narrow excited baryons are in fact *not* a feature of large N_c QCD; they are merely artifacts of the simple quark model

used in Ref. [33]. This chapter is organized as follows: We review the construction of baryon states in the quark-shell model and the significance of key matrix elements in Ref. [33]. Next, we use a quark-shell model Hamiltonian to show that the states used in Ref. [33] are not physical in large N_c QCD. In fact, the physical states are superpositions of both symmetric and mixed-symmetric spin-flavor representations.

2.2 Consistency Conditions and the Quark-shell Model

We begin our review of Pirjol and Yan's argument for narrow excited baryons by pointing out that the narrowness can arise for one of two reasons. They follow from Fermi's golden rule applied to decay processes, where the decay rate is given by

$$\text{Decay rate} = \frac{2\pi}{\hbar} |\mathcal{M}|^2 \times (\text{phase space}) \,. \tag{2.1}$$

The matrix element (or amplitude), $\mathcal{M}$, characterizes how strongly an initial state couples to its potential decay products. For excited baryons, the matrix element is proportional to the meson-baryon coupling, which is the important quantity in our study. The phase space (or density of final states) accounts for all the possible outcomes of a decay process. A state will be narrow if either the matrix element or the phase space for decay is small. According to Ref. [33], the meson-baryon coupling for the mixed-symmetric states is of order $O(N_c^{-1/2})$, and thus even when the phase space is of order $O(N_c^0)$, the decay rate vanishes as $N_c \to \infty$ and produces narrow states.

Pirjol and Yan's analysis [33] of excited baryons begins in a manner that is formally similar to that described in Sec. 1.4 of Chapter 1. Pions are scattered

off of excited baryons, and the N_c power counting rules are enforced for the total scattering amplitude. Any analysis of a physical scattering event presupposes that the target is stable; in Ref. [33], the target was a p-wave baryon, and it was taken to be narrow in the large N_c limit. This is a tenuous assumption unless the quark mass is taken to be large, in which case the baryon has no possible decay channels due to phase space limitations. For the sake of argument, we will work in such a world in the following and assume that results obtained can be safely extrapolated back to the physical world of light quarks. As noted in Sec. 2.1, it is by no means clear that such a procedure is justifiable, since the consistency conditions cannot legitimately be formulated for states that are unstable in large N_c QCD. However, for the present purpose this procedure is adequate since states may be narrow for one of two reasons: Either the phase space for decay is small (or zero) or the meson-baryon coupling is small. The claim of Ref. [33] is that mixed-symmetric states have a meson-baryon coupling that is of order $O(N_c^{-1/2})$, and thus even when the phase space is of order $O(N_c^0)$, they still have narrow widths. If the coupling is truly of order $O(N_c^{-1/2})$ as a result of general large N_c QCD arguments, this counting would be expected to hold regardless of whether the quark mass were taken to be light or heavy enough to suppress the phase space for decay. Conversely, if one can show even in this world of heavy quarks that the coupling to potential decay channels (which are now phase space suppressed) is generally of order $O(N_c^0)$ and not $O(N_c^{-1/2})$ for *all* low-lying states in the spectrum, then it is clear that large N_c QCD arguments alone do not predict a class of narrow states.

The analysis of Pirjol and Yan is composed of two parts: (i) A set of con-

sistency conditions for couplings of excited baryons to mesons (analogous to the consistency conditions for ground-state baryons) is derived. Functional forms of relations that solve these conditions are proposed and then verified by substitution into the condition equations. (ii) A simple nonrelativistic quark-shell model is used to motivate the functional forms proposed for the model-independent analysis. As a result of this quark model analysis, it is seen that the strength of the coupling between an excited baryon and a meson plus a ground-state baryon depends on the symmetry type of the excited baryon.

2.2.1 (i) Model-independent Part

In the model-independent part of Pirjol and Yan's analysis, the aforementioned consistency conditions were determined by imposing Witten's counting rules [17] (see Chapter 1) on the following scattering processes at large N_c:

$$\pi^a + B(\text{s-wave}) \;\rightarrow\; \pi^b + B'(\text{s-wave}), \tag{2.2}$$

$$\pi^a + B(\text{p-wave}) \;\rightarrow\; \pi^b + B'(\text{p-wave}), \tag{2.3}$$

$$\pi^a + B(\text{p-wave}) \;\rightarrow\; \pi^b + B'(\text{s-wave}), \tag{2.4}$$

where s-wave refers to the ground-state band of baryons modeled as having all quarks in a spatial s-wave; p-wave refers to excited levels that have quantum numbers consistent with a single quark excited into a p-wave ($\ell = 1$) orbital; a and b are isospin indices.

The analysis of process (2.2) is identical to that of Sec. 1.4. Recall that the irreducible tensor operator, X^{ia}, parameterizing the axial current matrix element

obeys the condition, $[X^{jb\dagger}, X^{ia}] = 0$ in the large N_c limit. The vanishing of this commutator is the leading-order consistency condition for ground-state baryons and is the key to the contracted SU(4) algebra [30, 29].

This procedure can be extended to the process (2.3) involving excited baryons if the current matrix element is parameterized in terms of a new operator Z^{ia}: $\langle B'|\bar{q}\gamma^i\gamma_5\tau^a q|B\rangle = N_c\langle B'|Z^{ia}|B\rangle$. As in the above case, which is described in Chapter 1, the scattering amplitude apparently diverges at large N_c in the absence of cancellations, and thus consistency requires that

$$[Z^{jb\dagger}, Z^{ia}] = 0, \tag{2.5}$$

in the large N_c limit. This condition is analogous to that for X^{ia}, meaning that solutions for Z^{ia} also fill irreducible representations of a contracted SU(4) algebra. These representations can be labeled by the magnitude of a spin vector $\vec{\Delta}$ such that $\vec{\Delta} = \vec{I} + \vec{J}$ (but only in the sense that the allowed eigenvalues of $\vec{\Delta}$ are determined by the vector addition rule of quantum mechanics; indeed, Ref. [33] uses a relative minus sign in their definition). Note that this operator (denoted by $\vec{K}$ in Ref. [39]) has a very simple interpretation in terms of chiral soliton models where $\vec{\Delta} = \vec{I} + \vec{J}$ in a true vector operator sense; the combined operator is called the "grand spin." See Sec. 3.2 of Chapter 3 for more information about grand spin in the context of meson-baryon scattering.

To extend this procedure to the process (2.4), we introduce two new operators, Y^a and $Q^{ij,a}$, in order to parameterize the current matrix elements between an s-

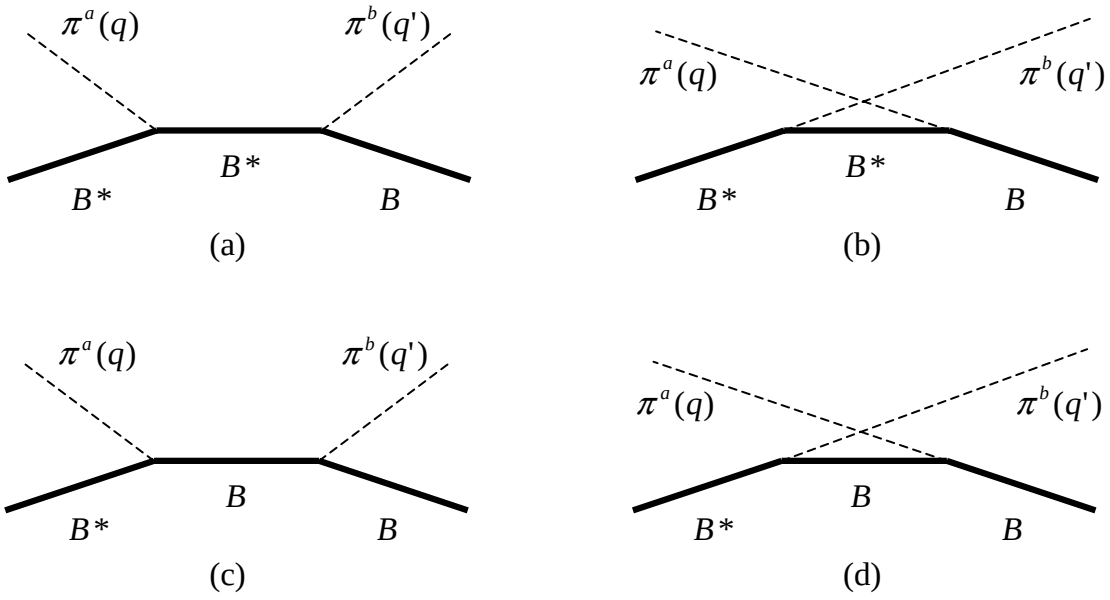

Figure 2.1: The tree level diagrams that contribute to meson-excited baryon scattering in Eq. (2.4). The B refers to a ground-state (s-wave) baryon, while the B^* refers to an excited (p-wave) baryon.

wave and p-wave baryon:

$$\langle B'|\bar{q}\gamma^0\gamma_5\tau^a q|B\rangle = N_c^{1/2}\langle B'|Y^a|B\rangle, \tag{2.6}$$

$$\langle B'|\bar{q}\gamma^i\gamma_5\tau^a q|B\rangle = N_c^{1/2}q^j\langle B'|Q^{ij,a}|B\rangle, \tag{2.7}$$

where q^μ is the momentum of the current and $|B'\rangle$ indicates the ground-state baryon. These expressions differ from those in Ref. [33] by the absorption of possible additional N_c powers and coefficients, $g(Y)$ and $g(Q)$, into the right-hand sides, which can be accommodated by the explicit rescaling of Y and Q. The scattering amplitude for (2.4) [See Fig. 2.1] still violates the Witten power-counting prediction if the matrix elements of Y and Q scale as $N_c^{-1/2}$ or larger (note that generic Witten counting rules suggest that Y and Q scale as N_c^0). In these cases, consistency

requires that

$$X^{ia}Y^{b\dagger} - Y^{b\dagger}Z^{ia} = 0, \tag{2.8}$$

$$X^{ib\dagger}Y^{a} - Y^{a}Z^{ib\dagger} = 0, \tag{2.9}$$

$$X^{ia}Q^{jk,\,b\dagger} - Q^{jk,\,b\dagger}Z^{ia} = 0, \tag{2.10}$$

$$X^{kb\dagger}Q^{ij,\,a} - Q^{ij,\,a}Z^{kb\dagger} = 0. \tag{2.11}$$

The set of consistency conditions in Eqs. (2.5) and (2.8)-(2.11) form the basis of Pirjol and Yan's model-independent analysis. Matrix elements of the operators Z, Y, and Q between baryon states $|J, J_3, I, I_3, \Delta\rangle$ can be found by solving this set. We repeat, for emphasis, that the minimum set of quantum numbers needed to construct solutions to the consistency conditions includes the baryon spin and isospin with their z-components and the Δ vector: $\{J, J_3, I, I_3, \Delta\}$. To find the solutions to Eqs. (2.8)-(2.11), we convert them into a set of algebraic equations by first reducing the matrix elements with the Wigner-Eckart theorem, then inserting a complete set of intermediate states ($\mathbf{1} = \sum |b\rangle \langle b|$), then projecting the expressions into a channel of fixed total angular momentum and isospin with the aide of Clebsch-Gordan coefficients. The Y^a matrix element, for example, is found in this manner to be

$$\begin{aligned}\langle J'{=}I', J'_3, I'_3|Y^a|J, J_3, I, I_3, \Delta\rangle &= g_Y(-1)^{1+2J} \\ &\times\sqrt{\frac{2I+1}{3(2J+1)}}\,\langle I'I'_3|I, 1; I_3, a\rangle\,\delta_{JJ'}\delta_{J_3J'_3}\delta_{\Delta 1},\end{aligned} \tag{2.12}$$

where the fact that $|B'\rangle$ is a ground-state baryon imposes the condition that $I'{=}J'$. The constant, g_Y, encodes the overall strength of the matrix element, including

any overall nontrivial N_c scaling. If the system scales according to the generic Witten rule, then $g_Y \sim O(N_c^0)$. If, for some special class of states, the coupling is characteristically smaller, then g_Y is less than order $O(N_c^0)$. Reference [33] calculates the matrix elements of Y^a in the quark-shell model and finds the same spin-flavor structure as is given by Eq. (2.12), regardless of the symmetry of the state $|B\rangle$. However, the N_c dependence of the coefficient g_Y in the quark-shell model is found to depend upon the symmetry of the excited states, with $g_Y \sim O(N_c^0)$ for spin-flavor symmetric states and $g_Y \sim O(N_c^{-1/2})$ for mixed-symmetric states. It is this scaling for the mixed-symmetric states that leads to the prediction of narrow baryon resonances. In the next section, we introduce the quark-shell model and use it to directly calculate the matrix elements of Y^a and $Q^{ij,a}$.

2.2.2 (ii) Model-dependent Part

We begin by discussing some features of quark models and, in particular, the quark-shell model. One can treat the quark model as a standard many-body problem in which each quark moves in a potential derived from the two-body or three-body interactions between quarks. However, treatments of this sort are technically difficult and the resulting wave functions are complicated, making it hard to extract useful information from them. It is possible to simplify the dynamics by considering a single-particle description in which the potential is created by all the other quarks. This approach is analogous to the shell model of nuclear physics that describes protons and neutrons in the nucleus. In the simple quark-shell model of Ref. [33], each excited baryon is treated as a single orbitally excited quark with

angular momentum ℓ acting on top of a spin-flavor symmetric core of $N_c - 1$ quarks. For the case of $N_c = 3$, the simplest version of the quark-shell model describes the ground-state baryons as three quarks in s-wave orbitals, filling a **20**-plet spin-flavor representation. The lowest-lying excited baryons have one quark in a p-wave orbital, also filling a **20**-plet spin-flavor representation [78, 39]. This version of the quark-shell model has been successful in describing the excited baryon spectrum and it is the most popular quark-based treatment of excited baryons in large N_c QCD [56, 40, 41, 42, 43, 44, 45, 46].

We can develop more sophisticated quark-shell models that incorporate configuration mixing in which the physical states are admixtures of different single-particle descriptions. These have the benefit of including particle correlations. However, for now, we will neglect configuration mixing in the quark-shell model.

The quark model wave function describing the N_c quarks is composed of three parts: (color) $\times$ (spatial) $\times$ (spin $-$ flavor). It is worth noting that in the present context "spin-flavor" refers to the spin and flavor of the quarks and not of the baryon. The Pauli principle requires that the complete wave function describing the baryon is antisymmetric under the exchange of any two (fermionic) quarks. Color confinement requires that the quark color labels form a fully antisymmetric singlet wave function, and thus the space and spin-flavor wave functions together must be symmetric. Only symmetric or mixed-symmetric spatial wave functions can be constructed when a single quark is excited. Therefore, the spin-flavor wave functions of the quark-shell model states are either symmetric (S) or mixed-symmetric (MS) under quark exchange.

We focus on the nonstrange states of SU(4), in which the distinction between the S and the MS representations is clean: Spin and isospin are related by $S=I$ for the S case and $|S-I| \leq 1$ for the MS case. This distinction may be neatly encoded by introducing the concept of P spin [33]: set $P=0$ for the S case and $P=1$ for the MS case. Thus, treating $\vec{P}$ as though it were a true angular momentum, one sees that the single triangle rule $\delta(SIP)$ characterizes both permutational symmetries (See Appendix B for a discussion of triangle rules).

The matrix elements of Z, Y, and Q in the quark model are obtained by defining the currents and constructing the baryon states in quark model language. Up to overall multiplicative constants of order unity, the currents in the quark model are [33]:

$$N_c\, Z^{ia} = \sigma^i \otimes \tau^a, \tag{2.13}$$

$$N_c^{1/2}\, Y^a = \frac{1}{\sqrt{3}} \sum_{j=-1}^{+1} (-)^{1-j} \sigma^j r^{-j} \otimes \tau^a, \tag{2.14}$$

$$N_c^{1/2}\, Q^{ka} = \sum_{i,j=-1}^{+1} \langle 2, k | 1, 1; j, i \rangle\, \sigma^j r^i \otimes \tau^a. \tag{2.15}$$

The σ, τ, and r operators act on the quark's spin, isospin, and orbital degrees of freedom, respectively. The spin-2, isospin-1 operator, Q^{ka} satisfies the same consistency conditions as $Q^{ij,a} = \sigma^j r^i \otimes \tau^a$ in Eqs. (2.10) and (2.11) of Sec. 2.2.1.

Reference [33] constructs quark model states of conserved or fixed (quark) spin (S, m_S), isospin (I, I_3), and orbital angular momentum (ℓ, m_ℓ) in such a manner that each is either symmetric or mixed-symmetric under spin-flavor exchanges. As an example, we will outline the construction of the mixed-symmetric states in the quark-shell model. We begin by writing the state obtained by adding the j^{th} quark

to a symmetric state of $N_c - 1$ quarks with spin and isospin i:

$$|SI; m_S I_3\rangle_j = \sum_{\substack{m_1 m_2 \\ \alpha_1 \alpha_2}} \langle S, m_S \mid i, \frac{1}{2}; m_1, m_2\rangle \, \langle I, I_3 \mid i, \frac{1}{2}; \alpha_1, \alpha_2\rangle \mid i, m_1, \alpha_1\rangle \otimes |\frac{1}{2}, m_2, \alpha_2\rangle_j \, . \tag{2.16}$$

We impose the mixed symmetry on the spin-flavor wave function by forming an expression that is antisymmetric under a permutation of the first quark with any one of the remaining $N_c - 1$ quarks in the baryon. This wave function is denoted by

$$|SI; m_S I_3\rangle_{[j,1]} = \frac{1}{\sqrt{2}} \left(|SI; m_S I_3\rangle_j - |SI; m_S I_3\rangle_1 \right) , \tag{2.17}$$

for $2 \leq j \leq N_c$. In order to form a completely symmetric baryon wave function as required by the Pauli principle (after accounting for the antisymmetric color labels), the spatial wave function must also be mixed symmetric under quark exchange. The spatial wave function has a form similar to Eq. (2.17) and is denoted by $|\ell; m_\ell\rangle_{[j,1]}$. After combining the spin-flavor and spatial parts into a completely symmetric wave function with well-defined spin and isospin, we arrive at our final result,

$$|SI\ell; m_S I_3 m_\ell\rangle = \frac{1}{\sqrt{N_c - 1}} \sum_{j=2}^{N_c} |SI; m_S I_3\rangle_{[j,1]} \otimes |\ell; m_\ell\rangle_{[j,1]} \, . \tag{2.18}$$

See Ref. [33] for a derivation of the normalization factor and the phase factor [suppressed in Eq. (2.18)].

It is not clear at the outset how to interpreted these states. Either these states may be taken to be eigenstates of some unspecified Hamiltonian $\mathcal{H}$ that is assumed to model QCD, or they may be taken as merely a convenient basis that allows one to enumerate the possible physical states. If they are eigenstates of $\mathcal{H}$, then the quantum numbers specifying the states must be associated with operators that

commute with $\mathcal{H}$ in order to be conserved. If this is the case, then the eigenstates of $\mathcal{H}$ include the narrow excited states predicted in Ref. [33] and incorporate a new large N_c QCD symmetry that stabilizes these states against decay. This apparent symmetry arises because $\mathcal{H}$ commutes separately with the (quark) spin and with the total angular momentum.

Note that if the states $|P, SI\ell; m_S I_3 m_\ell\rangle$ are merely used to form a basis set, superpositions of which form possible physical states, then one is faced with the issue of determining the extent of mixing between the basis states. If each physical state is predominantly a single basis state (with admixtures of other states characteristically suppressed in the large N_c limit), the system then acts much as it would above for the case where the states are treated as eigenstates of a QCD-like Hamiltonian: The physical eigenstates that are predominantly MS in spin-flavor are then narrow. However, if the mixing is of order $O(N_c^0)$, then the concept of a physical state that is predominantly mixed-symmetric is ill-defined, and all states allowed by phase space have widths of order $O(N_c^0)$.

It should also be observed that the quantum numbers $\{P, S, m_S, I, I_3, \ell, m_\ell\}$ denoting the quark-shell model states are different from those used in the (model-independent) consistency condition method of Sec. 2.2.1, $\{J, J_3, I, I_3, \Delta\}$. In particular, it should be noted that the there is no analog for the P quantum number (which specifies the nature of the spin-flavor symmetry of the quark model state) in the model-independent analysis. This raises the obvious question of whether or not the concept of the P spin has a well-defined meaning in large N_c QCD outside the context of the simple quark model.

The matrix elements of the currents in Eqs. (2.13)-(2.15) can be calculated with the quark model states described above [*e.g.*, Eq. (2.18)]. A **lengthy** calculation in Ref. [33] revealed the N_c scaling and detailed spin-flavor structure of the matrix elements of Y (and Q) between excited and ground-state baryons. It was found that

$$\underbrace{\langle P'=0,\ell'=0}_{S}|Y,Q|\underbrace{P=0,\ell\neq 0\rangle}_{S}\sim O(N_c^0), \tag{2.19}$$

while

$$\underbrace{\langle P'=0,\ell'=0}_{S}|Y,Q|\underbrace{P=1,\ell\neq 0\rangle}_{MS}\sim O(N_c^{-1/2}), \tag{2.20}$$

where the states are labeled by their P spin and excited quark orbital angular momentum, ℓ. Since the spin-flavor structure of the matrix elements is not relevant to our discussions, it was suppressed in the above equations. We note that the structure is identical to that of the solutions to the consistency condition equations in Sec. 2.2.1 [*e.g.*, see Eq. (2.12)]. This lends some support to the idea that the quark-shell model is an adequate calculation tool for excited baryons and that its predictions may be taken as general results of large N_c QCD. We shall see in the next section that this idea is not necessarily valid.

The excited baryon decay widths are determined by squaring the matrix elements of the physical states, dividing by the pion decay constant, f_π^2, and including the appropriate phase space factor [see Eq. (2.1)]. Recalling from Chapter 1 that $f_\pi^2\sim O(N_c^1)$ and the phase space is of order $O(N_c^0)$, it is straightforward to determine the scaling of the decay widths. If one assumes that the quark model assignments of states correspond to physical states (with only small admixtures of states with different quark model spin-flavor symmetries), then the decay width of a mixed-

symmetric baryon ($P=1$) is of order $O(N_c^{-1})$, while the decay width of a symmetric baryon ($P=0$) is of order $O(N_c^0)$. In the large N_c limit, the former vanishes. This result is important since it implies that *mixed-symmetric excited baryon states are narrow*. This would neatly explain the phenomenological fact that certain baryons are narrow enough to discern from the spectrum and would render the consistency argument of Ref. [33] valid for these states. However, these desirable results hinge on the physical baryon states corresponding to the quark model states in terms of their quantum numbers. In the following section, we face the question of whether this correspondence is realized in large N_c QCD.

2.3 Spin-flavor Symmetry Breaking and Baryon Decay Widths

In this section we focus on the issue of whether the physical baryon states truly correspond to the simple quark model states of Ref. [33], which, in effect, is the question of whether narrow excited baryons appear in large N_c QCD. If this is a generic large N_c QCD result, one would expect it to be seen in all models that correctly encode large N_c physics. Thus, to disprove it, we need only find some model that encodes the correct large N_c scaling rules for which it is untrue. We will consider a fairly general quark-shell model Hamiltonian that shares some essential properties with the QCD Hamiltonian. In particular, we consider the most general quark model for which the number of quarks in a given orbital is well defined. In practice, this restriction means one excludes operators that remove quarks from one orbital and place them in different orbitals. We impose this restriction to keep the

model tractable. Note, however, that even with this restriction, this Hamiltonian is considerably more general then the Hamiltonian implicitly used to construct the quark model states in the previous section.

Large N_c scaling rules *greatly* restrict the number of possible operators that contribute at order $O(N_c^0)$ or larger (and hence that can contribute in the large N_c limit [40, 41]). For example, as shown in Ref. [40, 41], the *only* operators that contribute at order $O(N_c^0)$ for states with a single excited quark are given by:

$$\mathcal{H} = c_1 \mathbf{1} + c_2\, \ell\cdot s + c_3\, \ell^{(2)} g\, G_c/N_c, \tag{2.21}$$

where ℓ, s, $\ell^{(2)}$, and g are the orbital, spin, $\Delta\ell = 2$ tensor, and combined spin-flavor (Gamow-Teller) operators, respectively, acting only on the excited quark, while G_c is the combined spin-flavor operator acting only on the core of unexcited quarks. The combined spin-flavor operator is a generator of SU(4), and has the following form in the quark model language:

$$G^{ia} \equiv \sum_{\alpha=1}^{N_c} q_\alpha^\dagger \left(\frac{\sigma^i}{2} \otimes \frac{\tau^a}{2}\right) q_\alpha \ , \tag{2.22}$$

where σ and τ are Pauli matrices in spin and isospin spaces, respectively. The rank-2 tensor $\ell^{(2)}$ takes the form

$$\ell_{ij}^{(2)} = \frac{1}{2}\{\, l_i, l_j \,\} - \frac{\ell^2}{3}\delta_{ij}. \tag{2.23}$$

Thus the operator $\ell^{(2)} g\, G_c/N_c$ in $\mathcal{H}$, shown with explicit indices, is $\ell_{ij}^{(2)} g_{ia}\, G_c^{ja}/N_c$. The factor of $1/N_c$ accounts for the two quark-quark-gluon couplings (each costing a factor of $1/\sqrt{N_c}$) needed to generate this operator.

The coefficients in $\mathcal{H}$ have the following scaling rules:

$$c_1 \sim N_c^1, \quad c_2 \sim N_c^0, \quad c_3 \sim N_c^0 \ . \tag{2.24}$$

The scaling of c_1 is a bit subtle. Most of the contribution to c_1 comes from the unexcited quarks in the core. Thus $c_1 = m_N + \delta c_1$ with the ground-state baryon mass, $m_N \sim O(N_c^1)$ and $\delta c_1 \sim O(N_c^0)$. In general, each coefficient contains corrections at all subleading powers of $1/N_c$.

Consider, as an example, the $\ell \cdot s$ operator. If this operator induces significant mixing [*i.e.*, of order $O(N_c^0)$] between the S and MS states of the basis described in Sec. 2.2.2, then this model—which correctly encodes the large N_c scaling rules—does not automatically give excited baryons that are weakly coupled in the large N_c limit. To begin, note that the $\ell \cdot s$ operator does not commute with the spin operator $\mathbf{S}$; that is, m_S is not generally a good quantum number for the Hamiltonian eigenstates. Thus, the operator does induce mixing between the states enumerated above. The central question becomes the scale of this mixing. If the mixing is small (or zero) in the large N_c limit, then a state with a fixed spin-flavor symmetry (either S or MS) is a well-defined object with symmetry-dependent properties.

Suppose one considers only states for which the excited quark is in an orbital with $\ell \neq 0$ (The case of $\ell = 0$ is special and is discussed below). This implies that the $\ell \cdot s$ operator mixes states of differing spin-flavor symmetry. Consider a state labeled by total angular momentum (J,J_3), total isospin (I, I_3), total (quark) spin (S), and P-spin: $|JJ_3; II_3(\ell, S = I + \rho)[P]\rangle$. The ρ (introduced in Refs. [40, 41]) plays a role similar to the P-spin of Sec. 2.2.2. It is a *number* that equals either ± 1 or 0 for the mixed-symmetric case ($P = 1$), or 0 for the symmetric case ($P = 0$). The states so labeled are identical to the ones enumerated in Sec. 2.2.1. The matrix element of $\ell \cdot s$ that connects two states in this basis of equal JJ_3, II_3, and ℓ but

different P-spin (*i.e.*, spin-flavor symmetry) is written as

$$\langle \ell \cdot s \rangle_{\rho'} \equiv \langle J J_3; I I_3(\ell, S'=I+\rho')[1] \, |\ell \cdot s| \, J J_3; I I_3(\ell, S=I)[0] \rangle. \tag{2.25}$$

This matrix element is computed for general ρ and ρ' in Ref. [40], but we present a more concise expression than their Eq. (A7):

$$\langle \ell \cdot s \rangle = (-1)^{J-I+\ell} \sqrt{\frac{3}{2}} \sqrt{\ell(\ell+1)(2\ell+1)(2S+1)(2S'+1)}$$
$$\times \left\{ \begin{array}{ccc} \ell & \ell & 1 \\ S & S' & J \end{array} \right\} \sum_{\eta=\pm 1} c_{\rho\eta} c_{\rho'\eta} (-1)^{(1-\eta)/2} \left\{ \begin{array}{ccc} 1 & \frac{1}{2} & \frac{1}{2} \\ I+\frac{\eta}{2} & S' & S \end{array} \right\}. \tag{2.26}$$

(See Appendix B for an introduction to the Wigner $6j$ symbol.) From here, we set $\rho = 0$ (meaning that $S = I$ for the S state in the ket) and calculate this matrix element for each value of ρ' in the mixed-symmetric bra. For $\rho' = 0$, we have:

$$\langle \ell \cdot s \rangle_0 = (-1)^{J-I+\ell+1} \sqrt{\frac{3}{2}} \sqrt{\ell(\ell+1)(2\ell+1)} (2S+1) c_{0-}^{\mathtt{MS}} c_{0+}^{\mathtt{MS}} \left\{ \begin{array}{ccc} \ell & \ell & 1 \\ S & S & J \end{array} \right\}$$
$$\times \left[\left\{ \begin{array}{ccc} 1 & \frac{1}{2} & \frac{1}{2} \\ I+\frac{1}{2} & S & S \end{array} \right\} + \left\{ \begin{array}{ccc} 1 & \frac{1}{2} & \frac{1}{2} \\ I-\frac{1}{2} & S & S \end{array} \right\} \right]. \tag{2.27}$$

The coefficients $c_{0-}^{\mathtt{MS}}$ and $c_{0+}^{\mathtt{MS}}$ are given by

$$\begin{aligned} c_{0-}^{\mathtt{MS}} &= -\sqrt{\frac{(S+1)(N_c-2S)}{N_c(2S+1)}}, \\ c_{0+}^{\mathtt{MS}} &= +\sqrt{\frac{S[N_c+2(S+1)]}{N_c(2S+1)}}, \end{aligned} \tag{2.28}$$

and are both of order unity in the large N_c limit. For $\rho' = \pm 1$, we have:

$$\langle \ell \cdot s \rangle_{\pm 1} = (-1)^{J-I+\ell+1} \sqrt{\frac{3}{2}} \sqrt{\ell(\ell+1)(2\ell+1)(2S+1)(2S+1\pm 2)}$$
$$\times c_{0\mp}^{\mathtt{MS}} \left\{ \begin{array}{ccc} \ell & \ell & 1 \\ S & S\pm 1 & J \end{array} \right\} \left\{ \begin{array}{ccc} 1 & \frac{1}{2} & \frac{1}{2} \\ I\pm\frac{1}{2} & S\pm 1 & S \end{array} \right\}. \tag{2.29}$$

In general, evaluation of these formulas for appropriate (physical) values of S, I, J, and ℓ yields nonzero matrix elements. The non-vanishing of MS $\to$ MS matrix elements is confirmed in Refs. [40, 41]. Moreover, in all of these cases the matrix element of $\langle \ell \cdot s \rangle$ is of order $O(N_c^0)$. Combining this with the scaling of Eq. (2.24) for the strength of the operator, implies that the $\ell \cdot s$ term in the Hamiltonian connects states of different spin-flavor symmetry with strength of order $O(N_c^0)$. Due to this mixing, an energy eigenstate of the quark-shell model cannot be described as having a well-defined spin-flavor symmetry. Thus, for this class of models there is no special set of weakly-coupled excited baryons at large N_c (at least for $\ell \neq 0$). Since these models encode generic large N_c scaling rules, one concludes that these rules alone do not imply that a set of weakly coupled states exists. Returning now to a world where the quarks are light enough so that the amount of phase space [which is of order $O(N_c^0)$] permits decays, one concludes that there is no generic argument for why such states should be narrow.

Note that an analogous argument could be made using the $\ell^{(2)} g G_c / N_c$ term in the Hamiltonian, which also leads to mixing of order $O(N_c^0)$. One might wonder whether there is some way to evade this conclusion by hoping for a type of cancellation between the $\ell^{(2)} g G_c / N_c$ and $\ell \cdot s$ terms. However, in general, the two terms are independent; their ratio is not fixed by large N_c QCD arguments. Moreover, although the operators commute at leading order in $1/N_c$, they are distinct—their matrix elements are not proportional to each other, even at leading order in $1/N_c$ [39, 40, 41, 57]. Hence, the only way for them to cancel in general is if they are both zero.

The conclusion that S and MS configurations are mixed in models of this type is valid for all cases except where the excited quark is in an $\ell=0$ orbital. However, it is clear that all of the matrix elements of $\ell \cdot s$ (where $\Delta\ell = 1$) and $\ell^{(2)} g G_c/N_c$ (where $\Delta\ell = 2$) between states with $\ell = 0$ are zero. Thus, the argument presented above does not exclude the possibility of weakly coupled, and thus narrow, $\ell = 0$ MS excited states. We note, however, that the quark model considered in this thesis, though more general than that implicitly used to construct the basis states, is by no means the most general one that one can consider. In particular, one can consider models with configuration mixing—that is, in which the physical states are admixtures of different single-particle descriptions (See Ref. [76]). Such mixing operators can induce admixtures between the S and MS states at order $O(N_c^0)$. It is easy to see how this can come about. An allowable operator can mix a state with a quark in an excited $\ell=0$ orbital and a state with a quark in an $\ell=1$ orbital that has total angular momentum (spin plus orbital) equal to $\frac{1}{2}$. Such mixing violates no symmetries of the system and is allowable at $O(N_c^0)$. Once such a state admixes with the $\ell=1$ orbitals, the previously considered operators induce mixing between the S and MS spin-flavor components.

The case of $\ell=1$ presents its own subtlety, the well-known problem in many-body physics of spurious modes associated with broken symmetries [76]. However, the existence of spurious modes does not alter the conclusions drawn above for the $\ell=1$ case. Since the discussion of spurious modes is outside the scope of this chapter, we defer it to Appendix A.

2.4 Conclusion

In this chapter, we have explored the issue of whether excited baryons with mixed-symmetric spin-flavor wave functions have decay widths that vanish in the large N_c limit. If previous claims that a set of states is automatically narrow in the large N_c limit were in fact generic, they would be both theoretically and phenomenologically significant. On the other hand, the assertion that such states are narrow is based only on calculations with a very simple quark model. We showed that the narrowness of these states claimed by Pirjol and Yan is an artifact of the simple quark model used in the calculations and is not, in fact, a generic feature of large N_c QCD. This was shown in the context of a slightly more general class of quark models that encode generic large N_c scaling rules by a demonstration that excited baryons cannot be assigned a well-defined, fixed spin-flavor symmetry; the symmetry configurations are admixed at order $O(N_c^0)$. This implies that the relative narrowness of baryon states observed in nature cannot be simply attributed to large N_c QCD scaling behavior. It also implies that the general model-independent analysis of Ref. [33] is not strictly correct because, without narrow states to serve as scattering targets, the large N_c QCD consistency condition analysis is not applicable. Fortunately, many of the conclusions of this analysis remain correct despite this deficiency, such as the predicted pattern of degeneracies [39] discussed in Sec. 2.1.

Chapter 3

Model-independent Linear Scattering Relations:

Pion-nucleon scattering

3.1 Pions as Hadronic Probes

Scattering particles off of each other is a time-honored method for investigating the properties and interactions of matter and for discovering new physical phenomena. The de Broglie wavelength of the injected particle changes with energy, allowing an experimenter to probe different attributes of a particle's properties and degrees of freedom. For example, as the energy of an electron beam incident on an atomic target increases, we are able to obtain information first about the electronic structure of the atom, then the atomic nucleus, its proton and neutron content, and finally the quarks. Our discussion in this chapter will concentrate on low-energy hadronic scattering in which quarks and gluons are not the relevant degrees of freedom, but rather nucleons, deltas, and pions.

Pions have been an important probe of hadronic properties for a long time and for many reasons. Foremost is their intimate role in the nucleon-nucleon interaction. According to the Yukawa model [58], pion exchange between protons and neutrons is the dominant source of the strong force that binds the atomic nucleus together. Another reason is their connection to the approximate chiral symmetry of QCD as

discussed in Chapter 1. Due to their pseudo-Goldstone boson nature, pions are very light compared to other hadrons and therefore stable against strong decays. The charged pions eventually decay via the weak interaction, while the chiral anomaly significantly reduces the lifetime of the neutral pion. Regardless of these decay channels, the lifetimes are long enough so that pions can be used to form particle beams and are easily detected. For these reasons, a great deal of experimental data for pion-baryon scattering and pion photoproduction has been compiled and analyzed over the last several decades.

In this chapter and the next, we will discuss pion-baryon scattering and pion photoproduction, respectively within the framework of large N_c QCD. In particular, we will show that amplitudes for these processes are not independent and can be linearly related. This follows from an expansion of the S matrix describing these processes that we derive in the next section.

3.2 Derivation of the S Matrix Expansion

In this section, we consider a pion scattering off of a nucleon at rest producing a pion and a baryon in the final state. We focus our attention on the case where nucleons and deltas are the final state baryons. We wish to compute the S matrix for this process using the techniques of large N_c QCD and the contracted SU(4) spin-flavor symmetry developed in Chapter 1. We begin by enumerating the relevant (conserved or fixed) quantum numbers of the system: The isospin of the pion ($I_\pi = 1, I_{\pi 3}$) and its initial and final orbital angular momentum about the baryon ($L, L_3; L', L'_3$), the

spin=isospin of the initial and final baryon ($R = \frac{1}{2}, R_3; R', R'_3$), the conserved total isospin (I_s, I_{s3}), and the conserved total angular momentum (J_s, J_{s3}). We employ the Wigner-Eckart theorem to eliminate any dependence on the quantum number projections and thus seek an expression for the reduced S matrix: $S_{LL'RR'I_sJ_s}(E)$, where E is the scattering energy.

Our calculation begins by considering the operators that contribute to the S matrix. Large N_c QCD becomes most useful when we consider the operator that connects the pions and baryons in the t-channel exchange picture (See Fig. 3.1). This operator does not carry baryon number, has isospin I_t and spin J_t and therefore obeys the large N_c QCD result of Eq. (1.6) that takes the form $\langle B'|\hat{O}^{(n)}_{I_t,J_t}/N_c^n|B\rangle \sim 1/N_c^{|I_t-J_t|}$. Thus, to leading order in the $1/N_c$ expansion, the dominant matrix elements and scattering amplitudes in the t-channel have $I_t = J_t \equiv \mathcal{J}$. This is the famous "$I_t = J_t$ rule" originally derived for meson-baryon scattering in the Skyrme model [59]. Although we are discussing the process from the t-channel point of view, this view can only be justified with large N_c QCD in the kinematic regime appropriate to the s-channel process, in which a meson of energy $O(N_c^0)$ scatters quasi-elastically from a massive, nonrelativistic baryon. Indeed, the t-channel process, requiring meson energies of order $O(N_c^1)$, is exponentially suppressed in large N_c QCD as mentioned in Sec. 1.3.

According to the $I_t = J_t$ rule, the leading order t-channel scattering amplitude is characterized by a smaller set of quantum numbers: $\tilde{s}^t_{\mathcal{J}LL'RR'}(E)$. Also, the dependence of this amplitude on the intrinsic baryon quantum numbers, $\{RR'\}$, can be factored out with the normalization of the baryon wavefunctions. Using the normaliza-

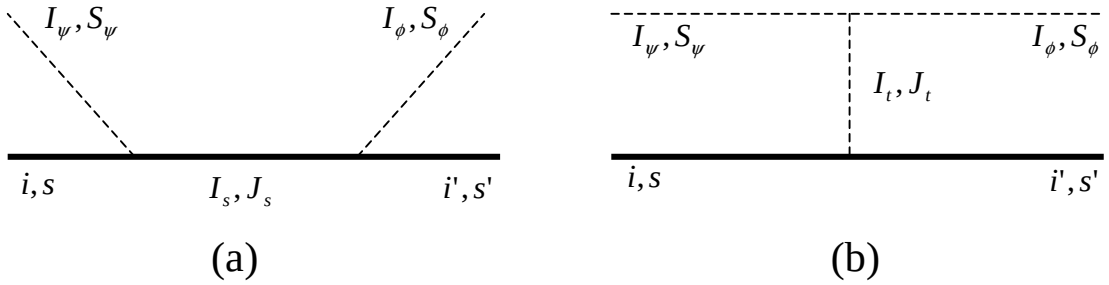

Figure 3.1: (a) The s-channel versus (b) t-channel meson-baryon scattering diagrams. The solid lines are baryons with isospin i, i' and spin s, s'. The dashed lines are mesons with isospin I_ψ, I_ϕ and spin S_ψ, S_ϕ. Appendix B presents the relationship between the quantum numbers in the two channels.

tion derived from either the contracted SU(4) group or the Skyrme model [24], the result of this factorization is $\tilde{s}^t_{\mathcal{J}LL'RR'}(E) = (-1)^{-2(R+R')}\sqrt{(2R+1)(2R'+1)}\hat{s}^t_{\mathcal{J}LL'}(E)$. To obtain $S_{LL'RR'I_sJ_s}(E)$, we must cross $\tilde{s}^t_{\mathcal{J}LL'RR'}(E)$ into the s-channel using standard angular momentum coupling algebra techniques involving Wigner $6j$ symbols outlined in Appendix B [59, 60]. Also see Ref. [61] for more details. The result of this crossing is

$$S_{LL'RR'I_sJ_s}(E) = \sum_{\mathcal{J}} \begin{bmatrix} I_\pi & R' & I_s \\ R & I_\pi & \mathcal{J} \end{bmatrix} \begin{bmatrix} L' & R' & J_s \\ R & L & \mathcal{J} \end{bmatrix} s^t_{\mathcal{J}LL'}(E) + O(N_c^{-1}) \quad (3.1)$$

where $s^t_{\mathcal{J}LL'}(E)$ is called the *reduced amplitude*. It is proportional to $\hat{s}^t_{\mathcal{J}LL'}(E)$ with the other quantum number-dependent factors absorbed inside. Note that an error of $O(N_c^{-1})$ is included since our derivation produces only the leading order result. The square brackets (called $[6j]$ symbols) are real numbers related to Wigner's $6j$

symbols by

$$\left\{ \begin{array}{ccc} a & b & e \\ c & d & f \end{array} \right\} \equiv \frac{(-1)^{-(b+d+e+f)}}{([a][b][c][d])^{1/4}} \left[\begin{array}{ccc} a & b & e \\ c & d & f \end{array} \right], \tag{3.2}$$

where $[X] \equiv 2X + 1$. This notation serves to make the formulas more compact and transparent since it displays only the relevant factors. The $[6j]$ symbol still retains many important properties of the Wigner $6j$ symbol (See Appendix B). Among these properties are four triangle rules:

$$\left\{ \begin{array}{ccc} j_1 & j_2 & j_{12} \\ j_3 & J & j_{23} \end{array} \right\} \propto \delta(j_1 j_2 j_{12}) \delta(j_2 j_3 j_{23}) \delta(j_1 j_{23} J) \delta(j_{12} j_3 J), \tag{3.3}$$

which dictate which values of $\mathcal{J}$ contribute to the sum in Eq. (3.1). It is worth noting that Eq. (3.1) can be generalized to mesons with arbitrary spin and isospin [62]. For example, the η has isospin zero and the ω has spin one. The case for isospin zero will be important in Sec. 4.1 and is trivial to derive from Eq. (3.1); simply insert $I_\pi \to 0$ in the $[6j]$ symbol.

Equation (3.1) is an important result and deserves some comments. The expansion of the physically measurable S matrix in terms of reduced amplitudes was first made in the context of the Skyrme model [24, 25]. In this case, the reduced amplitudes are amplitudes for pions scattering off of solitons in which the quantum number $K \equiv I + J$ is conserved. The solitons are then projected into well-defined baryon states as discussed in Sec. 1.3, producing the $[6j]$ symbols and a sum over K numbers (equivalent to our sum over $\mathcal{J}$). It is possible to evaluate the reduced amplitudes directly from the Skyrme model (or any other chiral soliton model), which yields $S_{LL'RR'I_sJ_s}(E)$ using Eq. (3.1). The detailed behavior of these amplitudes

can then be used to predict values for baryon resonance observables such as phase shifts and absorption parameters [25, 24, 63, 64]. A slightly different derivation of Eq. (3.1) clearly demonstrates that it is a model-independent result to leading order in $1/N_c$ (Ref. [39]).

Our attempt to find the detailed behavior of $S_{LL'RR'I_sJ_s}(E)$ has resulted in the expansion in terms of other unknown functions ($s^t_{\mathcal{J}LL'}(E)$) shown in Eq. (3.1). We know of no simple way to use a model-independent analysis of large N_c QCD to evaluate the reduced amplitudes to obtain $S_{LL'RR'I_sJ_s}(E)$. However, Eq. (3.1) is still useful for understanding some aspects of hadronic physics. The key point is that the set of quantum numbers needed to describe the S matrix, $\{LL'RR'I_sJ_s\}$ is smaller than the set specifying the reduced amplitudes, $\{\mathcal{J}LL'\}$. This implies that there are fewer reduced amplitudes than S matrix elements and they are shared among several different S matrices. This has many important consequences in hadronic phenomenology. One is that degeneracies exist in the excited baryon spectrum to leading order in $1/N_c$ [39] that can be labeled by the quantum number K. In the study of baryon resonances, resonances in a given channel correspond to a pole in the S matrix, which must appear in one of its associated reduced amplitudes. This pole is then shared among S matrix elements for different scattering channels through the reduced amplitude, creating the degeneracies. Certain decay properties of the N(1535) and N(1650) baryons can also be explained in this analysis [39]. In particular, it is predicted and confirmed that N(1535) couples *strongly* to the ηN channel and *weakly* to the πN channel, while the coupling preference is reversed for N(1650).

A second consequence is that the set of S matrix elements for a given initial angular momentum (L) is linearly dependent. Linear algebra can be used to eliminate the unknown reduced amplitudes, $s^t_{\mathcal{J}LL'}$ and produce model-independent linear relations among different physically measurable scattering amplitudes. Relations of this type for $\pi N \to \pi N$ and $\pi N \to \pi\Delta$ scattering were first derived by Hayashi, Eckart, Holzwarth, and Walliser [25] and Mattis and Peskin [24] in the Skyrme model. The linear relations display no explicit energy dependence and require only experimentally extracted scattering data for validation. In this respect, they provide an excellent test of large N_c QCD and are the focus of this chapter and the next. We present linear relations in the following sections and demonstrate their great ability to fit the experimental data.

So far we have only considered the leading order term in the $1/N_c$ expansion of the scattering S matrix. The contracted SU(4) group formalism provides a straightforward method to extend the result to the next order in the $1/N_c$ expansion. This follows directly from Eq. (1.6). According to that formula, if we construct the most general term that violates the "$I_t = J_t$ rule" by one unit, that is if $|I_t - J_t| = 1$, then we incur a penalty of one factor of $1/N_c$. The procedure is the following: We will add the two terms for $I_t = J_t \pm 1$ with a $1/N_c$ factor to Eq. (3.1), yielding an S matrix that includes all next-to-leading order effects. The result of this procedure is

$$S_{LL'RR'I_sJ_s}(E) = \sum_{\mathcal{J}} \begin{bmatrix} I_\pi & R' & I_s \\ R & I_\pi & \mathcal{J} \end{bmatrix} \begin{bmatrix} L' & R' & J_s \\ R & L & \mathcal{J} \end{bmatrix} s^t_{\mathcal{J}LL'}(E)$$

$$-\frac{1}{N_c}\sum_x \begin{bmatrix} I_\pi & R' & I_s \\ R & I_\pi & x \end{bmatrix} \begin{bmatrix} L' & R' & J_s \\ R & L & x+1 \end{bmatrix} s^{t(+)}_{xLL'}(E)$$

$$-\frac{1}{N_c}\sum_y \begin{bmatrix} I_\pi & R' & I_s \\ R & I_\pi & y \end{bmatrix} \begin{bmatrix} L' & R' & J_s \\ R & L & y-1 \end{bmatrix} s^{t(-)}_{yLL'}(E) + O(N_c^{-2}), \qquad (3.4)$$

where the $s^{t(\pm)}_{xLL'}(E)$ functions are the reduced t-channel amplitudes corresponding to $s^t_{\mathcal{J}LL'}(E)$ for the two possible ways of combining I_t and J_t such that $|I_t - J_t| = 1$. Note that an error of $O(N_c^{-2})$ is included since our $1/N_c$ expansion includes only the leading order and next-to-leading order terms. This expansion is one of the main achievements of this thesis. It is possible to continue in this manner with the remaining terms in the $1/N_c$ expansion, but this has limited utility for πN scattering as discussed in Sec. 3.4.

If linear dependence remains in the system of equations for a πN scattering process, then we can construct linear relations that hold to next-to-leading order (NLO) in $1/N_c$; these have small errors of order $O(N_c^{-2})$. In so far as the $1/N_c$ expansion is useful, these NLO relations should be more robust against experimental scrutiny than their leading order counterparts. Indeed, for the cases of πN scattering and pion photoproduction, we find this to be true qualitatively.

3.3 Pion-nucleon Scattering Relations

We begin our discussion of pion-nucleon scattering relations by deriving the leading order (LO) formulas of Refs. [24, 25]. To this end, we need only the leading order terms of Eq. (3.4) (*i.e.*, the formula in Eq. (3.1)). We will derive the next-to-leading

order expressions in the next section.

Before deriving the LO linear relations, it is helpful to discuss restrictions on the reduced amplitudes $s^t_{\mathcal{J}LL'}(E)$ and the pion angular momentum $\{L, L'\}$ due to the symmetries of the strong interaction. Time-reversal invariance of the πN scattering process dictates that the S matrix is symmetric under the exchange of initial and final states (characterized by the quantum numbers $\{L, R\}$ and $\{L', R'\}$, respectively). We see that the symmetry properties of the $[6j]$ symbols (inherited from the $6j$ symbols) imply that the product in Eq. (3.1) is invariant under this exchange (See Appendix B). Thus, the reduced amplitudes must also be symmetric (*i.e.*, $s^t_{\mathcal{J}LL'}(E) = s^t_{\mathcal{J}L'L}(E)$) in order to maintain the symmetries of QCD. The triangle rules of the $[6j]$ symbols also encode important restrictions on the change in the pion orbital angular momentum, $\Delta L \equiv |L' - L|$. In order to get a non-zero $[6j]$ symbol for the $\pi N \to \pi N$ reaction, the allowed change is $\Delta L = 0, 1$. For $\pi N \to \pi\Delta$, the allowed change is $\Delta L = 0, 1, 2$.

We can further restrict the possible values of ΔL by considering parity. The strong interaction conserves parity, meaning the world described by a position $\vec{r}$ is the same as the one described by $-\vec{r}$. A particle is assigned a number ± 1 depending on its parity properties: A particle field with negative parity (-1) reverses sign under the application of the parity operator. Pseudo-scalar mesons like the pion have a (-1) parity. Particles with orbital angular momentum L have a parity $(-1)^L$ derived from the angular part of their wavefunction, $Y^L_m(\theta, \phi)$. The parity of a system is the product of the parity of its parts. Thus the pion-baryon system has a total conserved parity of $(-1)^{L+1}$. The $\Delta L = 1$ possibility is forbidden by

parity conservation since $P = (-1)^{L+1} = (-1)^{L'+1}$, meaning that ΔL must be an even number. To summarize, the permitted cases are $\Delta L = 0$ for $\pi N \to \pi N$ and $\Delta L = 0, 2$ for $\pi N \to \pi\Delta$.

The procedure for deriving the linear relations is straightforward. First, we write out the expansion in Eq. (3.1) for all the possible total isospin and angular momentum values for a given L (and noting that $I_\pi = 1$ and real initial target baryons are always nucleons, $R = 1/2$): $I_s = \{\frac{1}{2}, \frac{3}{2}\}$ and $J_s = L \pm \frac{1}{2}$. Next, we algebraically eliminate the reduced amplitudes, $s^t_{\mathcal{J}LL'}(E)$ to produce the linear relations. We present them now using the more compact notation, $S_{LLRR'I_sJ_s} \to S^{\pi R'}_{L,2I_s,2(J_s-L)}$, or $S_{LL'RR'I_sJ_s} \to S^{\pi R'}_{L,L',2I_s,2(J_s-L)}$ if $L \neq L'$ and with R' represented by the baryon's symbol:

$$S^{\pi N}_{L,3,-1} = \frac{L-1}{4L+2} S^{\pi N}_{L,1,-1} + \frac{3L+3}{4L+2} S^{\pi N}_{L,1,+1} + \mathcal{O}(N_c^{-1}), \tag{3.5}$$

$$S^{\pi N}_{L,3,+1} = \frac{3L}{4L+2} S^{\pi N}_{L,1,-1} + \frac{L+2}{4L+2} S^{\pi N}_{L,1,+1} + \mathcal{O}(N_c^{-1}), \tag{3.6}$$

$$S^{\pi\Delta}_{L,3,-1} = \frac{4(L-1)}{\sqrt{10}(2L+1)} S^{\pi\Delta}_{L,1,-1} + \frac{3}{2L+1}\left[\frac{(L+1)(2L+3)(2L-1)}{10L}\right]^{1/2} S^{\pi\Delta}_{L,1,+1} + \mathcal{O}(N_c^{-1}), \tag{3.7}$$

$$S^{\pi\Delta}_{L,3,+1} = \frac{3}{2L+1}\left[\frac{L(2L+3)(2L-1)}{10(L+1)}\right]^{1/2} S^{\pi\Delta}_{L,1,-1} + \frac{4(L+2)}{\sqrt{10}(2L+1)} S^{\pi\Delta}_{L,1,+1} + \mathcal{O}(N_c^{-1}), \tag{3.8}$$

and

$$\sqrt{L+1}\, S^{\pi\Delta}_{L,L+2,1,+1} = -\sqrt{L+2}\, S^{\pi\Delta}_{L+2,L,1,+3} + \mathcal{O}(N_c^{-1}), \tag{3.9}$$

$$\sqrt{L+1}\, S^{\pi\Delta}_{L,L+2,3,+1} = -\sqrt{L+2}\, S^{\pi\Delta}_{L+2,L,3,+3} + \mathcal{O}(N_c^{-1}), \tag{3.10}$$

and

$$\sqrt{10(L+1)}S^{\pi\Delta}_{L,L+2,3,+1} = +\sqrt{L+2}S^{\pi\Delta}_{L+2,L,1,+3} + \mathcal{O}(N_c^{-1}), \tag{3.11}$$

$$S^{\pi\Delta}_{L+2,L,1,+3} = -\sqrt{10}S^{\pi\Delta}_{L+2,L,3,+3} + \mathcal{O}(N_c^{-1}), \tag{3.12}$$

and

$$S^{\pi N}_{L,1,-1} - S^{\pi N}_{L,1,+1} = \sqrt{\frac{2L-1}{L+1}}S^{\pi\Delta}_{L,1,-1} + \sqrt{\frac{2L+3}{L}}S^{\pi\Delta}_{L,1,+1} + \mathcal{O}(N_c^{-1}), \tag{3.13}$$

where each S matrix element is evaluated at the same scattering energy, E. Note that the LO relations fall into three distinct classes: (1) Linear combinations involving only $\pi N \to \pi N$ amplitudes [Eqs. (3.5) & (3.6)] and (2) $\pi N \to \pi\Delta$ amplitudes [Eqs. (3.7)–(3.12)], and (3) a mixture of the two reactions [Eq. (3.13)]. Class 2 further divides into linear combinations for $L = L'$ and proportionalities for $L \neq L'$.

Values for each S matrix element ($S^{\pi R'}_{L,2I_s,2(J_s-L)}$ or $S^{\pi R'}_{L,L',2I_s,2(J_s-L)}$) over an appropriate energy range can be found in the available experimental data tables [69]. Using these extracted amplitudes in the above relations for each L, we find they generally compare well with experiment. Mattis and Peskin found that overall agreement improves with higher energy and higher L-valued partial waves [24]. As typical examples, we consider relations (3.5) and (3.6) for two different L values [See Appendix C for more a complete collection of plots]. Inserting $L = 2$ into Eq. (3.5) gives $D_{33} = \frac{1}{10}D_{13} + \frac{9}{10}D_{15}$, where the partial wave is denoted by the $L_{2I,2J}$ notation for elastic pion-nucleon scattering. Inserting $L = 3$ into Eq. (3.6) gives $F_{37} = \frac{9}{14}F_{15} + \frac{5}{14}F_{17}$. In Figures 3.2 and 3.3, we plot the real and imaginary part of the dimensionless T matrix [$T \equiv (S-1)/2i$] as a function of center-of-mass energy

W for the πN system. A more in-depth discussion of this scattering data is deferred to Sec. 3.5.

Figures 3.2 and 3.3 demonstrate that the relations are able to effectively reproduce some features of a partial wave including peaks and the background. Note in Fig. 3.3 that while the detailed structure of the peaks is correct, there is a shift between them of about 230 MeV. This hints that the shift is caused by the same $1/N_c$ effect of Sec. 1.4 that causes the ~ 290 MeV mass difference between the delta and nucleon. While the leading order analysis cannot capture this physics, an extension of the linear relations to the next order in the $1/N_c$ expansion should improve the predictions.

While most of the LO relations follow the data nicely, notable exceptions are Eqs. (3.11) and (3.12) with the $\sqrt{10}$ coefficient. This mystery was noticed by Mattis and Peskin [24] and we present the resolution in the following section.

3.4 NLO Pion-nucleon Scattering Relations

The linear relations of the previous section were derived from the leading order term in the S matrix expansion and thus had an error of order $O(N_c^{-1})$. It is possible to derive linear relations with errors of order $O(N_c^{-2})$ by using the expansion in Eq. (3.4) that includes the next-to-leading order terms. This method for improving the accuracy of linear relations is superior to attempts to fix the LO relations of Sec. 3.3 through modifications of the Skyrme model [65]. Those results only capture some of the $1/N_c$ effects.

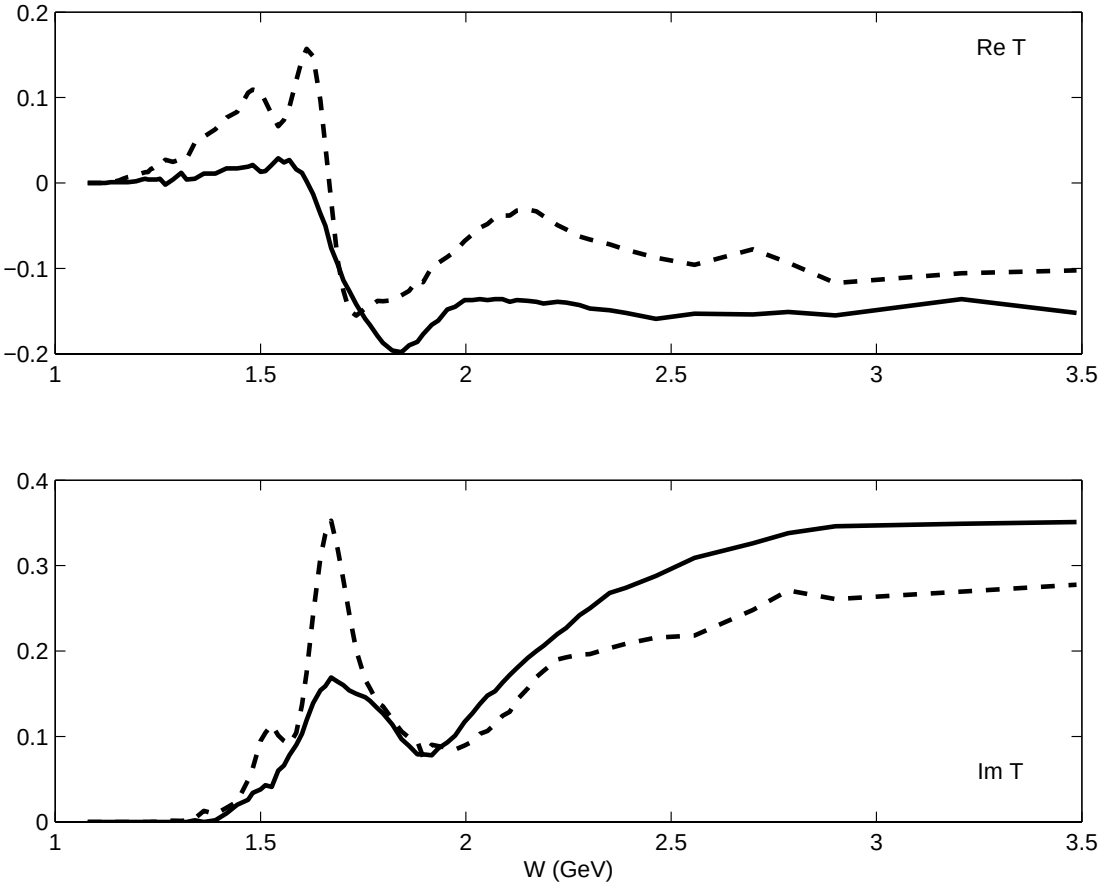

Figure 3.2: Experimentally determined D_{33} partial-wave amplitude (solid curve) for $\pi N \rightarrow \pi N$ scattering compared to the combination predicted by Eq. (3.5): $\frac{1}{10}D_{13} + \frac{9}{10}D_{15}$ (dotted curve). The data is provided by SAID [69].

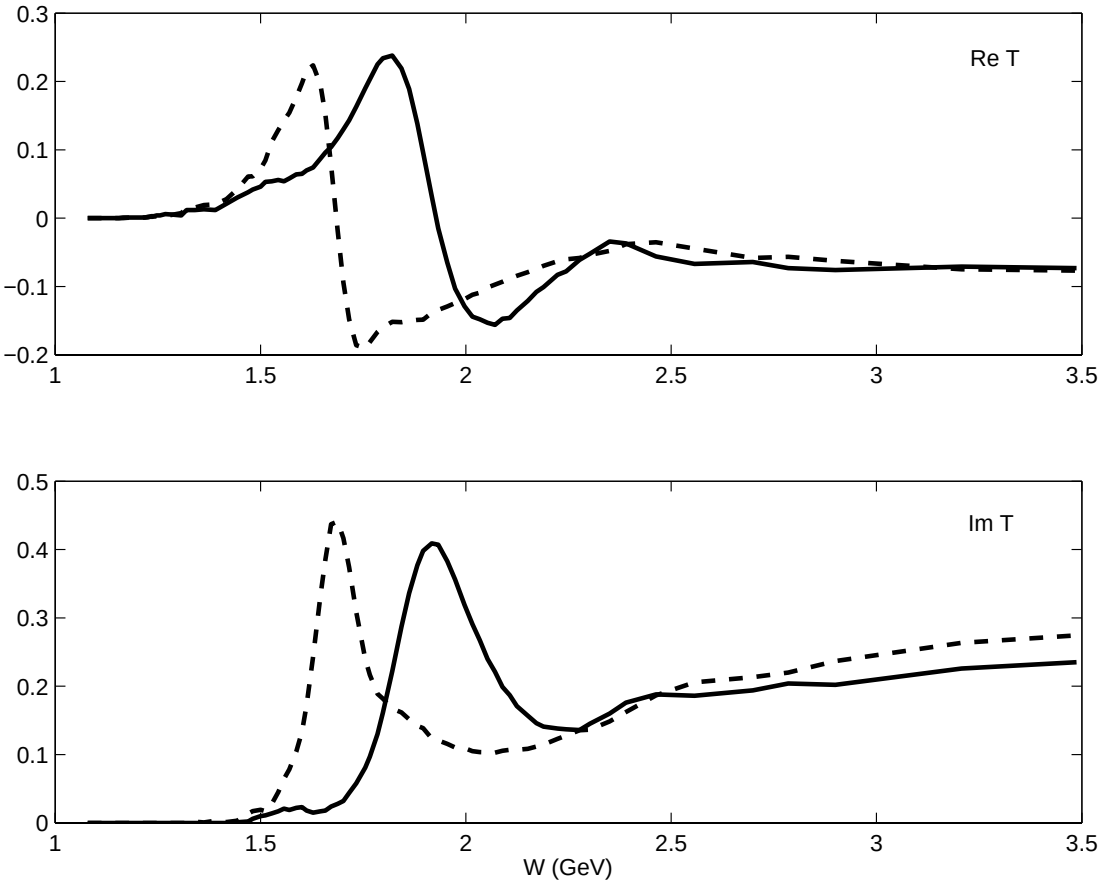

Figure 3.3: Experimentally determined F_{37} partial-wave amplitude (solid curve) for $\pi N \rightarrow \pi N$ scattering compared to the combination predicted by Eq. (3.6): $\frac{9}{14}F_{15} + \frac{5}{14}F_{17}$ (dotted curve). The data is provided by SAID [69].

Let us first consider the reactions $\pi N \to \pi N$ and $\pi N \to \pi\Delta$ when the pion orbital angular momentum is unchanged: $L = L'$. There are eight physical amplitudes corresponding to the different ways to add the spin and isospin of the pion and the nucleon in the two reactions: $I_s = \frac{1}{2}, \frac{3}{2}$ and $J_s = L \pm \frac{1}{2}$. We can expand these in terms of seven reduced amplitudes using Eq. (3.4). Therefore, there is only one relation among the physical amplitudes with all references to the reduced amplitudes eliminated. This relation is:

$$\begin{aligned} S^{\pi N}_{L,1,-1} - S^{\pi N}_{L,1,+1} &= \sqrt{\frac{2L-1}{L+1}} S^{\pi\Delta}_{L,1,-1} + \sqrt{\frac{2L+3}{L}} S^{\pi\Delta}_{L,1,+1} \\ &\quad + \left[\frac{2}{3} \left(S^{\pi N}_{L,3,-1} - S^{\pi N}_{L,3,+1} \right) + \frac{1}{3} \left(S^{\pi N}_{L,1,-1} - S^{\pi N}_{L,1,+1} \right) \right. \\ &\quad + \frac{1}{3}\sqrt{\frac{5}{2}} \left(\sqrt{\frac{2L-1}{L+1}} S^{\pi\Delta}_{L,3,-1} + \sqrt{\frac{2L+3}{L}} S^{\pi\Delta}_{L,3,+1} \right) \\ &\quad \left. - \frac{5}{6} \left(\sqrt{\frac{2L-1}{L+1}} S^{\pi\Delta}_{L,1,-1} + \sqrt{\frac{2L+3}{L}} S^{\pi\Delta}_{L,1,+1} \right) \right] \\ &\quad + O(N_c^{-2}). \end{aligned} \tag{3.14}$$

The left hand side and the first two terms resemble one of the original LO relations [Eq. (3.13)], but there is a correction term in the square brackets. The $1/N_c$ corrections to the terms in the square bracket from Eqs. (3.5)–(3.8) precisely cancel the corrections to Eq. (3.13), yielding a result that holds to order $O(N_c^{-2})$. It is natural that the only NLO relation that exists for $L = L'$ is a mixture of πN and $\pi\Delta$ amplitudes due to all the additional unknown reduced amplitudes included in Eq. (3.4). Equation (3.13) works rather well empirically (see the plots in Ref. [24]), and we defer a discussion of the possible effects of the correction term to Sec. 3.5.

Now we consider the reactions for which the pion orbital angular momentum

is changed by two units, $L = L' \pm 2$. The parity arguments of Sec. 3.3 restrict this case to the $\pi N \to \pi\Delta$ reaction. There are four physical amplitudes that can be expressed in terms of two reduced amplitudes. This implies the existence of two NLO linear relations:

$$\sqrt{L+1}\, S^{\pi\Delta}_{L,L+2,1,+1} = -\sqrt{L+2}\, S^{\pi\Delta}_{L+2,L,1,-1} + O(N_c^{-2}), \tag{3.15}$$

$$\sqrt{L+1} S^{\pi\Delta}_{L,L+2,3,+1} = -\sqrt{L+2}\, S^{\pi\Delta}_{L+2,L,3,-1} + O(N_c^{-2}). \tag{3.16}$$

These resemble two of the LO relations [*cf.* Eqs. (3.9), (3.10)]. However, we have now shown that they hold at NLO in $1/N_c$, and thus, to the extent that the $1/N_c$ expansion applies to these observables, one expects that these relations hold better than the generic LO predictions. As discussed in the following section, we show that this is, in fact, experimentally true. These formulae also constitute a resolution to the $\sqrt{10}$ mystery of Mattis and Peskin [24] mentioned in Sec. 3.3: Those authors unknowingly held a LO relation [Eqs. (3.11), (3.12)] to the same level of performance as a NLO one.

We note that all of our NLO relations involve the $\pi N \to \pi\Delta$ reaction. This is natural due to the large number of reduced amplitudes introduced at NLO in $1/N_c$; therefore, more physical amplitudes are required to algebraically eliminate them. These predictions however are problematic to verify experimentally as will be discussed in Sec. 3.5. The main point is that the delta is unstable in the $N_c = 3$ world and extensive modeling is required to extract its scattering amplitudes from the data.

In principle, our "$I_t = J_t$ rule" method can be applied again to derive the

$1/N_c^2$ terms in the S matrix expansion, as noted in Sec. 3.2. However, we note that such a procedure is of minimal utility for describing pion-nucleon scattering in the physical $N_c = 3$ world. The resulting triangle rules appearing in the $1/N_c^2$ corrections, applied to terms with a nucleon ($R = \frac{1}{2}$) in the initial state, cannot be satisfied for any baryon in the $R' = I = J$ multiplet of the large N_c world; this forces the $6j$ symbols to vanish, thus terminating the expansion. Therefore, it appears that we have exhausted the number of experimentally accessible NLO relations in pion-nucleon scattering. There are no relations that hold at next-to-next-to-leading order in the $1/N_c$ expansion (*i.e.*, have order $O(N_c^{-3})$ errors).

Before proceeding with the experimental tests of our new relations, we note in passing an interesting consistency check of the Weinberg-Tomozawa relation for scattering lengths. According to soft-pion theorems of chiral symmetry, the s-wave pion-nucleon scattering lengths for the isospin $I = \frac{1}{2}, \frac{3}{2}$ channels ($a_{1/2}$, $a_{3/2}$) are related to leading order in the chiral expansion by [14]

$$a_{1/2} = -2a_{3/2} = \frac{g_V^2}{\pi f_\pi^2} \frac{m_\pi m_N}{m_\pi + m_N} + O(m_\pi/m_N), \tag{3.17}$$

where m_π and m_N and the pion and nucleon mass, respectively and $g_V \sim O(N_c^0)$ is the vector current coupling. This relation is experimentally well satisfied; the ratio $a_{1/2}/a_{3/2}$ equals -2 to within 5% [66]. The scattering length (a) is related to the S matrix by $S = \exp[2ika]$ for small values of pion momenta, k. Using the leading order $1/N_c$ expansion of Eq. (3.1), we find that the S matrices for $L = 0$, $J = \frac{1}{2}$ with $I = \frac{1}{2}, \frac{3}{2}$ are equal (*i.e.*, $S_{I=1/2} = S_{I=3/2} = s^t_{000}/2\sqrt{3}$), apparently implying that $a_{1/2} = a_{3/2}$, in contradiction of the Weinberg-Tomozawa relation.

However, after imposing the N_c scaling for the various factors from Chapter 1, we find that the function on the right hand side of Eq. (3.17) is of order $O(N_c^{-1})$. Therefore, to leading order in $1/N_c$, the scattering lengths should vanish. For consistency with this result, chiral symmetry imposes the constraint $\frac{\partial}{\partial k} s^t_{000}|_{k\to 0} = 0$ to all orders in $1/N_c$. This was originally uncovered by Mattis and Peskin [24], but a trivial "0 = 0" consistency check of this relation is unsatisfactory. Since this prediction holds at next-to-leading in $1/N_c$, we gain some insight into this problem by considering our NLO expansion in Eq. (3.4). Carrying out the sum in Eq. (3.4) for $L = 0$, $J = \frac{1}{2}$ and $I = \frac{1}{2}, \frac{3}{2}$, we have

$$S_{I=1/2} = \left[\frac{1}{2\sqrt{3}} s^t_{000}\right] + \left[-\sqrt{\frac{2}{3}} s^{t(-)}_{100} \frac{1}{N_c}\right], \tag{3.18}$$

$$S_{I=3/2} = \left[\frac{1}{2\sqrt{3}} s^t_{000}\right] + \left(-\frac{1}{2}\right)\left[-\sqrt{\frac{2}{3}} s^{t(-)}_{100} \frac{1}{N_c}\right]. \tag{3.19}$$

At next-to-leading order in $1/N_c$, the relative factor of -2 between the scattering lengths in Eq. (3.17) follows directly from the $-1/2$ in Eq. (3.19). This constitutes a satisfying nontrivial consistency check of the Weinberg-Tomozawa relation in the $1/N_c$ expansion.

It is not necessary that the two expansions (chiral and $1/N_c$) produce the same result. Cases are known (*e.g.*, predictions for the charge radius of the nucleon) in which the limits do not commute [67]. The problem can be traced to the inclusion of the delta particle. In the large N_c limit, the delta and nucleon are degenerate in mass (see Chapter 1) and both contribute to pion loops in Feynman diagrams for an observable. This can be seen more clearly when we compute the diagrams in terms of the parameter, $d \equiv (m_\Delta - m_N)/m_\pi$. Note that $d \to \infty$ in the chiral limit

$(m_\pi \to 0)$ and $d \to 0$ in the large N_c limit since $m_\Delta - m_N \sim O(N_c^{-1})$. Quantities with strong d dependence can vary drastically depending on the ordering of the two limits. In the case of the Weinberg-Tomozawa relation, we properly accounted for the order $O(N_c^{-1})$ effects and demonstrated consistency between the two predictions.

3.5 Experimental Check of the NLO Pion-nucleon Relations

In principle, all three linear relations derived in Sec. 3.4 (for each allowed value of L) can be tested with available experimental data. The amplitudes we will use come from a partial-wave analysis applied to raw data from scattering experiments. These experiments use charged pions produced in proton collisions which are then magnetically directed into bubble chambers. The chambers are filled with either hydrogen gas serving as proton targets or deuterium serving as neutron targets. The pion energy-momentum is selected with magnetic fields and the scattering cross section is inferred from detector signals and the visible particle tracks. The partial-wave amplitudes are treated as complex parameters and fitted to the measured cross sections at each energy with a χ^2-minimization analysis. Clebsch-Gordan coefficients allow us to account for the z-components of the spin and isospin quantum numbers for particular charged reactions (*e.g.*, $\pi^+ p \to \pi^0 \Delta^{++}$), so the final result is a partial-wave amplitude $LL'_{2I_s,2J_s}$ as a function of scattering energy for $\pi N \to \pi N$ and $\pi N \to \pi \Delta$.

The extraction of partial-wave amplitudes for the $\pi N \to \pi N$ reaction from the large amount of reliable (though old) data is straightforward. However, all of

the NLO relations of Sec. 3.4 involve the reaction $\pi N \to \pi\Delta$. The extraction of partial-wave amplitudes for $\pi N \to \pi\Delta$ is complicated by the fact that the delta decays strongly to πN. This decay occurs because the chiral limit dominates the large N_c limit; the pion mass is smaller than the delta-nucleon mass difference. The delta lifetime is on the order of 10^{-23} seconds and thus the final state observed in the laboratory is $\pi\pi N$. The observed reaction $\pi N \to \pi\pi N$ can take several intermediate routes. For example, it is possible to produce a ρ vector meson ($m_\rho = 776$ MeV), $\pi N \to \rho N$, which then decays strongly to two pions. The $\pi N \to \pi\Delta$ partial waves must therefore be extracted with a model that distinguishes events in the observed reaction $\pi N \to \pi\pi N$ that pass through an intermediate delta resonance and which do not.

The $\pi N \to \pi\Delta$ partial-wave amplitude data therefore necessarily contains some model dependence, making it somewhat less reliable. Due to this uncertainty, much less attention has been paid to these reactions and the set of analyzed data is far more sparse. Fortunately, the Δ is an extremely prominent resonance (understandable in the context of large N_c QCD), and hence it is believed that the model dependence should be rather modest.

For the comparisons presented in this section, we use results from the isobar model analysis of Manley, Arndt, Goradia, and Teplitz [68], which is readily available through the SAID program at George Washington University [69]. The analysis is presented in terms of the dimensionless T matrix [$\mathbf{T} \equiv (\mathbf{S} - \mathbf{1})/2i$] rather than the S matrix. This causes no complications, since any extra factors and terms cancel in our formulas. The results of Ref. [68] are presented in terms of the center-of-mass

energy W of the πN system in the range 1340–1910 MeV. While this range is merely that presented by the most up-to-date analysis, it is appropriate for a test of our $\pi N \to \pi\Delta$ scattering relations. Our assumption that the baryon is at rest becomes tenuous at impact energies slightly higher than 1910 MeV because the delta's recoil can no longer be neglected.

We first consider Eq. (3.14) and restrict our attention to $1 \leq L \leq 3$. The lower bound is an elementary consequence of angular momentum conservation, while the upper bound reflects limitations of the available data. Even with this restriction we see that for each L, Eq. (3.14) requires partial-wave amplitudes that are, unfortunately, not available in the data set. For example, the amplitudes PP_{31}, PP_{13}, DD_{33}, and FF_{17} are not given. Mattis and Peskin were able to circumvent this problem in their LO comparisons [24] by rewriting the unknown amplitudes in terms of known ones using formulas Eqs. (3.7) & (3.8). We have no such luxury; inserting Eqs. (3.7) & (3.8) into our NLO relation [Eq. (3.14)] simply introduces an error of order $O(N_c^{-1})$ and effectively converts it to a LO relation. Since our goal is to test the extent to which a NLO relation is more experimentally effective than a LO one, this type of substitution would be counterproductive. We therefore make no assumptions about these unknown partial-wave amplitudes and thus cannot test the validity of Eq. (3.14) at the present time.

We now consider Eqs. (3.15) and (3.16) and restrict our attention to $0 \leq L \leq 1$. The upper bound is again the limit of available data. Fortunately, there is sufficient analyzed data to study these relations for the $L = 0$ case. To test the $1/N_c$ expansion, we will compare the quality of the agreement of these NLO relations with

the $L = 0$ LO relations, Eqs. (3.11) & (3.12). Both sets of predictions involve only the $\pi N \to \pi\Delta$ reaction and we view the loss of predictive power due to modeling the $\pi N \to \pi\Delta$ partial-wave amplitudes as a comparable systematic uncertainty for the two types of relations. Our predictions are as follows:

$$SD_{11} = -\sqrt{2}\, DS_{13} + O(N_c^{-2}), \tag{3.20}$$

$$SD_{31} = -\sqrt{2}\, DS_{33} + O(N_c^{-2}), \tag{3.21}$$

and

$$SD_{11} = +\sqrt{20}\, DS_{33} + O(N_c^{-1}), \tag{3.22}$$

$$SD_{31} = +\frac{1}{\sqrt{5}}\, DS_{13} + O(N_c^{-1}), \tag{3.23}$$

where the first two equations are the NLO relations (see Fig. 3.4) and the second two are the LO relations (see Fig. 3.5).

It is immediately apparent that the NLO relations agree with experiment considerably better than their LO analogs. For the NLO relations, the gross structure of the amplitudes is clearly discernible on both the left- and right-hand sides of the relation. In contrast, the LO relations are much less robust in describing the data. We note that the LO relations tested here work much more poorly than those involving only the $\pi N \to \pi N$ amplitudes (See Figs. 3.2 and 3.3). We also note that the reported errors in the real and imaginary parts of the T matrix at each energy point are less than 0.04 for the partial-waves considered here [69] and are thus too small to explain the difference in the level of agreement.

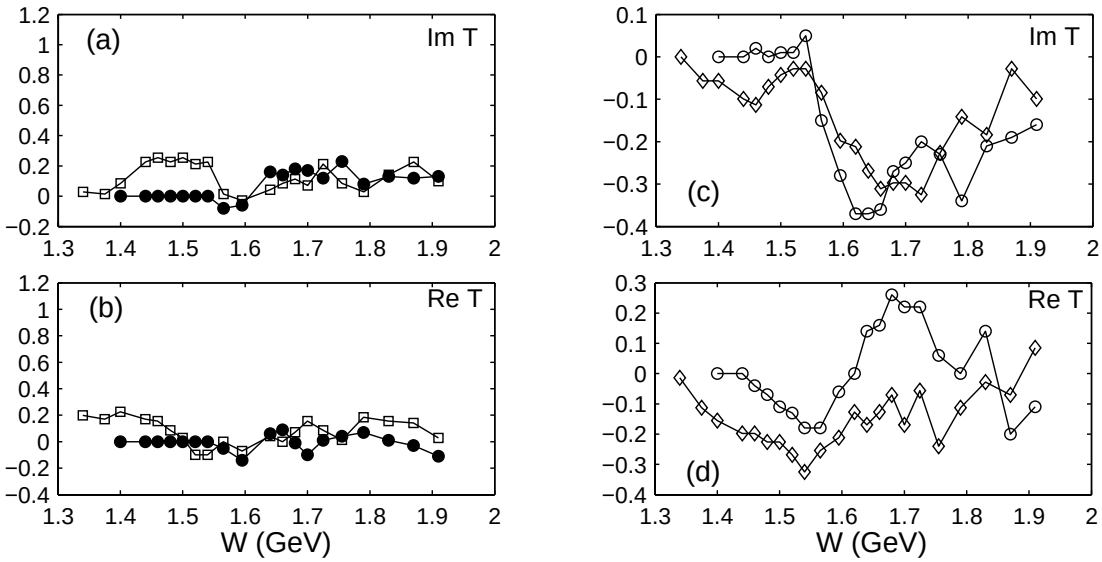

Figure 3.4: Experimentally determined $\pi N \to \pi\Delta$ amplitudes SD_{11} and SD_{31} compared to the predictions of Eqs. (3.20), (3.21). In plots (a) and (b), the closed circle ($\bullet$) is SD_{11} and the box is $-\sqrt{2}\,DS_{13}$. In plots (c) and (d), the open circle ($\circ$) is SD_{31} and the diamond ($\diamond$) is $-\sqrt{2}\,DS_{33}$. The data is provided by SAID [69].

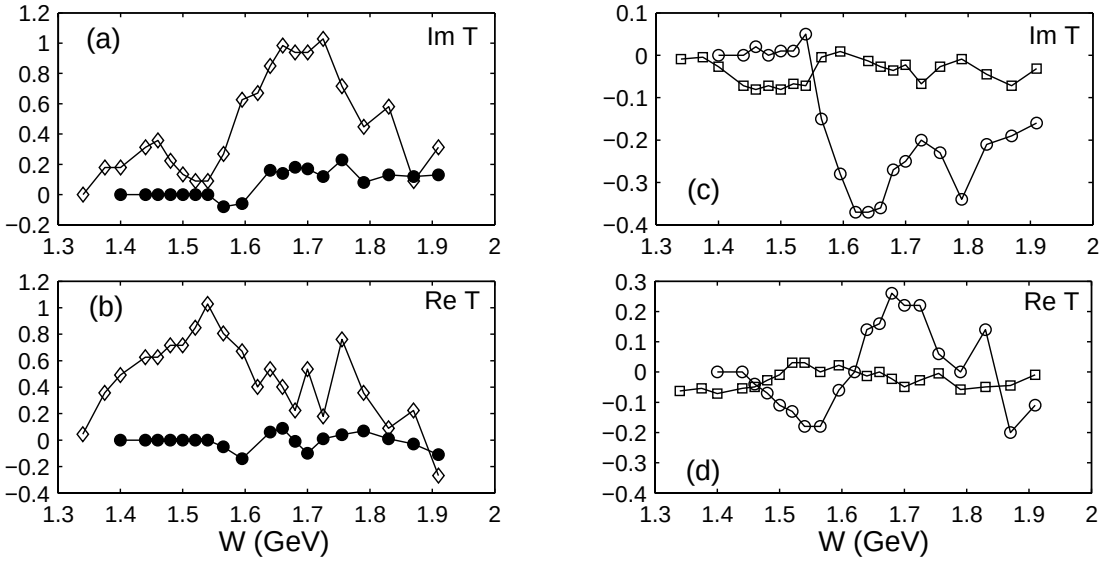

Figure 3.5: Experimentally determined $\pi N \to \pi\Delta$ amplitudes SD_{11} and SD_{31} compared to the predictions of Eqs. (3.22), (3.23). In plots (a) and (b), the closed circle ($\bullet$) is SD_{11} and the diamond ($\diamond$) is $+\sqrt{20}\,DS_{33}$. In plots (c) and (d), the open circle ($\circ$) is SD_{31} and the box is $+1/\sqrt{5}\,DS_{13}$. The data is provided by SAID [69].

3.6 Summary

In the previous sections, we have demonstrated the power and utility of the $1/N_c$ expansion for describing pion-nucleon scattering. We have shown that the contracted SU(4) spin-flavor symmetry that emerges in large N_c QCD allows us to make non-trivial predictions that are testable by data. Given the rigor of large N_c QCD, these predictions passed all experimental expectations, thus helping us to understand some rather complicated features of hadronic physics. This understanding can be expanded by considering the photoproduction of pions off of nucleons as done the next chapter.

In this chapter, we have shown that the symmetries of large N_c QCD create linear dependence among amplitudes for pion-nucleon scattering. This allows us to derive model-independent linear relations that were directly confirmed using experimental data. In the following chapter, the techniques developed here will be applied to pion photoproduction.

-.-

Chapter 4

Model-independent Linear Scattering Relations:

Pion Photoproduction

4.1 Pion Photoproduction

The production of pions with real or virtual photons ($\gamma N \to \pi N$) is another important source of hadronic information. In pion electroproduction, electrons emit virtual photons that are absorbed by a nucleon, creating an intermediate state that then couples to a pion and nucleon. In pion photoproduction, a nucleon absorbs gamma rays from electron bremsstrahlung, then decays into a pion and nucleon. The key difference is that a virtual photon has an additional longitudinal propagation mode that is forbidden for an on-shell (real) spin-1 photon. The pion production process can be symbolically described as $\langle \pi N \left| H_\pi \right| N^* \rangle \langle N^* \left| H_\gamma \right| \gamma N \rangle$, where N^* is the intermediate state and H_π and H_γ are the pionic and electromagnetic interaction operators, respectively. Given that $\langle \pi N \left| H_\pi \right| N^* \rangle$ is well-studied and documented as indicated by Sec. 3.5, pion production gives us access to the electromagnetic interaction through $\langle N^* \left| H_\gamma \right| \gamma N \rangle$. In this section, we focus on pion photoproduction and derive an S matrix expansion similar to Eq. (3.1) for electromagnetic multipole amplitudes. In the next section, we will derive linear relations among multipole amplitudes that hold to leading order (LO) and next-to-leading order (NLO) in $1/N_c$.

In Sec. 4.3, we compare all the predicted relations with experimental data.

Pion photoproduction can be described by the same S matrix expansion in Eq. (3.1) derived for πN scattering once certain modifications are made to account for the electromagnetic interaction. These modifications include assigning the initial "pion" with the spin and isospin quantum numbers of a photon. Although the photons are spin 1, one traditionally precombines the photon spin with its orbital angular momentum about the nucleon target. This gives the usual multipole angular momentum (ℓ) for scattering processes involving radiation [70]. Since ℓ represents all the sources of angular momentum for the photon, its intrinsic spin may effectively be set to zero, as with the pion.

The photon has the interesting property that it interacts with hadrons through either an isoscalar ($I_\gamma = 0$) or isovector current ($I_\gamma = 1$). The operators that connect the hadronic and photonic isospin currents have distinct properties in large N_c QCD. The dominant isovector coupling of a photon to a nucleon enters through the combined spin-flavor operator, G^{ia}, introduced in Sec. 2.3, which in a quark model representation is

$$G^{ia} \equiv \sum_{\alpha=1}^{N_c} q_\alpha^\dagger \left(\frac{\sigma^i}{2} \otimes \frac{\tau^a}{2} \right) q_\alpha \ , \tag{4.1}$$

where σ and τ are Pauli matrices in spin and isospin spaces, respectively. We sum α over the N_c quark fields, q_α, in the nucleon. It should be noted that this operator does not require a quark model to be well defined. However, the quark model exactly reproduces the results of the contracted SU(4) symmetry and is a simple way to implement the group theory [29]–it is often joked that this is the "poor

man's" way to do group theory. In the field-theoretic context, q_α simply stands for an interpolating field with the quantum numbers of a current quark, whose effect, summed over α, completely exhausts the full nucleon wave function [71]. In the same quark model language, the (spin-dependent) isoscalar coupling enters via the operator

$$J^i \equiv \sum_{\alpha=1}^{N_c} q_\alpha^\dagger \left(\frac{\sigma^i}{2}\right) q_\alpha \ . \tag{4.2}$$

The two operators differ in that the matrix elements of G^{ia} are of order $O(N_c^1)$ for ground-state baryons due to the collective effect of the N_c quarks, while the matrix elements of J^i are, by construction, of order $O(N_c^0)$ for ground-state baryons like the nucleon.

The S matrix expansion of Eq. (3.1) does not reflect the different N_c scaling for isospin couplings discussed above. The scaling must be put in by hand by adding to the leading isovector ($I_\gamma = 1$) terms additional isoscalar ($I_\gamma = 0$) terms suppressed by an explicit factor of $1/N_c$.

This suppression follows from the isospin symmetry breaking in the electromagnetic interaction since both isoscalar and isovector currents couple to the photon spin operator. However, a truly spinless isoscalar meson (*viz.*, the η) can couple through the operator

$$\mathbf{1} \equiv \sum_{\alpha=1}^{N_c} q_\alpha^\dagger q_\alpha \ , \tag{4.3}$$

whose nucleon matrix elements are of order $O(N_c^1)$, and therefore couples just as strongly to nucleons as pions do through the isovector coupling, Eq. (4.1).

We are now ready to proceed with the derivation of pion photoproduction

multipole amplitudes from Eq. (3.1). We substitute $R = R' = \frac{1}{2}$ for the nucleons and $I_\pi = 1$ for the pion. We also have $I_\gamma \in \{0, 1\}$ for the photon, where we sum the two cases to get the full physical amplitude. The result for a particular I_γ is

$$S^{I_\gamma}_{\ell L \frac{1}{2} \frac{1}{2} I_s J_s}(E) = \sum_{\mathcal{J}} \begin{bmatrix} 1 & \frac{1}{2} & I_s \\ \frac{1}{2} & I_\gamma & \mathcal{J} \end{bmatrix} \begin{bmatrix} L & \frac{1}{2} & J_s \\ \frac{1}{2} & \ell & \mathcal{J} \end{bmatrix} s^{t, I_\gamma}_{\mathcal{J} \ell L}(E). \tag{4.4}$$

We need to evaluate this expansion for a particular electromagnetic transition and charge channel. Processes involving radiation proceed through an electric or magnetic transition depending on the relative parity of the initial and final states as determined by ℓ and L. If $(\ell - L)$ is odd, then the transition is electric and described by an electric multipole amplitude ($M^{\mathrm{e}}_{\ell L J_s}$). If $(\ell - L)$ is even, then the transition is magnetic and described by a magnetic multipole amplitude ($M^{\mathrm{m}}_{\ell L J_s}$). It is possible to be even more specific since our initial and final baryons are both spin $\frac{1}{2}$ particles (*viz.*, the nucleons): In the magnetic case, the photon and pion have the same orbital angular momentum ($\ell = L$), whereas in the electric case, there is a change of one unit ($\ell = L \pm 1$).

In order to project $\gamma N \to \pi N$ into a particular charge channel, we need to specify the z-component of isospin for the incoming nucleon (m_I) and for the pion (ν). With the appropriate Clebsch-Gordan coefficients describing the initial and final states, we have:

$$M^{\lambda I_\gamma, m_I \nu}_{\ell L I_s J_s}(E) = \left(\begin{array}{cc|c} 1 & \frac{1}{2} & I_s \\ \nu & m_I - \nu & m_I \end{array} \right) \left(\begin{array}{cc|c} I_\gamma & \frac{1}{2} & I_s \\ 0 & m_I & m_I \end{array} \right) S^{\lambda I_\gamma}_{\ell L \frac{1}{2} \frac{1}{2} I_s J_s}(E), \tag{4.5}$$

where the index $\lambda \in \{\mathrm{e}, \mathrm{m}\}$ indicates the type of electromagnetic transition and the isospin of the photon ($I_\gamma \in \{0, 1\}$) has been left unevaluated. Finally, we must sum

over all possible the total isospin states.

Let us summarize before proceeding with the NLO additions to the $1/N_c$ expansion. The multipole amplitude that describes pion photoproduction is a sum of the isoscalar and isovector expansions. The isoscalar piece is suppressed by a factor of $1/N_c$ relative to the isovector piece. Therefore an expansion to consistent order in $1/N_c$ requires the inclusion of NLO amplitudes for only the isovector channel. The structure of the isovector amplitudes [Eq. (4.5) with $I_\gamma = 1$] is identical to the πN scattering case [see Eq. (3.1)] and the construction of the NLO amplitudes will follow exactly as in Sec. 3.2. The NLO term is

$$\begin{aligned} M_{\ell L I_s J_s}^{\lambda 1, m_I \nu\,(\mathrm{NLO})}(E) \;=\; & \frac{1}{N_c} \left(\begin{array}{ccc|c} 1 & & \frac{1}{2} & I_s \\ & & & \\ \nu & m_I - \nu & & m_I \end{array} \right) \left(\begin{array}{ccc|c} 1 & & \frac{1}{2} & I_s \\ & & & \\ 0 & m_I & & m_I \end{array} \right) \\ & \times \left\{ \sum_x \left[\begin{array}{ccc} 1 & \frac{1}{2} & I_s \\ & & \\ \frac{1}{2} & 1 & x \end{array} \right] \left[\begin{array}{ccc} L & \frac{1}{2} & J_s \\ & & \\ \frac{1}{2} & \ell & x+1 \end{array} \right] s_{x\ell L}^{t\lambda(+)}(E) \right. \\ & \left. + \sum_y \left[\begin{array}{ccc} 1 & \frac{1}{2} & I_s \\ & & \\ \frac{1}{2} & 1 & y \end{array} \right] \left[\begin{array}{ccc} L & \frac{1}{2} & J_s \\ & & \\ \frac{1}{2} & \ell & y-1 \end{array} \right] s_{y\ell L}^{t\lambda(-)}(E) \right\}. \end{aligned} \tag{4.6}$$

The total multipole amplitude expansion, including all leading order and next-to-leading order terms in the $1/N_c$ expansion, is the sum

$$M_{\ell L J_s}^{\lambda, m_I \nu} = \sum_{I_s} \left(M_{\ell L I_s J_s}^{\lambda 1, m_I \nu} + \frac{1}{N_c} M_{\ell L I_s J_s}^{\lambda 0, m_I \nu} + M_{\ell L I_s J_s}^{\lambda 1, m_I \nu\,(\mathrm{NLO})} \right). \tag{4.7}$$

An expression for multipole amplitudes similar to this one was previously derived in the Skyrme model [26, 27]. However, that derivation did not utilize large N_c QCD as a constraint–the isoscalar and isovector operators are treated equally and the

$M_{\ell L I_s J_s}^{\lambda 1, m_I \nu\,(\mathrm{NLO})}$ term is absent–and thus did not yield any truly model-independent predictions.

Equation (4.7) can be evaluated for particular values of $\{m_I, \nu\}$ and we will show that linear dependence among these quantities exists, meaning we can derive linear relations. These are discussed in the following section.

4.2 Pion Photoproduction Relations

In this section, we derive nine linear relations among pion photoproduction amplitudes that follow from Eq. (4.7). They hold to LO or NLO in $1/N_c$ and compare reasonably well with experiment as demonstrated in Sec. 4.3 below. Before proceeding, we must consider an important restriction that isospin invariance imposes on the individual charge channels.

Charge conservation limits the number of pion photoproduction channels to four: $\gamma p \to \pi^+ n$, $\gamma n \to \pi^- p$, $\gamma p \to \pi^0 p$, $\gamma n \to \pi^0 n$. However, due to the isospin invariance of the strong interaction, only three of these channels are independent. This can be seen explicitly once we decompose the amplitude for the charge channels in terms of the isospin amplitudes appropriate for the reaction to proceed via the isovector current with an intermediate $I = \frac{3}{2}$ state ($T_V^{3/2}$) or $I = \frac{1}{2}$ state ($T_V^{1/2}$), or via the isoscalar current with an $I = \frac{1}{2}$ state (T_S):

$$\begin{aligned}
A(\gamma p \to \pi^+ n) &= \frac{\sqrt{2}}{3} T_V^{3/2} - \frac{\sqrt{2}}{3} T_V^{1/2} + \sqrt{\frac{2}{3}} T_S, \\
A(\gamma n \to \pi^- p) &= \frac{\sqrt{2}}{3} T_V^{3/2} - \frac{\sqrt{2}}{3} T_V^{1/2} - \sqrt{\frac{2}{3}} T_S, \\
A(\gamma p \to \pi^0 p) &= \frac{2}{3} T_V^{3/2} + \frac{1}{3} T_V^{1/2} - \sqrt{\frac{1}{3}} T_S,
\end{aligned}$$

$$A(\gamma n \to \pi^0 n) \;=\; \frac{2}{3}\,T_V^{3/2} + \frac{1}{3}\,T_V^{1/2} + \sqrt{\frac{1}{3}}\,T_S, \tag{4.8}$$

where we have summed over all the total isospin states with the appropriate Clebsch-Gordan coefficients. Note that this system is linearly dependent and thus one of the amplitudes can be written in terms of the other three. Since all the species in $\gamma n \to \pi^0 n$ are neutral, this reaction is difficult to study experimentally and isospin freedom allows us to ignore its amplitudes:

$$A(\gamma n \to \pi^0 n) = A(\gamma p \to \pi^0 p) + \sqrt{1/2}\,\Big[\,A(\gamma p \to \pi^+ n) - A(\gamma n \to \pi^- p)\,\Big]. \tag{4.9}$$

Given this restriction, the set of multipole amplitudes $[M_{\ell L J_s}^{\lambda,m_I\nu}(E)]$ describing the three remaining channels can be written in terms of a still *smaller* set of reduced amplitudes $[s_{\mathcal{J}\ell L}^{t\lambda,I_\gamma}(E),\, s_{y\ell L}^{t\lambda(-)}(E),\, s_{x\ell L}^{t\lambda(+)}(E)]$. Thus one expects this linear dependence to yield relations among the physically measurable amplitudes.

Linear relations can be derived at both LO and NLO in the $1/N_c$ expansion. In order to find the LO relations, we work only with the LO terms in Eq. (4.7) (*i.e.*, disregard the $1/N_c$-suppressed terms, $\frac{1}{N_c}M_{\ell L I_s J_s}^{\lambda 0,m_I\nu}$, $M_{\ell L I_s J_s}^{\lambda 1,m_I\nu\,(\mathrm{NLO})}$). To find the relations that hold to NLO in $1/N_c$, we use the complete expression. Since the electric and magnetic transitions have distinct expansions, we investigate them separately.

We use a more convenient notation than $M_{\ell L J_s}^{\lambda,m_I\nu}$ for the multipole amplitudes to present our relations. The total angular momentum J_s will be represented by the equivalent information of the sign in $J_s = L \pm \frac{1}{2}$. The channel will not be represented by the numerical superscripts, $\{m_I, \nu\}$, but by the more illuminating and traditional nuclear reaction notation, $N(\pi)N'$. For example, $M_{L+1,L,L+\frac{1}{2}}^{\mathrm{e},\frac{1}{2},+1}$ will be replaced by $M_{L+1,L,+}^{\mathrm{e},p(\pi^+)n}$.

We begin with the expansion of the electric multipole amplitudes. There are six physical amplitudes corresponding to the two ways of combining the pion and nucleon angular momenta, $J_s = L \pm \frac{1}{2}$, for each of the three independent charged reactions. To LO in $1/N_c$ these depend on only two reduced amplitudes implying four linear relations. Two of these are

$$M^{\mathrm{e},\,p(\pi^+)n}_{L-1,L,-} = M^{\mathrm{e},\,n(\pi^-)p}_{L-1,L,-} + O(N_c^{-1}) \ (L \geq 2), \tag{4.10}$$

$$M^{\mathrm{e},\,p(\pi^+)n}_{L+1,L,+} = M^{\mathrm{e},\,n(\pi^-)p}_{L+1,L,+} + O(N_c^{-1}) \ (L \geq 0). \tag{4.11}$$

These relations follow simply from the isospin symmetry of isovector amplitudes, since the isoscalar component of the photon current is absent at leading order in $1/N_c$ as discussed in Sec. 4.1. This can be seen explicitly with Eq. (4.8) if we set $T_S \to 0$ to get $A(\gamma p \to \pi^+ n) = A(\gamma n \to \pi^- p) + O(N_c^{-1})$.

The other two LO relations imply the vanishing of the electric multipole amplitudes for the $\gamma p \to \pi^0 p$ reaction at leading order in $1/N_c$:

$$M^{\mathrm{e},\,p(\pi^0)p}_{L\pm1,L,\pm} = 0 + O(1/N_c) \ . \tag{4.12}$$

After extrapolating to the real world of $N_c = 3$, one expects these amplitudes to be about a factor of $N_c = 3$ smaller (on average) than those of the charge-exchange reactions. Indeed, a qualitative check of experimental data [69, 74] reveals this to be the case for low energies a safe distance away from resonances. A more in-depth discussion of this case is presented in Sec. 4.3 below.

Once the NLO terms in Eq. (4.7) are included, four new reduced amplitudes appear and the linear dependence of the set of electric multipole amplitudes dis-

appears. Therefore, there are no electric multipole linear relations among these reactions that hold to NLO in $1/N_c$.

Turning to the magnetic transition, one sees that only two reduced amplitudes are needed to describe the six physical amplitudes to leading order in $1/N_c$. This yields four LO linear relations for $L \geq 1$:

$$M^{\mathrm{m},\,p(\pi^0)p}_{L,L,-} = M^{\mathrm{m},\,p(\pi^0)p}_{L,L,+} + O(N_c^{-1}), \tag{4.13}$$

$$M^{\mathrm{m},\,p(\pi^+)n}_{L,L,-} = M^{\mathrm{m},\,n(\pi^-)p}_{L,L,-} = -\frac{L+1}{L} M^{\mathrm{m},\,p(\pi^+)n}_{L,L,+} = -\frac{L+1}{L} M^{\mathrm{m},\,n(\pi^-)p}_{L,L,+}. \tag{4.14}$$

Two of these [$M^{\mathrm{m},\,p(\pi^+)n}_{L,L,-} = M^{\mathrm{m},\,n(\pi^-)p}_{L,L,-} + O(N_c^{-1})$, $M^{\mathrm{m},\,p(\pi^+)n}_{L,L,+} = M^{\mathrm{m},\,n(\pi^-)p}_{L,L,+} + O(N_c^{-1})$] follow from isospin symmetry among the isovector amplitudes as mentioned earlier in reference to the electric transition case.

The NLO terms in Eq. (4.7) introduce only three more reduced amplitudes, meaning that one linear relation remains at NLO in $1/N_c$. Indeed, one might have anticipated that a NLO relation would be found for the magnetic rather than the electric transition case. This follows because there are fewer quantum number combinations (thus fewer amplitudes) in the magnetic transition case since only $\ell = L$ is allowed. The NLO relation for $L \geq 1$ is

$$M^{\mathrm{m},\,p(\pi^+)n}_{L,L,-} = M^{\mathrm{m},\,n(\pi^-)p}_{L,L,-} + \left(-\frac{L+1}{L}\right)\left[M^{\mathrm{m},\,p(\pi^+)n}_{L,L,+} - M^{\mathrm{m},\,n(\pi^-)p}_{L,L,+}\right] + O(N_c^{-2}). \tag{4.15}$$

We see that this is a linear combination of the LO relations in Eq. (4.14); it is the unique combination for which the NLO corrections (in brackets) cancel. One expects this relation to hold empirically a factor of $N_c = 3$ better than its LO counterpart in Eq. (4.14).

In the following section, we test these predictions using the available experimental data for pion photoproduction.

4.3 Experimental Check of the Pion Photoproduction Relations

In principle, all nine linear relations included in Eqs. (4.10)–(4.15) (for each allowed value of L), plus the smallness of Eqs. (4.12), can be tested through a comparison with available experimental data. The numbers we will use are the result of a partial-wave analysis applied to raw data from pion photoproduction experiments. In a typical experiment [73], an electron beam creates photons (gamma rays) which are directed towards a target of liquid hydrogen (proton targets) or deuterium (neutron targets). The differential cross section for the photon-nucleon scattering is measured by detecting the final state particles. The partial-wave analysis follows a procedure similar to that used for πN scattering (see Sec. 3.5) and the final result is a set of complex *electromagnetic multipoles*, as defined below. As we will see below, photon-decay couplings will play an important role in our experimental check. These are extracted from the multipoles by fitting the resonant part of the amplitude to a Breit-Wigner form.

For our comparisons, we use the electromagnetic multipole data presented by the SAID program [69] at George Washington University and the MAID 2003 program [74] at Universität Mainz. Although one requires only a single data set, it is useful to check the extent to which the model dependence of the data analysis used by the two groups affects our comparisons. We find that the difference is not

significant when applied to the LO relations, but tends to make our NLO relation unconvincing. As discussed below, the ultimate verification of the NLO relation requires a "resonant parameter test" using photon-decay couplings (*helicity amplitudes*) taken from the Particle Data Group [38]. It should also be noted that the sign of the $p\,(\pi^+)\,n$ amplitudes appearing in the data sets is often reversed (in MAID, for example) compared to those fixed by the standard Condon-Shortley convention used in this thesis.

We now introduce the notation used in the experimental data tables. The *electromagnetic multipoles* are given in terms of our multipole amplitudes by

$$\begin{aligned} M^{\mathrm{e}}_{L-1,L,-} &= +\beta\sqrt{L(L-1)}\,E_{L-}, \\ M^{\mathrm{e}}_{L+1,L,+} &= +\beta\sqrt{(L+2)(L+1)}\,E_{L+}, \\ M^{\mathrm{m}}_{L,L,+} &= -\beta\sqrt{L(L+1)}\,M_{L+}, \\ M^{\mathrm{m}}_{L,L,-} &= -\beta\sqrt{L(L+1)}\,M_{L-}, \end{aligned} \tag{4.16}$$

where [26]

$$\beta \equiv -f_\pi\sqrt{\frac{k_\gamma}{2\pi\alpha}} \tag{4.17}$$

is an energy scale with $f_\pi \approx 93\,\mathrm{MeV}$, $\alpha \approx 1/137$, and k_γ being the photon center-of-mass momentum. This factor cancels from all linear relations and therefore is irrelevant to this work. In fact, as seen from Sec. 4.2, each term in any one of our linear relations has the same prefactors of β and L entering via Eq. (4.16). The relations therefore take the same form when written in terms of the electromagnetic multipoles. For easy referencing purposes, we present our nine relations in the

experimental notation:

$$E_{L-}^{p(\pi^+)n} = E_{L-}^{n(\pi^-)p} + O(N_c^{-1}) \ (L \geq 2), \tag{4.18}$$

$$E_{L+}^{p(\pi^+)n} = E_{L+}^{n(\pi^-)p} + O(N_c^{-1}) \ (L \geq 0), \tag{4.19}$$

$$E_{L\pm}^{p(\pi^0)p} = 0 + O(N_c^{-1}), \tag{4.20}$$

$$M_{L-}^{p(\pi^0)p} = M_{L+}^{p(\pi^0)p} + O(N_c^{-1}) \ (L \geq 1), \tag{4.21}$$

$$M_{L-}^{p(\pi^+)n} = M_{L-}^{n(\pi^-)p} = -\frac{L+1}{L} M_{L+}^{p(\pi^+)n} = -\frac{L+1}{L} M_{L+}^{n(\pi^-)p} \ (L \geq 1), \tag{4.22}$$

$$M_{L-}^{p(\pi^+)n} = M_{L-}^{n(\pi^-)p} + \left(-\frac{L+1}{L}\right) \left[M_{L+}^{p(\pi^+)n} - M_{L+}^{n(\pi^-)p}\right] + O(N_c^{-2}). \tag{4.23}$$

Before presenting plots comparing our predictions to data, we describe what suitable agreement among the relations entails. Each partial wave consists of a continuum punctuated by occasional resonances. Our relations should be taken at face value in the continuum regions. Therefore, if the two sides of a relation in such a region are expected to have only order $O(N_c^{-2})$ corrections, but the agreement is much poorer, then one can say that the relation fails. However, even in such a case, one must question whether the method of extracting the partial wave might be at fault. For example, the $L=4$ results for Eqs. (4.22) and (4.23) differ greatly between MAID (Figs. 4.6 & 4.7) and SAID (Fig. 4.8), with the former much more supportive of our relations; but without further information, one cannot definitively say which scenario is correct. Fortunately, this effect does not occur in most cases.

In the resonant regions, the agreement between amplitudes is much less impressive for a variety of reasons. Foremost, the delta resonance may appear prominently in some partial waves although the delta is not a resonance at all in large N_c QCD, but a stable partner of the nucleon (See Chapter 1). The delta of the $N_c = 3$ world

is unstable only because the pion mass (139 MeV) is smaller then the delta-nucleon mass difference (290 MeV) which is an order $O(N_c^{-1})$ effect. Thus, the chiral limit which fixes the pion mass wins out over the large N_c limit which determines the delta-nucleon mass difference. There also exist multiplets of true resonances degenerate in mass to order $O(N_c^{-1})$ as mentioned in Sec. 3.2 [39], and these appear as bumps in the two sides of relations at relatively shifted positions: For a preview, see the $L = 2$ cases in Figs. 4.6 and 4.8. In such cases, we rely upon an analysis ("resonant parameter test" described below) introduced in Ref. [27] of comparing the extracted resonant amplitudes (helicity amplitudes) directly. As we shall see, the agreement of the resonant parameters in the $L = 2$ case turns out to be very satisfactory.

In all the following plots, we present both the real and imaginary parts of the electromagnetic multipoles measured in units of $10^{-3}/m_{\pi^+}$ in terms of the center-of-mass energy W of the γN system in the range, 1.1–2.0 GeV. This energy range reflects the limitations of the data tables, as does the maximum value of pion angular momentum ($L = 5$) [69, 74].

We begin with an illustration of the electric multipole results, Eqs. (4.18)–(4.20). In Fig. 4.1 we plot the left-hand side (l.h.s.) and right-hand side (r.h.s.) of Eq. (4.18) for $L = 2$–5, and similarly for Eq. (4.19) with $L = 0$–5 in Figs. 4.2 and 4.3. It is immediately clear that the relations are convincing, particularly in the energy range below resonances. Recall that these relations follow from the isospin symmetry of isovector amplitudes and it is well established that isoscalar amplitudes are suppressed compared to isovector amplitudes. The $1/N_c$ expansion

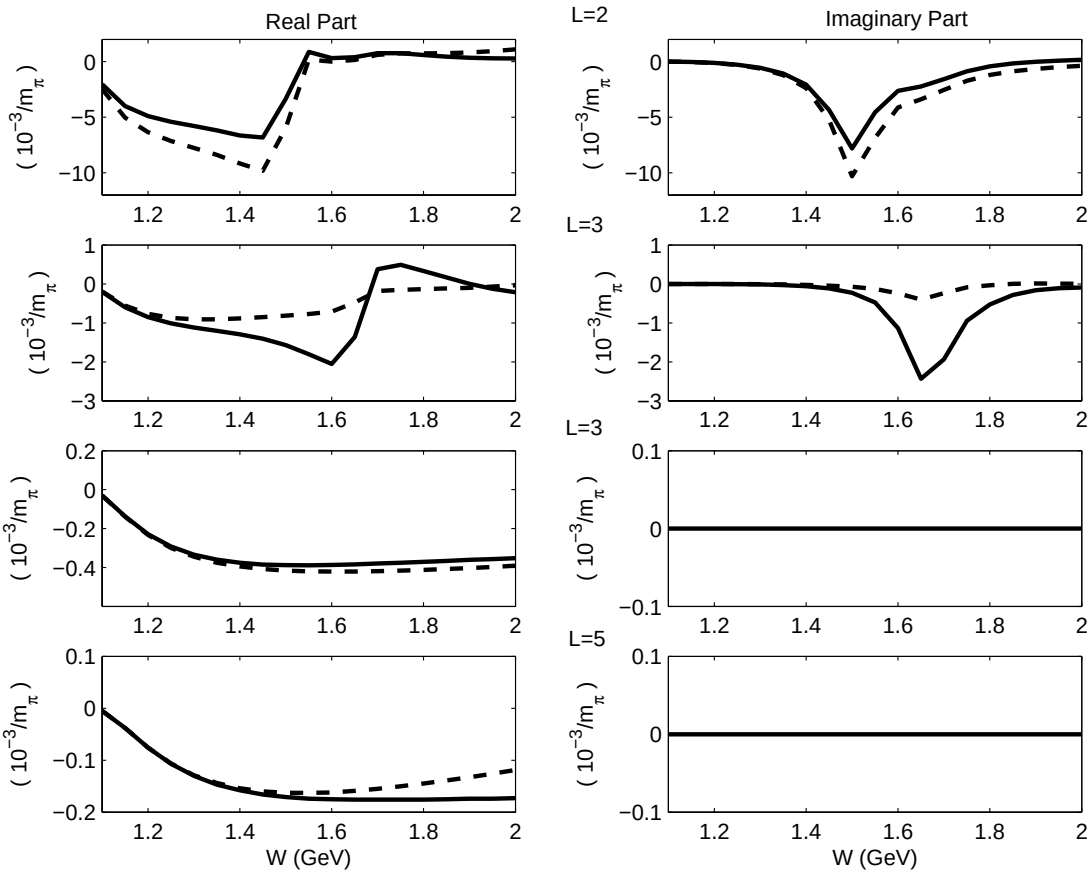

Figure 4.1: Experimentally determined electric multipoles provided by MAID [74]. The solid lines indicate the l.h.s. of Eq. (4.18), while the dashed lines indicate the r.h.s.

simply provides an expectation for the relative magnitude of the difference; indeed, the agreement often seems better than $1/N_c$, or 1 part in 3.

Comparing Eq. (4.20) with data is more difficult. One may, for example, superimpose plots of $E_{L\pm}^{p(\pi^0)p}$ with the corresponding charge-exchange amplitudes and ask whether the former are truly of order $O(N_c^{-1})$ smaller than the latter. Since both of these amplitudes have their own unique structure as functions of energy, an averaging procedure is necessary and a decisive result is not immediately

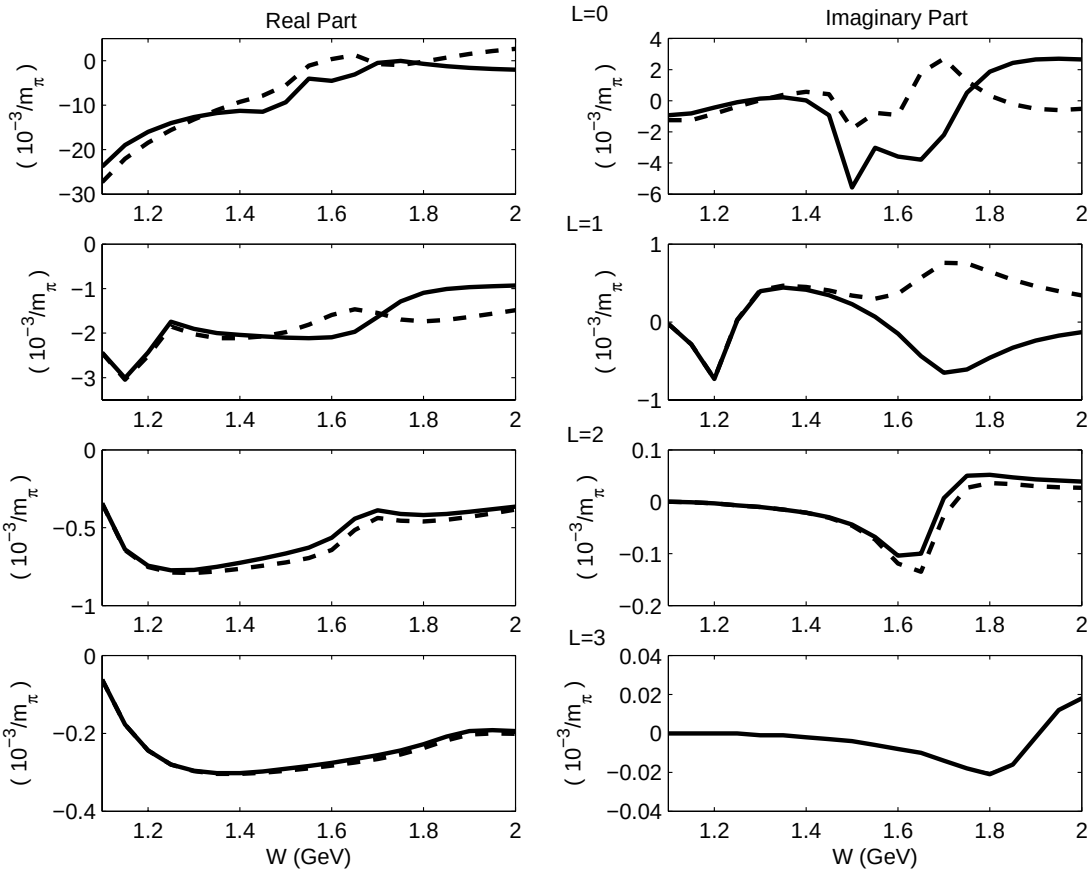

Figure 4.2: Experimentally determined electric multipoles provided by MAID [74]. The solid lines indicate the l.h.s. of Eq. (4.19), while the dashed lines indicate the r.h.s.

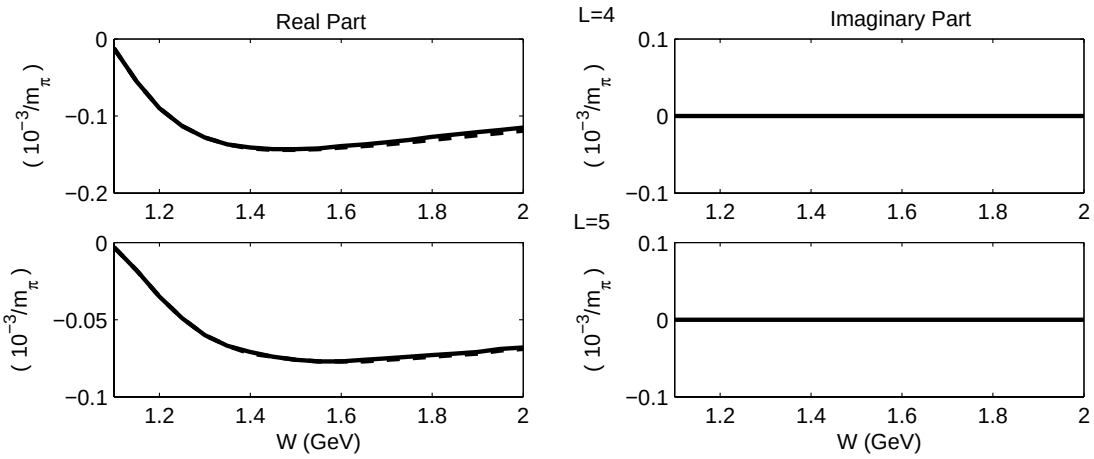

Figure 4.3: Experimentally determined electric multipoles provided by MAID [74]. The solid lines indicate the l.h.s. of Eq. (4.19), while the dashed lines indicate the r.h.s.

visible. We therefore do not include such plots in this thesis. Indeed, there are certain energy values where the $p(\pi^0)p$ electric multipoles are actually larger than their charged counterparts, particularly for the imaginary parts in the lower partial waves. However, the $p(\pi^0)p$ electric multipoles tend to be smaller overall at most energies, in general agreement with Eq. (4.20).

We next plot the two sides of the $p(\pi^0)p$ magnetic relation, Eq. (4.21) in Figs. 4.4 and 4.5 for $L=1$–5. Agreement for the $L=1$ partial wave is particularly poor because of the presence of the $\Delta^+(\mathrm{P}_{33})$ resonance at $W \approx 1.23$ GeV, which, in the large N_c limit, is a stable partner of the nucleons. As L increases, however, one observes an increasingly satisfactory comparison. Even in $L=2$, where the resonances $\mathrm{D}_{13}(1520)$ and $\mathrm{D}_{15}(1675)$ appear separated and quite different in amplitude, there is good reason for optimism as we show below in a resonance parameter test

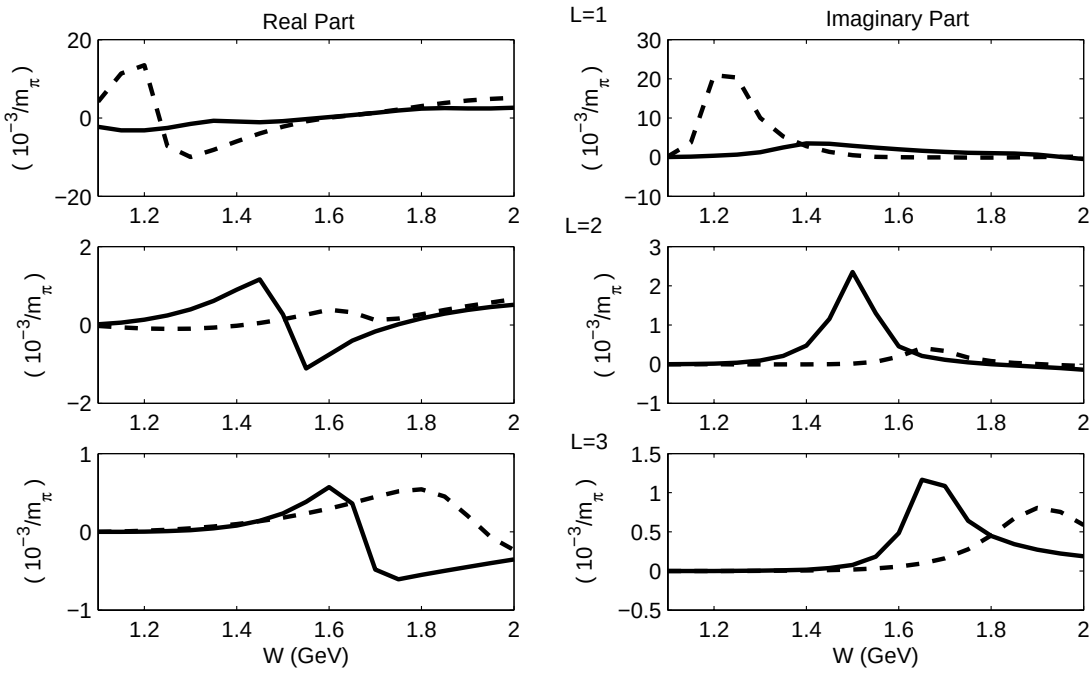

Figure 4.4: Experimentally determined magnetic multipoles provided by MAID [74]. The solid lines indicate the l.h.s. of Eq. (4.21), while the dashed lines indicate the r.h.s.

for the charge-changing magnetic multipoles.

Turning now to the charged magnetic multipole relations, we simultaneously test both LO [leftmost of Eq. (4.22)] and NLO [Eq. (4.23)] relations in a single set of plots for $L = 1$–5. It is appropriate to compare these relations, so we can test the extent to which a NLO relation is more experimentally effective than a LO one. In each plot, three curves appear corresponding to $M_{L-}^{p(\pi^+)n}$ [the l.h.s. of Eqs. (4.22) and (4.23)] and the r.h.s.'s of the LO and NLO relations. Since the NLO relations are more sensitive to the modeling effects of the data analysis, we present these combinations using both the MAID (Figs. 4.6 & 4.7) and the SAID (Fig. 4.8) data.

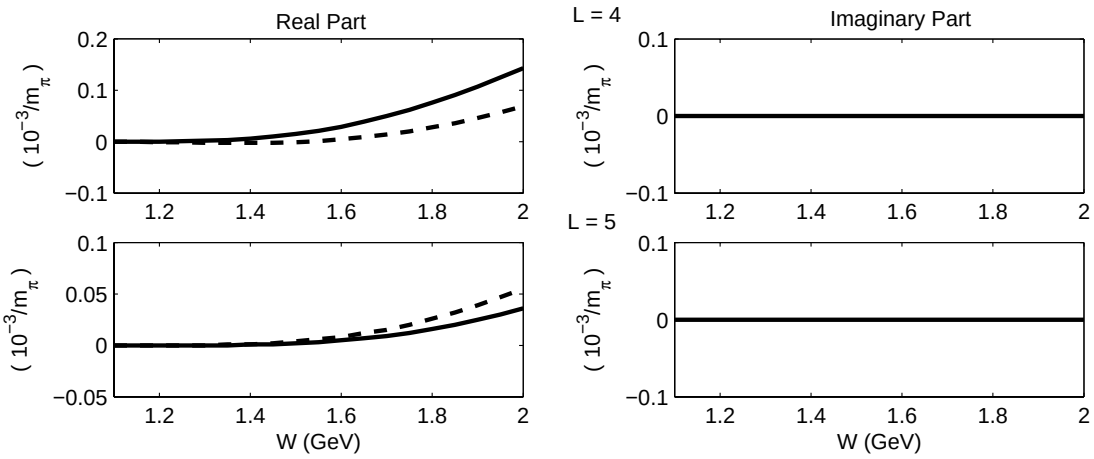

Figure 4.5: Experimentally determined magnetic multipoles provided by MAID [74]. The solid lines indicate the l.h.s. of Eq. (4.21), while the dashed lines indicate the r.h.s.

The SAID multipole amplitudes and the magnetic multipoles are related by:

$$M_{L\pm}^{p(\pi^+)n} = -\sqrt{2}\left(L_{1,\,2L\pm1}pM - \frac{1}{3}L_{3,\,2L\pm1}pM\right),$$
$$M_{L\pm}^{n(\pi^-)p} = +\sqrt{2}\left(L_{1,\,2L\pm1}nM + \frac{1}{3}L_{3,\,2L\pm1}nM\right).$$

One can draw several interesting conclusions from these figures. First, the LO relations definitely have merit, particularly in the energy range below the appearance of resonances. This is true for all partial waves, real and imaginary parts alike. However, the addition of the correction term to the NLO relation does not seem to greatly improve agreement between the two curves; indeed, in certain low partial waves (*e.g.*, $L=1$), the addition of NLO terms seems to make the agreement worse. However, a clue to what is happening may be inferred from the fact the NLO term in square brackets in Eq. (4.23) may introduce resonances completely absent from the LO term.

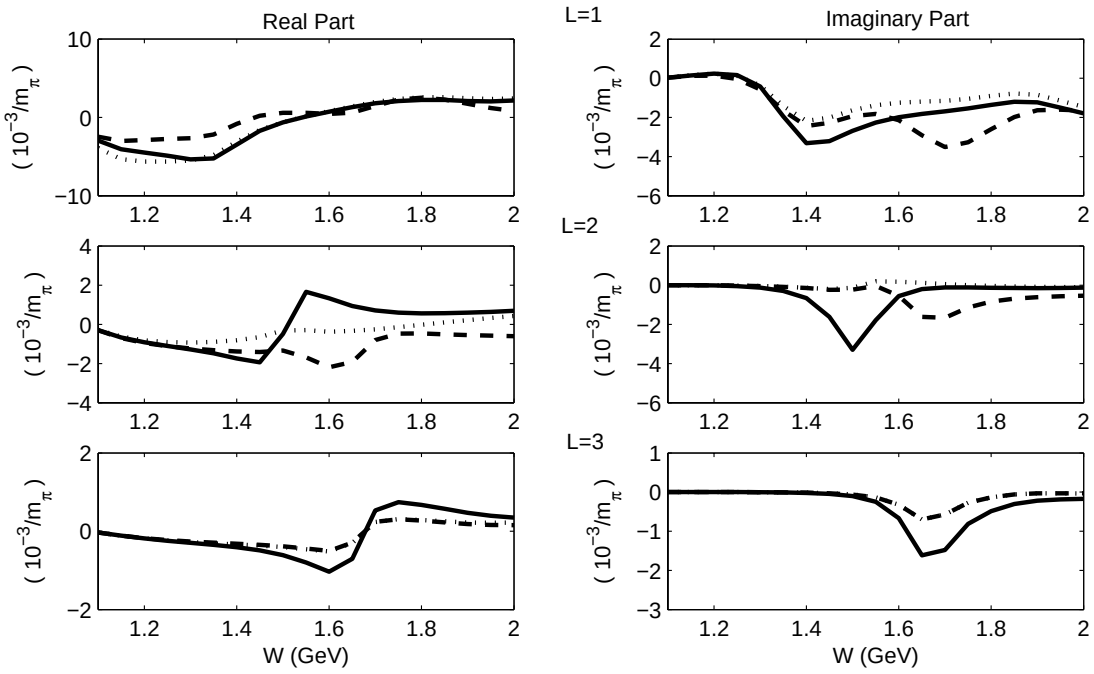

Figure 4.6: Experimentally determined magnetic multipoles provided by MAID [74]. The solid lines indicate the l.h.s. of Eqs. (4.22) and (4.23), while the dotted lines indicate the LO relation [first r.h.s. of Eq. (4.22)] and the dashed lines indicate the NLO relation [l.h.s. of Eq. (4.23)].

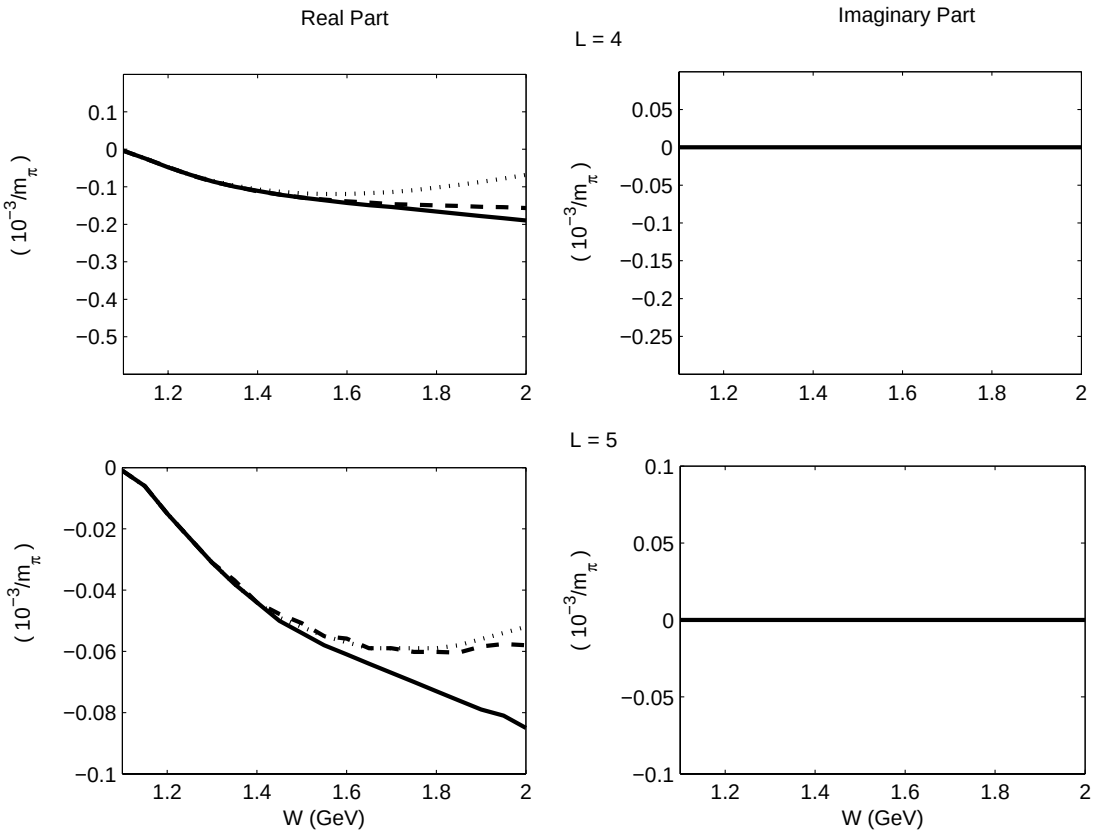

Figure 4.7: Experimentally determined magnetic multipoles provided by MAID [74]. The solid lines indicate the l.h.s. of Eqs. (4.22) and (4.23), while the dotted lines indicate the LO relation [first r.h.s. of Eq. (4.22)] and the dashed lines indicate the NLO relation [l.h.s. of Eq. (4.23)].

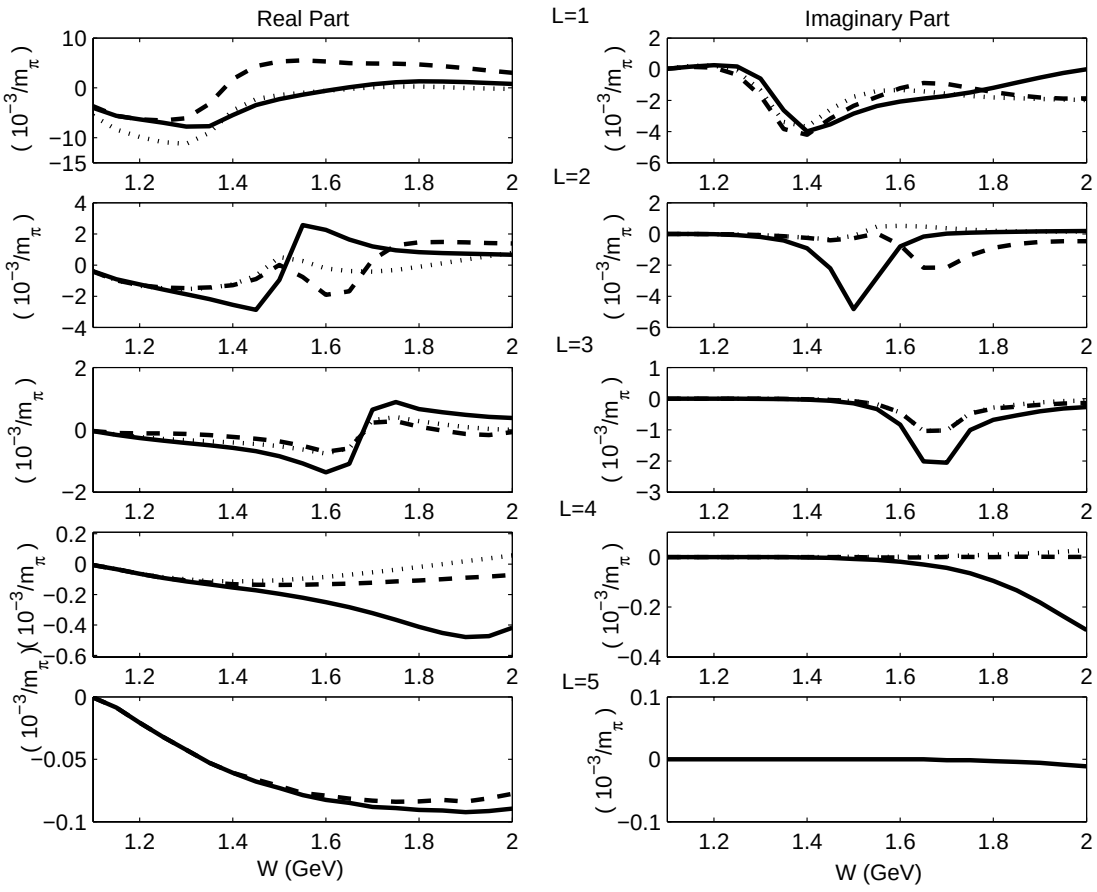

Figure 4.8: Experimentally determined magnetic multipoles provided by SAID [69]. As before, the solid lines indicate the l.h.s. of Eqs. (4.22) and (4.23), while the dotted lines indicate the LO relation [first r.h.s. of Eq. (4.22)] and the dashed lines indicate the NLO relation [l.h.s. of Eq. (4.23)].

These plots reveal the strong effect of resonances in the lower partial waves on the quality of our predictions. This was noted earlier by Schwesinger *et al.* [27] when they attempted to compare their Skyrme model relations with experiment. Rather than comparing the electromagnetic multipoles along the full energy range, they proposed an alternate testing method using the resonance parameters (obtainable through the helicity amplitudes) for the relevant resonances.

Such an approach is all the more sensible in the $1/N_c$ expansion, where resonances that would be degenerate in the large N_c limit may differ in mass by as much as 300 MeV. For example, the delta-nucleon mass difference of about 290 MeV is formally only an order $O(N_c^{-1})$ effect. One should not be surprised if LO and NLO terms differ by bumps that are shifted in energy with respect to each other.

One can proceed in a similar manner to that of Ref. [27], once Eqs. (4.22) and (4.23) are written in terms of the Walker helicity amplitudes [75] A^p, A^n, B^p, and B^n, which are, respectively, proportional to the helicity amplitudes $A^p_{1/2}$, $A^n_{1/2}$, $A^p_{1/2}$, and $A^n_{3/2}$ at each resonance given in the *Review of Particle Properties* [38]. In the present case, each of these amplitudes may have a total angular momentum of either $J = L \pm \frac{1}{2}$. The conversion between these amplitudes is outlined in Appendix D; the final result is:

$$[A^p - A^n]_{L-} + \frac{1}{2}(L-1)\,[B^p - B^n]_{L-} = 0 + O(N_c^{-1}), \tag{4.24}$$

and

$$\begin{aligned}&[A^p - A^n]_{L-} + \tfrac{1}{2}(L-1)\,[B^p - B^n]_{L-}\\ &+ [A^p - A^n]_{L+} - \tfrac{1}{2}(L+2)\,[B^p - B^n]_{L+} = 0 + O(N_c^{-2}).\end{aligned} \tag{4.25}$$

We now consider each partial wave and insert the resonance couplings for nearby $I=\frac{1}{2}$ resonances into the above formulas (paired $I=\frac{3}{2}$ resonances appear to occur too high in energy to significantly influence these plots). After consulting the *Review of Particle Properties* [38], one sees that only $L=2$ provides a meaningful test since $D_{13}(1520)$ and $D_{15}(1675)$ can be grouped together as distinct resonances (with a mass difference of about 155 MeV) appearing in one of the plotted partial waves. This is fortunate, because the $L=2$ plot is the most inconclusive of those discussed above (See Figs. 4.6 & 4.7 and 4.8). Resonances in other partial waves are either poorly resolved or separated too far apart to make a convincing match. We evaluate the l.h.s.'s of Eqs. (4.24) and (4.25), and also show in curly braces the sum of the absolute values of each term to demonstrate the extent of the cancellations. If the $1/N_c$ expression is working, the l.h.s. in the first should be about 1/3 of the corresponding factor in braces, and that in the second should be about 1/9. See Appendix D for details; the result is

$$\text{l.h.s.}\,(4.24) \;=\; -38.4 \pm 5.6 \;\; \{100.9\} \;\times 10^{-3}\,\text{GeV}^{-1}, \tag{4.26}$$

$$\text{l.h.s.}\,(4.25) \;=\; -18.2 \pm 8.5 \;\; \{140.2\} \;\times 10^{-3}\,\text{GeV}^{-1}. \tag{4.27}$$

Expressed as absolute value ratios, the results are 0.38 ± 0.06 and 0.13 ± 0.06, respectively. Noting that $1/N_c \approx 0.33$ and $1/N_c^2 \approx 0.11$, one sees that the behavior is exactly what one would expect from the $1/N_c$ expansion. We conclude that Eq. (4.23) and the $1/N_c$ expansion work well, even though the presence of somewhat separated resonances obscures agreement over the full energy range.

4.4 Summary

In this chapter, we have shown that the symmetries of large N_c QCD create linear dependence among amplitudes for pion photoproduction, using the techniques of the previous chapter. This allows us to derive model-independent linear relations that can be directly confirmed with experimental data. The agreement between our predictions and experiments is very satisfactory and gives us further encouragement for the $1/N_c$ expansion as a powerful tool for understanding hadronic physics.

Appendix A

The Role of Spurious Modes in Excited Baryon Descriptions

In Chapter 2, we showed that certain operators in a general quark model Hamiltonian can connect states of different spin-flavor symmetry. This has been shown for all values of the excited quark's orbital angular momentum, l. The case of $l = 1$, however, requires special attention due to the issue of spurious states.

Traditionally, one attempts to calculate the states of an N_c-body field theory within a single-particle potential model such as the Hartree-Fock, Tamm-Dancoff, or random-phase approximation [76]. In each case, a spurious state corresponding to the collective motion of the particles' center of mass is generated. Its appearance can be traced to a violation of translational invariance that occurs in solving for the states when one replaces a translationally invariant many-body problem with a shell model which violates translational invariance. This state is not a genuine excitation of the quarks and should be disregarded. We note that since the spurious center of mass motion is vectorial in nature (it is associated with the total momentum, $\vec{P}$), one expects that it manifests itself only in channels that transform vectorially, which means the $\ell = 1$ channels.

A systematic method for isolating the spurious states has not been established. One must first calculate all the states and then find those that are simply translations of the center of mass. However, the spurious states generated by the random-phase

approximation (RPA) can easily be eliminated by rejecting solutions to the RPA equations having a zero energy eigenvalue [77]. Procedures relying on 'conserving approximations' that maintain 'consist symmetries' at each step in the calculation yield spurious states also. However, to their advantage, these procedures may allow one to quickly identify a spurious state; for example, as a zero-energy pole in the particle-hole Green's function [76]. We emphasize that in all cases the spurious states and their properties are only revealed after the complete calculation.

Once a spurious state is identified, the behavior of its spin-flavor wavefunction under permutation can be determined. There is no *a priori* method for determining the spin-flavor symmetry of the spurious state before the complete calculation. However, it is known that in a harmonic oscillator basis, the $l = 1$ spurious mode has a spin-flavor symmetry that is symmetric under permutation [78]. This has led some to believe that $l = 1$ symmetric states may be immediately discarded on the grounds that they do not represent internal excitations. We know that this is not a generally valid way to proceed prior to enumerating all the states.

The problem of spurious modes as discussed here is generic in quark-shell models. In principle, it is separate from the issue of relevance to this thesis, that of whether the spin-flavor symmetric and mixed-symmetric states mix strongly in forming the physical excited baryon states. One should follow the strategy given above: Using the quark-shell model, calculate all of the $\ell = 1$ modes and discard the ones that are mostly spurious. The general arguments given in Sec. 2.3 show that the states so generated have strong mixing of order $O(N_c^0)$, and this is sufficient for our purpose. One expects the physical $\ell = 1$ state to exhibit strong mixing between

states of different spin-flavor symmetries, and hence one expects the states to have decay widths of order $O(N_c^0)$.

Thus, we conclude that our previous arguments are valid even for $\ell = 1$ states. We note, however, that the entire issue is moot. At the end of the day, the problem of spurious states is a disease of quark-shell models. They appear in translationally-invariant quark models with *ad hoc* truncations that create them. Of course, we introduced these models following the treatment of Ref. [33] and then generalized them to show that quark-shell models have mixing of order $O(N_c^0)$ between different spin-flavor symmetries. Such models are computationally tractable. Of course, in principle one may use *any* model consistent with large N_c QCD scaling to establish this point. Ideally, one should consider models that do not suffer from the spurious mode problem, in order to completely avoid the issue. One might consider, for example, a translationally invariant model of N_c quarks interacting among themselves. Such a model obviously has the drawback that it is computationally hard to solve. However, for our purposes the only issue of relevance is whether quark spin, $\mathbf{S}$, is a good quantum number. If the model has tensor interactions between quarks at leading order [which is $1/N_c$, leading to order $O(N_c^0)$ matrix elements when quark combinatorics are included], then quark spin is not a good quantum number, and even in the absence of explicit computation one expects generic mixing of order $O(N_c^0)$ between states of different spin-flavor symmetry.

-.-

Appendix B

Wigner's 6j Symbols and their Applications

This appendix is meant to serve as an introduction to the group theory required to derive Eq. (3.1). We will discuss the Wigner $6j$ symbol and its properties and the crossing relations for quantum numbers between different scattering channels. Most of the material from this appendix can be found in Ref. [79].

Consider the addition of three angular momenta (j_1, j_2, j_3) to form the sum, J: $J = j_1 + j_2 + j_3$. There is no unique way to combine the three angular momenta due to the associative nature of vector addition. In fact, we can imagine two distinct coupling schemes, as depicted in Fig. B.1 [80]:

$$\text{(a)} \quad j_{12} = j_1 + j_2, \;\; j_{12} + j_3 = J, \tag{B.1}$$

$$|(j_1 j_2) j_{12}, j_3; JM\rangle = \sum_{\substack{m_1 m_2 \\ m_3 \mu_{12}}} \langle j_1 j_2; m_1 m_2 | j_{12} \mu_{12}\rangle \, \langle j_{12} j_3; \mu_{12} m_3 | JM\rangle \, | \, m_1 m_2 m_3 \rangle \, ,$$

$$\text{(b)} \quad j_{23} = j_2 + j_3, \;\; j_1 + j_{23} = J, \tag{B.2}$$

$$|j_1, (j_2 j_3) j_{23}; JM\rangle = \sum_{\substack{m_1 m_2 \\ m_3 \mu_{23}}} \langle j_2 j_3; m_2 m_3 | j_{23} \mu_{23}\rangle \, \langle j_1 j_{23}; \mu_1 m_{23} | JM\rangle \, | \, m_1 m_2 m_3 \rangle \, .$$

For each coupling scheme, we show the basis kets in the $(2j_1+1)(2j_2+1)(2j_3+1)$-dimensional space spanned by the vectors, $| \, m_1 m_2 m_3\rangle \equiv | \, j_1 m_1\rangle \, | \, j_2 m_2\rangle \, | \, j_3 m_3\rangle$. The two representations below Eqs. (B.1) and (B.2) are connected by a unitary transformation. The coefficients of this unitary transformation are given in terms of the Wigner $6j$ symbol:

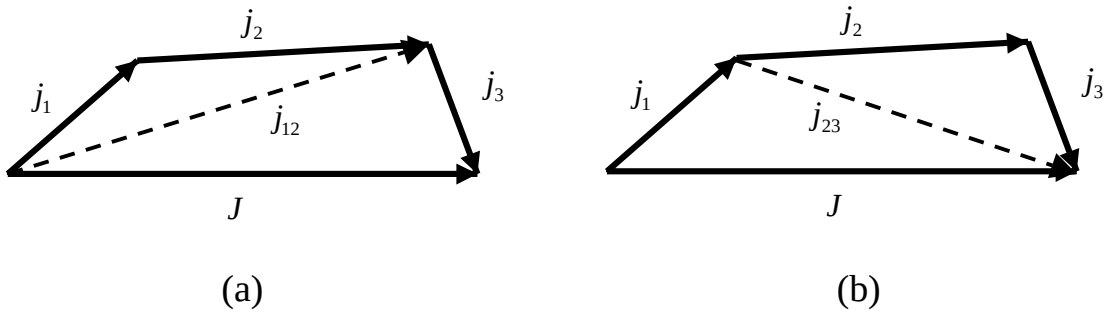

Figure B.1: The two different coupling schemes from Eqs. (B.1) and (B.2).

$$|(j_1 j_2) j_{12}, j_3; JM\rangle = \sum_{j_{23}} \sqrt{(2j_{12}+1)(2j_{23}+1)}(-1)^{j_1+j_2+j_3+J} \times \left\{ \begin{array}{ccc} j_1 & j_2 & j_{12} \\ j_3 & J & j_{23} \end{array} \right\} |j_1, (j_2 j_3) j_{23}; JM\rangle \,. \tag{B.3}$$

This is the defining relation for the $6j$ symbol, denoted by the curly brackets; the other factors are chosen so that the $6j$ symbol has useful symmetry properties to be discussed below. We note that it is possible to relate $6j$ symbols to Clebsch-Gordan coefficients [79]. The $6j$ symbol is important in all situations where angular momenta are being recoupled; even when there are more than three angular momenta.

The $6j$ symbol has many interesting properties that are relevant for this thesis. Foremost, the $6j$ symbol is a real number and is non-zero only when four triangle rules are satisfied:

$$\left\{ \begin{array}{ccc} j_1 & j_2 & j_{12} \\ j_3 & J & j_{23} \end{array} \right\} \propto \delta(j_1 j_2 j_{12}) \delta(j_2 j_3 j_{23}) \delta(j_1 j_{23} J) \delta(j_{12} j_3 J), \tag{B.4}$$

where $\delta(abc) = 1$ if c is among the set $\{a+b,\, a+b-1, \cdots,\, |a-b|+1,\, |a-b|\}$ and is zero otherwise. The $6j$ symbols encode two symmetries under a permutation of the

elements. Namely, the $6j$ symbol is invariant under a permutation of its columns and an exchange of two elements in the top row with the corresponding elements in the bottom row. A nice way to summarize these symmetries is to say that the six angular momenta (j_1, j_2, j_3, j_{12}, j_{23}, J) form the sides of a tetrahedron.

In Sec. 3.3, these symmetries were used to describe the behavior of the reduced amplitudes under the time-reversal operation. The main point is that the product of $6j$ symbols in Eq. (3.1) is invariant under time-reversal because of the permutation symmetry discussed above. That is,

$$\left\{ \begin{array}{ccc} I_\pi & R' & I_s \\ R & I_\pi & \mathcal{J} \end{array} \right\} \left\{ \begin{array}{ccc} L' & R' & J_s \\ R & L & \mathcal{J} \end{array} \right\} = \left\{ \begin{array}{ccc} I_\pi & R & I_s \\ R' & I_\pi & \mathcal{J} \end{array} \right\} \left\{ \begin{array}{ccc} L & R & J_s \\ R' & L' & \mathcal{J} \end{array} \right\}. \tag{B.5}$$

In Sec. 4.1, the case for $I_\gamma = 0$ requires the explicit form of the $6j$ symbol with a zero element. This has a compact closed form:

$$\left\{ \begin{array}{ccc} j & j' & 0 \\ J & J' & g \end{array} \right\} = (-1)^{j+J+g} \frac{\delta_{jj'}\delta_{JJ'}}{\sqrt{(2j+1)(2J+1)}}\, \delta(jJg). \tag{B.6}$$

Other values for the $6j$ symbols have been tabulated and can be found in ancient texts or with computer programs.

The $6j$ symbols find many applications in atomic and molecular spectroscopy and scattering. We focus on hadronic scattering due to its relevance to Chapters 3 and 4. Consider the three ways to describe a two-body scattering event (See Fig. B.2), called a channel: s, t, u.

$$\begin{aligned} (s) \quad & A + B \to C + D, \\ (t) \quad & A + \bar{C} \to \bar{B} + D, \\ (u) \quad & A + \bar{D} \to \bar{B} + C. \end{aligned} \tag{B.7}$$

Each channel is characterized by an amplitude that depends on the set of angular momentum and isospin quantum numbers, including the total spin and isospin. Crossing between any two channels (*i.e.*, projecting the quantum numbers for one channel into another) involves disentangling the vector sums and re-coupling them; this is accomplished with a $6j$ symbol. The channels that concern us most for hadronic scattering are the s- and t-channel (See Fig. B.2). Let us first consider only the isospin quantum numbers that describe this channel. We will denote the total isospin by I_s, I_t for the s- and t-channel, respectively. The isospin for each particle in Eqs. (B.7) is denoted by its label (A, B, C, or D) in a subscript. The amplitude describing the s-channel process is $A_s(I_s)$, and similarly for the t-channel. They are related in general by

$$A_s(I_s) = \sum_{I_t} (X_{st})_{I_s,\, I_t} A_t(I_t), \tag{B.8}$$

where the crossing matrix $(X_{st})_{I_s,\, I_t}$ is given by [60]

$$(X_{st})_{I_s,\, I_t} = \xi_{st}(2I_t + 1) \begin{Bmatrix} I_A & I_B & I_s \\ I_D & I_C & I_t \end{Bmatrix}. \tag{B.9}$$

The phase, ξ_{st}, depends on whether particles B and C have integer or half-integer quantum numbers. For our case of πN scattering and pion photoproduction, B is a nucleon with half-integer spin and isospin and C is a pion or photon with integer spin and isospin. Therefore, we have [60] $\xi_{st} = (-1)^{I_s + I_t + I_B}$.

We now have the tools needed to derive the S matrix expansion in Chapter 3. We use the crossing relations in both spin and isospin space to obtain Eq. (3.1). We begin in the t-channel of πN scattering and define the scattering amplitude as

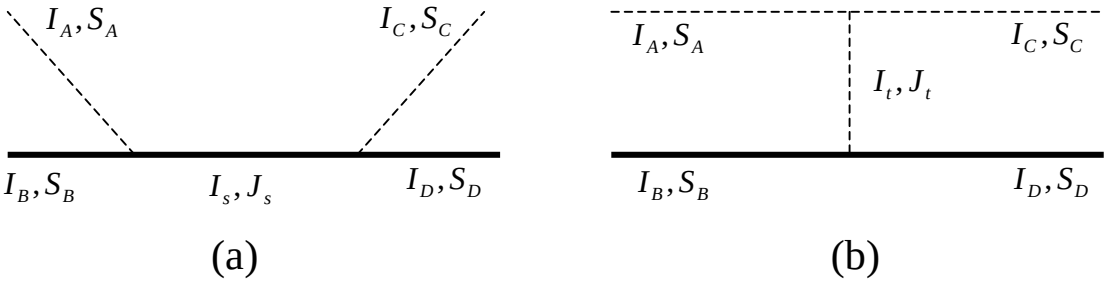

Figure B.2: (a) The s-channel versus (b) t-channel meson-baryon scattering diagrams. The solid lines are baryons with isospin I_B, I_D and spin S_B, S_D. The dashed lines are mesons with isospin I_A, I_C and spin S_A, S_C. The I_s, J_s and I_t, J_t are the total isospin and spin in their respective channels.

$\bar{s}^t_{I_t J_t L L' R R'}$. Crossing to the s-channel in both spin and isospin space with Eqs. (B.8) and (B.9) yields

$$\begin{aligned} S_{LL'RR'I_sJ_s} &= \textstyle\sum_{I_tJ_t}(-1)^{(I_t+J_t+I_s+J_s+2R')}(2I_t+1)(2J_t+1) \\ &\times \begin{Bmatrix} I_\pi & R' & I_s \\ R & I_\pi & \mathcal{J} \end{Bmatrix} \begin{Bmatrix} L' & R' & J_s \\ R & L & \mathcal{J} \end{Bmatrix} \bar{s}^t_{I_tJ_tLL'RR'}. \end{aligned} \tag{B.10}$$

According to the $I_t = J_t$ rule of large N_c QCD [20], we can define the t-channel amplitude, $\tilde{s}^t_{\mathcal{J}LL'RR'}$ with $\mathcal{J} \equiv I_t = J_t$, and eliminate one of the summation indices. This gives us

$$\begin{aligned} S_{LL'RR'I_sJ_s} &= \textstyle\sum_{\mathcal{J}}(-1)^{(2\mathcal{J}+I_s+J_s+2R')}(2\mathcal{J}+1)^2 \\ &\times \begin{Bmatrix} I_\pi & R' & I_s \\ R & I_\pi & \mathcal{J} \end{Bmatrix} \begin{Bmatrix} L' & R' & J_s \\ R & L & \mathcal{J} \end{Bmatrix} \tilde{s}^t_{\mathcal{J}LL'RR'}. \end{aligned} \tag{B.11}$$

This expression is equivalent to Eq. (3.1), though further simplification is possible. As indicated in Sec. 3.2, the baryon wave functions can be used to factor out the

$\{R\,R'\}$ dependence on the amplitude,

$$\tilde{s}^t_{\mathcal{J}LL'RR'} = (-1)^{2(R+R')}\sqrt{(2R+1)(2R'+1)}\hat{s}^t_{\mathcal{J}LL'}. \tag{B.12}$$

In order to produce an expression that explicitly displays only the relevant factors, we define the $[6j]$ symbols:

$$\left\{ \begin{array}{ccc} a & b & e \\ c & d & f \end{array} \right\} \equiv \frac{(-1)^{-(b+d+e+f)}}{([a][b][c][d])^{1/4}} \left[\begin{array}{ccc} a & b & e \\ c & d & f \end{array} \right], \tag{B.13}$$

where $[X] \equiv 2X+1$. The normalization and phases of the $[6j]$ symbol cancel many unimportant factors in our expression. Factors which are introduced by the $[6j]$ symbols can be conveniently absorbed into the definition of the *reduced amplitude*, $s^t_{\mathcal{J}LL'}$. The final result is simply Eq. (3.1).

Appendix C

Plots of Leading Order Pion-nucleon Scattering Relations

In Sec. 3.3, we presented linear relations among partial-wave amplitudes for πN scattering. Equations (3.5)–(3.13) hold to leading order in the $1/N_c$ expansion and can be tested with experimental data [69]. In this appendix, we display additional plots of the linear relations to supplement those offered in Sec. 3.3. We hope these will help develop a better appreciation for the quality of experimental agreement for the leading order predictions.

Evaluating Eq. (3.6) for $L = 0$ yields the prediction: $S_{31} = S_{11}$. This equality is also known as the Chew-Low theorem [81] and is plotted in Fig. C.1.

Evaluating Eq. (3.5) for $L = 1$ yields $P_{31} = P_{13}$, shown in Fig. C.2.

Evaluating Eq. (3.5) for $L = 3$ yields $F_{35} = \frac{1}{7}F_{15} + \frac{6}{7}F_{17}$, shown in Fig. C.3.

To test Eq. (3.13) with available data, we must combine Eqs. (3.5)–(3.8) to eliminate the partial waves that are absent in the data tables. Since all these rela-

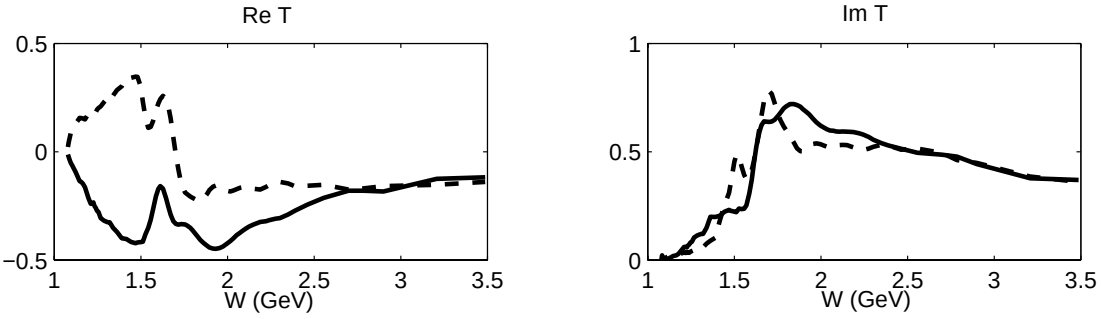

Figure C.1: The solid line is S_{31} and the dashed line is S_{11}.

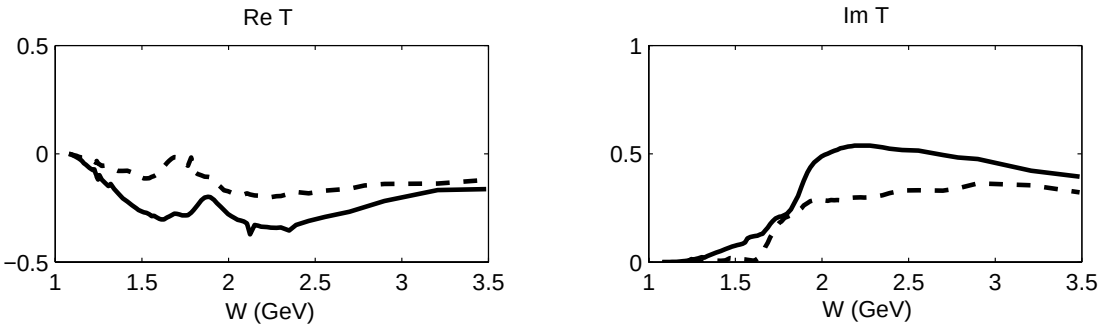

Figure C.2: The solid line is P_{31} and the dashed line is P_{13}.

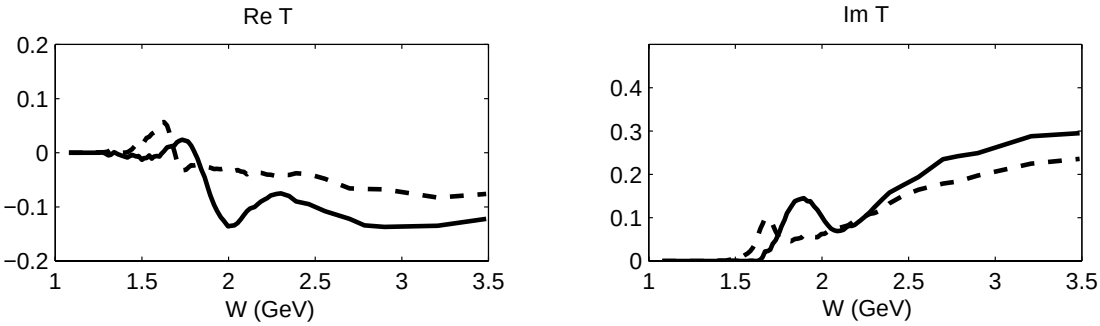

Figure C.3: The solid line is F_{35} and the dashed line is the linear combination $\frac{1}{7}F_{15} + \frac{6}{7}F_{17}$.

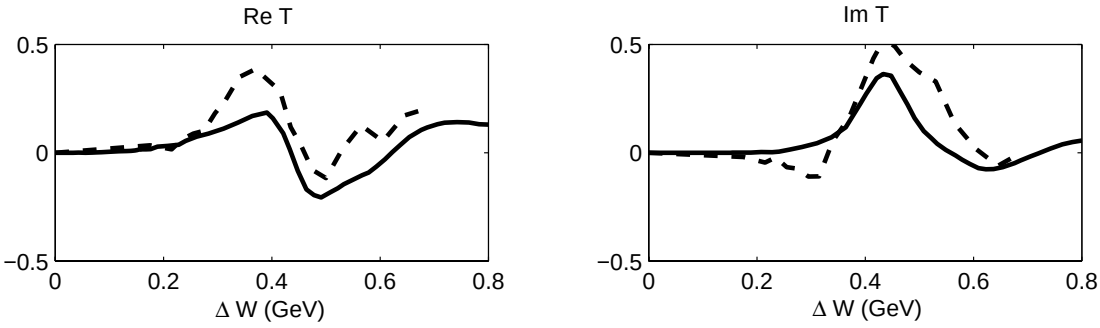

Figure C.4: The solid line is $\frac{1}{\sqrt{2}}(D_{13} - D_{33})$ and the dashed line is the linear combination $\frac{9}{10\sqrt{2}}DD_{13} + \frac{9\sqrt{7}}{20}DD_{15}$.

tions hold to leading order in $1/N_c$, the final relation will also hold to this order. An example for $L = 2$ is $\frac{1}{\sqrt{2}}(D_{13} - D_{33}) = \frac{9}{10\sqrt{2}} DD_{13} + \frac{9\sqrt{7}}{20} DD_{15}$, shown in Fig. C.4.

-.-

Appendix D

Resonant Parameter Test

This appendix is a guide to the resonant parameter test of pion photoproduction introduced in Chapter 4 (Sec. 4.3) with the goal of understanding the arithmetic that leads to the calculations of Eqs. (4.26) and (4.27). The procedure is to change the basis of our linear relations from magnetic multipoles $M_{L\pm}$ to helicity amplitudes. Helicity is the projection of the system's total spin vector along the photon's direction of propagation. For the γN system, the helicity has a total of four possible values $\{-\frac{3}{2}, -\frac{1}{2}, \frac{1}{2}, \frac{3}{2}\}$. These reduce to two values $\{\frac{1}{2}, \frac{3}{2}\}$ once we account for the parity and time-reversal invariance of the strong and electromagnetic interactions. Helicity amplitudes are numbers that parameterize the resonant part of a multipole at the resonance energy. The relationship between the helicity amplitudes and multipoles will become clear as we change bases.

We begin by introducing the Walker helicity elements [75], $A_{L\pm}$ and $B_{L\pm}$ for total angular momentum $J = L \pm \frac{1}{2}$. The labels A and B refer to an initial γN state with helicity $\frac{1}{2}$ and $\frac{3}{2}$, respectively. They are related to the magnetic multipoles for $L \geq 1$ by [Ref. [75], Eq. (25)]:

$$M_{L+} = \frac{1}{L+1}\left[A_{L+} - \frac{1}{2}(L+2)B_{L+}\right], \tag{D.1}$$

$$M_{L-} = \frac{1}{L}\left[A_{L-} + \frac{1}{2}(L-1)B_{L-}\right]. \tag{D.2}$$

These should be regarded as eight equations: two for each of the four possible pion

photoproduction reactions.

We now decompose the Walker helicity elements (represented collectively by the symbol $\mathcal{A}$) in isospin space for the individual charge-exchange channels: $\mathcal{A}(\gamma p \to \pi^+ n) = \sqrt{1/3}\,\mathcal{A}^\Delta + \sqrt{2/3}\,\mathcal{A}^p$ and $\mathcal{A}(\gamma n \to \pi^- p) = \sqrt{1/3}\,\mathcal{A}^\Delta - \sqrt{2/3}\,A^n$, where $\mathcal{A}^\Delta$ is the amplitude for the reaction with an $I = \frac{3}{2}$ intermediate state and $\mathcal{A}^p$ ($\mathcal{A}^n$) is for an $I = \frac{1}{2}$ intermediate state with a proton (neutron) in the initial state. Substituting these formulas and cancelling a common $(1/L)(\sqrt{2/3})$ factor yields our penultimate result, Eqs. (4.24) and (4.25).

The Walker helicity elements evaluated at a resonant energy (W_R) can be then be written in terms of helicity amplitudes $A^p_{1/2}$, $A^p_{3/2}$, $A^n_{1/2}$, and $A^n_{3/2}$, whose numerical values are tabulated in Ref. [38] for many baryons. The subscript indicates the helicity of the state, while the superscript indicates the initial nucleon. The relationship between these two representations is given by Eqs. (9.8) and (9.9) of Ref. [27]:

$$\begin{aligned} \text{Im } A^{p,n}_{L\pm}\Big|_{W_R} &= \mp f A^{p,n}_{1/2}\ , \\ \text{Im } B^{p,n}_{L\pm}\Big|_{W_R} &= \pm f \sqrt{\frac{16}{(2J-1)(2J+3)}}\, A^{p,n}_{3/2}\ , \\ f &= \sqrt{\frac{1}{(2J+1)\pi}\frac{k_\gamma}{k_\pi}\frac{m_N}{m_R}\frac{\Gamma_\pi}{\Gamma^2}}\ . \end{aligned} \tag{D.3}$$

The k_γ and k_π are the momenta magnitudes in the center-of-mass frame of the photon and pion, respectively. These are given by a straightforward kinematic calculation:

$$k_b = \frac{\sqrt{[m_R^2 - (m_N - m_b)^2][m_R^2 - (m_N + m_b)^2]}}{2m_R}, \tag{D.4}$$

where the subscript b stands for the photon ($m_\gamma = 0$ GeV) or the pion ($m_\pi \approx$

0.139 GeV). The m_N and m_R are the nucleon ($m_N \approx 0.939$ GeV) and resonance masses, and Γ_π and Γ are the pionic and total widths of the resonance, respectively.

While the pion photoproduction linear relations derived in Chapter 4 hold for all energy values, the resonance parameter approach assumes that we evaluate the amplitudes at a single resonance energy. To consistently implement this approach, we need to pick baryons from the spectrum that share a common resonance energy (*i.e.*, have similar masses). For our purposes, a mass difference on the order of the delta-nucleon splitting ($\sim$ 290 MeV) is reasonable in light of large N_c QCD. As pointed out in Chapter 4, the baryons $D_{13}(1520)$ and $D_{15}(1675)$ fit this criteria for $L = 2$. The data for these baryons is presented in Table D.1. The results of Eqs. (4.26) and (4.27) now follow from trivial substitution.

State	λ	A^p_λ ($10^{-3}\text{GeV}^{-1/2}$)	A^n_λ ($10^{-3}\text{GeV}^{-1/2}$)	Γ (GeV)	Γ_π/Γ	k_γ (GeV)	k_π (GeV)
$D_{13}(1520)$	$\frac{1}{2}$	-24 ± 9	-59 ± 9	0.120	0.55	0.470	0.456
	$\frac{3}{2}$	$+166 \pm 5$	-139 ± 11				
$D_{15}(1675)$	$\frac{1}{2}$	$+19 \pm 8$	-43 ± 12	0.150	0.45	0.576	0.565
	$\frac{3}{2}$	$+15 \pm 9$	-58 ± 13				

Table D.1: Helicity amplitudes, decay widths, and momenta for $L = 2$ resonances [38]. The momenta are calculated from Eq. (D.4).

-.-

BIBLIOGRAPHY

[1] H. Fritzsch, M. Gell-Mann, H. Leutwyler, Phys. Lett. **B47**, 365 (1973).

[2] O.W. Greenburg, Phys. Rev. Lett. **13**, 598 (1964).

[3] H.D. Politzer, Phys. Rev. Lett. **30**, 1346 (1973).

D.J. Gross and F. Wilczek, Phys. Rev. Lett. **30**, 1346 (1973).

[4] J.D. Bjorken, Phys. Rev. **179**, 1547 (1969).

R.P. Feynman, Phys. Rev. Lett. **23**, 1415 (1969).

[5] M.E. Peskin and Schroeder, *An Introduction to Quantum Field Theory* (Perseus, New York, 1995).

[6] M. Gell-Mann and Y. Ne'eman, *The Eightfold Way* (Benjamin, New York, 1965).

[7] A. Chodos, R.L. Jaffe, K. Johnson, C.B. Thorn, and V. Weisskopf, Phys. Rev. D **9**, 3471 (1974).

A. Chodos, R.L. Jaffe, K. Johnson, and C.B. Thorn, Phys. Rev. D **10**, 2599 (1974).

[8] J. Sakurai, Ann. Phys. **11**, 1 (1960).

J. Sakuari, *Currents and Mesons* (University of Chicago Press, 1969).

[9] G.T.H. Skyrme, Proc. R. Soc. London **A260**, 127 (1961).

[10] I. Zahed, G.E. Brown, Phys. Reports **142**, 1 (1986).

[11] E. Witten, Nucl. Phys. **B223**, 422 (1983).

E. Witten, Nucl. Phys. **B223**, 433 (1983).

[12] G. Adkins, C. Nappi, and E. Witten, Nucl. Phys. **B228**, 552 (1983).

[13] Cheng and Li, *Gauge Theory of Elementary Particle Physics* (Clarendon Press, London, 1984).

[14] S. Weinberg, Phys. Rev. Lett. **17**, 616 (1966).

Y. Tomozawa, Nuovo Cimento **46A**, 707 (1966).

[15] H.J. Rothe, *Lattice Gauge Theories: An Introduction* (World Scientific, New Jersey, 1997).

[16] G. 't Hooft, Nucl. Phys. **B72**, 461 (1974).

[17] E. Witten, Nucl. Phys. **B160**, 57 (1979).

[18] A. Belitsky and T.D.Cohen, Phys. Rev. C **65**, 064008 (2002).

[19] M.K. Banerjee, T.D. Cohen, and B.A. Gelman, Phys. Rev. C **65**, 034011 (2002).

[20] D.B. Kaplan and A.V. Manohar, Phys. Rev. C **56**, 76 (1997).

[21] T.D. Cohen and B.A. Gelman, Phys. Lett. **B540**, 227 (2002).

[22] T.D. Cohen and D.C. Dakin, Phys. Rev. C **68**, 017001 (2003).

[23] S. Coleman, *Aspects of Symmetry* (Cambridge University Press, New York, 1985).

[24] M.P. Mattis and M.E. Peskin, Phys. Rev. D **32**, 58 (1985).

[25] A. Hayashi, G. Eckart, G. Holzwarth, and H. Walliser, Phys. Lett. B **147**, 5 (1984).

[26] C. Eckart and B. Schwesinger, Nucl. Phys. **A458**, 620 (1986).

[27] B. Schwesinger, H. Weigel, G. Holzwarth, and A. Hayashi, Phys. Reports **173**, 173 (1989).

[28] G. S. Adkins and C. R. Nappi, Nucl. Phys. **B249**, 507 (1985).

[29] R.F. Dashen, E. Jenkins, and A.V. Manohar, Phys. Rev. D **49**, 4713 (1994).

[30] J.-L. Gervais and B. Sakita, Phys. Rev. Lett. **52**, 87 (1984); Phys. Rev. D **30**, 1795 (1984).

[31] R.F. Dashen and A.V. Manohar, Phys. Lett. B **315**, 425 (1993); **315**, 438 (1993).

[32] D.B. Kaplan and M.J. Savage, Phys. Lett. B **365**, 244 (1996)

[33] D. Pirjol and T.-M. Yan, Phys. Rev. D **57**, 1449 (1998).

[34] T.D. Cohen and R.F. Lebed, Phys. Rev. D 70, 096015 (2004); hep-ph/0504200 (2005).

[35] T.D. Cohen, D.C. Dakin, R.F. Lebed, and A. Nellore, Phys. Rev. D **70**, 056004 (2004).

[36] T.D. Cohen, D.C. Dakin, R.F. Lebed, and A. Nellore, Phys. Rev. D **69**, 056001 (2004).

[37] T.D. Cohen, D.C. Dakin, R.F. Lebed, and D.R. Martin, Phys. Rev. D **71**, 076010 (2005).

[38] Particle Data Group, Phys. Lett. B **592**, 1 (2004).

[39] T.D. Cohen and R.F. Lebed, Phys. Rev. D **67**, 096008 (2003); Phys. Rev. Lett. **91**, 012001 (2003); Phys. Rev. D **68**, 056003 (2003).

[40] C.E. Carlson, C.D. Carone, J.L. Goity, and R.F. Lebed, Phys. Rev. D **59**, 114008 (1999).

[41] C.E. Carlson, C.D. Carone, J.L. Goity, and R.F. Lebed, Phys. Lett. B **438**, 327 (1998).

[42] C.D. Carone, H. Georgi, L. Kaplan, and D. Morin, Phys. Rev. D **50**, 5793 (1994).

[43] J.L. Goity, Phys. Lett. B **414**, 140 (1997).

[44] C.L. Schat, J.L. Goity, and N.N. Scoccola, Phys. Rev. Lett. **88**, 102002 (2002); J.L. Goity, C.L. Schat, and N.N. Scoccola, Phys. Rev. D **66**, 114014 (2002).

[45] C.E. Carlson and C.D. Carone, Phys. Lett. **B441**, 363 (1998); Phys. Rev. D **58**, 053005 (1998).

[46] C.E. Carlson and C.D. Carone, Phys. Lett. **B484**, 260 (2000).

[47] E. Jenkins, Phys. Lett. B **315**, 441 (1993).

[48] R.F. Dashen, E. Jenkins, and A.V. Manohar, Phys. Rev. D **51**, 3697 (1995).

[49] E. Jenkins and R.F. Lebed, Phys. Rev. D **52**, 282 (1995).

[50] M.A. Luty and J. March-Russell, Nucl. Phys. **B426**, 71 (1994); M.A. Luty, J. March-Russell, and M.J. White, Phys. Rev. D **51**, 2332 (1995).

[51] C.D. Carone, H. Georgi, and S. Osofsky, Phys. Lett. B **322**, 227 (1994).

[52] A.J. Buchmann and R.F. Lebed, Phys. Rev. D **62**, 096005 (2000).

[53] A.J. Buchmann and R.F. Lebed, Phys. Rev. D **67**, 016002 (2003).

[54] E. Jenkins, X. Ji, and A.V. Manohar, Phys. Rev. Lett. **89**, 242001 (2002).

[55] T.D. Cohen, Phys. Lett. B **554**, 28 (2003).

[56] D. Pirjol and T.-M. Yan, Phys. Rev. D **57**, 5434 (1998).

[57] D. Pirjol and C. Schat, Phys. Rev. D **67**, 096009 (2003).

[58] H. Yukawa, Proc. Phys.-Math. Soc. Japan **17**, 48 (1935).

[59] M.P. Mattis and M. Mukerjee, Phys. Rev. Lett. **61**, 1344 (1988).

[60] C. Rebbi and R. Slanksy, Rev. Mod. Phys. **42**, 68 (1970).

[61] M.P. Mattis and E. Braaten, Phys. Rev. D **39**, 2737 (1989).

[62] M.P. Mattis, Phys. Rev. Lett. **56**, 1103 (1986); Phys. Rev. D **39**, 994 (1989); Phys. Rev. Lett. **63**, 1455 (1989).

[63] H. Walliser and G. Eckart, Nuc. Phys. A **429**, 514 (1984).

[64] M.P. Mattis and M. Karliner, Phys. Rev. D **31**, 2833 (1985).

[65] R.D. Amado, M. Oka, and M.P. Mattis, Phys. Rev. D **40**, 3622 (1989).

[66] W.R. Gibbs, L. Ai, and W.B. Kaufmann, Phys. Rev. C **57**, 784 (1998).

[67] T.D. Cohen, Rev. Mod. Phys. **68**, 599 (1996).

[68] D. Mark Manley, R.A. Arndt, Y. Goradia, and V.L. Teplitz, Phys. Rev. D **30**, 904 (1984).

[69] The SAID data is available at George Washington University's Center for Nuclear Studies website: http://gwdac.phys.gwu.edu.

[70] V.B. Berestetskii, E.M. Lifshitz, and L.P. Pitaevskii, *Relativistic Quantum Theory*
(Addison-Wesley Publishing, Reading, Massachusetts, 1971).

[71] A.J. Buchmann and R.F. Lebed, Phys. Rev. D **62**, 096005 (2000).

[72] A.J. Buchmann, J.A. Hester, and R.F. Lebed, Phys. Rev. D **66**, 056002 (2002).

[73] See the Jefferson Laboratory website: http://www.jlab.org/div_dept/physics_division/.

[74] The MAID data is available at the Universität Mainz Institute for Nuclear Physics website: http://www.kph.uni-mainz.de/maid/.

[75] R.L. Walker, Phys. Rev. **182**, 1729 (1969).

[76] These issues are discussed in certain treatments of many-body physics. See for example, J.-P. Blaizot and G. Ripka, *Quantum Theory of Finite Systems* (MIT Press, Cambridge, 1986).

[77] G.E. Brown, *Unified Theory of Nuclear Models and Forces* (North-Holland, Amsterdam, 1967).

[78] F.E. Close, *An Introduction to Quarks and Partons* (Academic, London, 1979).

[79] A.R. Edmonds, *Angular Momentum in Quantum Mechanics* (Princeton Univ. Press, Princeton, NJ, 1996).

[80] A. Messiah, *Quantum Mechanics* (North Holland Publishing, New York, 1961).

[81] V. Makhankov, Y. Rybakov, and V. Sanyuk, *The Skyrme Model* (Springer-Verlag, New York, 1993).